DRAFT

BMI-2104
Volume IV

Radionuclide Release Under Specific LWR Accident Conditions

Volume IV
PWR, Ice Condenser Containment Design

Prepared by
J. A. Gieseke, P. Cybulskis, R. S. Denning,
M. R. Kuhlman, K. W. Lee, H. Chen

Battelle Columbus Laboratories
Columbus, Ohio 43201

July 1984

DRAFT

BMI-2104
Volume IV

Radionuclide Release Under Specific LWR Accident Conditions

Volume IV
PWR, Ice Condenser Containment Design

Prepared by
J. A. Gieseke, P. Cybulskis, R. S. Denning,
M. R. Kuhlman, K. W. Lee, H. Chen

Battelle Columbus Laboratories
Columbus, Ohio 43201

July 1984

Prepared for
Office of Nuclear Regulatory Research
U.S. Nuclear Regulatory Commission
Washington, D.C. 20555

ACKNOWLEDGMENTS

Battelle's Columbus Laboratories wishes to acknowledge and express appreciation for the computer codes made available for this program by Sandia National Laboratory, Battelle's Pacific Northwest Laboratories, and the Kernforschungszentrum Karlsruhe, and for the computations and consultation provided by Sandia and the Oak Ridge National Laboratories. Further, members of the Peer Review Group have contributed significantly to this effort by providing comments, suggestions, and information on various reactor systems design.

The support of the U.S. Nuclear Regulatory Commission is gratefully acknowledged, and is the untiring leadership of the NRC staff, particularly Mel Silberberg and Mike Jankowski.

The diligent efforts of many Battelle staff members contributed to the preparation of this report. The following list identifies those staff making major contributions:

RJ Avers
GT Brooks
EP Bryant
R Freeman-Kelly
CS Jarrett
H Jordan
RG Jung
DJ Lehmicke
MB Neher
DR Rhodes
PM Schumacher
RO Wooton.

TABLE OF CONTENTS

TABLE OF CONTENTS
(Continued)

1.0 EXECUTIVE SUMMARY

This is Volume 4, dealing with the Sequoyah nuclear power plant, of a seven-volume report of work done at Battelle's Columbus Laboratories to estimate the amount of radioactive material that could be released from light water reactor (LWR) power plants under specific, hypothetical accident conditions. To make these estimates, five power plants were selected that represent the major categories of LWRs: three pressurized water reactors (PWRs) and two boiling water reactors (BWRs). Specifications and data from these plants, along with data from laboratory experiments, were input to computer codes designed to describe various conditions prevailing inside an operating reactor. Ultimately, these computer codes provide an estimate of how much radioactive material would be able to escape to the environment if a specific series of events (an "accident sequence") took place.

Volume 4 of this report deals with the Sequoyah Power station, a Westinghouse PWR with an ice condenser containment. The specific accident sequences investigated for the Sequoyah plant were selected to represent cases of high risk, severe consequences, and most importantly, a wide range of physical conditions. The computer codes used to analyze the accident sequences were the best available, including the new MARCH 2 code. Other power plants included in the study are Surry PWR (Volumes 1 and 5); Peach Bottom BWR (Volume 2); Grand Gulf BWR (Volume 3); and Zion PWR (Volume 6). The seventh volume will address technical questions raised as a result of the peer review of this work during its performance.

The possibility of radioactive material being released to the environment has long been the focus of considerable public concern about the safety of nuclear power plants. Since 1962, several major reports have addressed that concern by using computer codes to estimate the release of fission products (radioactive material produced during reactor operations) to the reactor containment building, and thence to the environment, during a hypothetical severe accident. Although these analyses have improved over the years, in terms of how realistically they describe what happens during a hypothetical accident, it has not previously been possible to apply the various codes consistently to follow the transport of fission products along their flow path

from the core to the environment. This limitation resulted in piecemeal, parametric estimates of release.

The research results reported here are intended to provide a systematic, sequential application of the codes as well as to present analyses performed with improved computational procedures. It is to be recognized that this report describes an analytical approach for estimating radionuclide transport and deposition which incorporates individual physical and chemical processes or mechanisms. This approach is being evaluated for use in predicting the amount fission product release (the "source term") to the environment for specific reactors and accident sequences. When verified, these prediction techniques are expected to be more specific and perhaps to supersede generic tables of release fractions provided by previous analyses.

The purpose of this report is then to:

(1) Develop updated release-from-plant fission product source terms for four types of nuclear power plants and for accident sequences invovling a range of conditions. The estimated source terms are to be based on consistent step-by-step analyses using improved computational tools for predicting radionuclide release from the fuel and radionuclide transport and deposition.

(2) Determine the effects on fission product releases associated with major differences in plant design and accident sequences.

(3) Provide in-plant time- and location-dependent distributions of fission product mass for use in equipment qualification.

Approach

This study was conducted by selecting specific plants and accident sequences and then using consistent and improved analyses of fission product release from fuel and radionuclide transport and deposition to predict fission product release to the environment for these specific cases. The approach comprises a sequence of steps; in the combined analysis, the results are specific to a particular set of accident conditions, and each step is based on results from analyses of the previous step.

The Sequoyah Plant

Sequoyah Unit 1 was selected to characterize ice-condenser PWR designs. Typical of these designs, Sequoyah 1 has ice stored in a closed compartment between the upper and lower volumes of the containment. During an accident, the ice serves as a large, passive heat sink to condense steam and reduce containment temperature and pressure. The ice-condenser compartment is normally closed but opens up when containment pressure increases, and fans circulate air through the ice bed.

The primary containment of Sequoyah 1 is a cylindrical steel shell with a hemispherical dome, with a flat bottom supported by a reinforced concrete mat. Internal design pressure is 10.8 psig (0.07 MPa). The primary containment is surrounded by a reinforced concrete shield building.

An additional safety feature of Sequoyah 1 is the provision of hydrogen igniters to burn hydrogen that may be generated during severe accidents before hazardous levels are reached.

Accident Sequences Chosen for Study

The following accident sequences were selected because they represent high-risk situations with potentially severe consequences and because they involve a considerable range in physical conditions:

S_2HF Sequence:

- Small-break Loss-of-Coolant Accident (LOCA).
- Delayed failure of Emergency Core Cooling and Containment Spray Recirculation systems.
- Air return fans and hydrogen igniters are operable.

TML Sequence:

- Transient, loss of power conversion system, auxiliary feedwater, and primary coolant makeup.
- Containment safety features (air recirculation fans, containment sprays, hydrogen igniters) are operable.

TMLB' Sequence:

- Transient, complete loss of electric power, leading to loss of power conversion, auxiliary feedwater, and primary coolant makeup systems.
- Containment safety features (containment sprays, containment cooling systems) are not available.

Computer Codes Used in the Study

The efforts described here build on previous computer modeling work performed at Battelle-Columbus, at Sandia, and in the Federal Republic of Germany, and on experimental and model evaluation studies performed at Oak Ridge, EG&G Idaho, Sandia, and Pacific Northwest Laboratories. In addition to the calculations performed at Battelle-Columbus, calculations of thermal-hydraulic behavior and fission product release related to molten core-concrete interactions were performed by Sandia. Research efforts specifically directed toward increasing our understanding of fission product release and transport under severe accident conditions are under way at the laboratories listed above, as well as at other research installations around the world. Over the next few years, it is expected that considerable progress will be made in this area. Therefore, this report must be considered as an expression of current knowledge, with the expectation of future validation or modification of the calculated fission product releases.

The first step in analyzing accident sequences was to collect plant design data and perform thermal-hydraulic calculations. Thermal-hydraulic conditions in the reactor over time were estimated with the MARCH 2 code, and detailed thermal-hydraulic conditions for the reactor's primary coolant system were estimated with the MERGE code, developed specifically for this program.

The time-dependent core temperatures from the MARCH 2 code were used as input to another code developed for this program, CORSOR, which predicts time- and temperature-dependent releases of radionuclides from the fuel inside the reactor pressure vessel. Releases of radionuclides from the interaction of the melted reactor core with the concrete outside the reactor vessel were estimated by Sandia National Laboratories using their computer code, VANESA.

Using the MARCH/MERGE-predicted thermal-hydraulic conditions and the CORSOR-predicted radionuclide release rates as input, a newly developed

version of the TRAP-MELT code was used to predict vapor and particulate transport in the primary coolant circuit. Transport and deposition of radionuclides in the containment were calculated using the NAUA-4 code. For treating fission product deposition in the ice condenser compartments, the NAUA code was used in a form modified to include the deposition mechanisms from the ICEDF code for this special geometry.

The calculations performed in this study were of a "best estimate" type. Whenever possible, input was derived from experimental measurements. Data employed in these analyses include vapor deposition velocities, aerosol deposition rates, aerosol agglomeration rates, fission product release rates from fuel, particle sizes formed from vaporizing/condensing fuel materials, engineering correlations for heat and mass transfer, and physical properties of various fuel, fission product, and structural materials.

Summary of Results

The results for the release of fission products from the fuel during the period of fuel heatup and melting in-vessel and during ex-vessel attack of the concrete in the present study do not differ markedly from the results of earlier analyses. Essentially all of the volatile fission products are predicted to be released from the fuel in all cases.

The retention of fission products during their transport through the reactor coolant system has not been addressed in any depth in earlier studies. In the current study the retention in the primary coolant system has been found to be quite substantial, with approximately 80 percent of the iodine and cesium predicted to be retained. The uncertainty regarding the ultimate fate of fission products deposited on primary system surfaces is quite substantial, however, because of the likely heating of these surfaces by the decaying fission products and their possible reevolution.

The results of the containment transport analyses in the present study indicate significant potential for fission product attenuation. As would be expected, the environmental source terms are seen to depend on the timing of containment failure, with earlier failure leading to larger releases. The ice condenser was found to typically remove about half of the airborne radioactivity passing through it. The operation of containment sprays and air return

fans was found to lead to substantial reduction in the potential release to the environment.

The ice condenser containment was found to be potentially vulnerable to large hydrogen burns. For the accident conditions and modeling assumptions considered, significant pressure loads were predicted even considering operation of the hydrogen igniters; large pressure loads resulted when the burning was predicted to propagate into the upper compartment of the containment.

The magnitudes of the environmental fission product source terms predicted in this study are significantly lower than those of earlier assessments, such as WASH-1400 and RSSMAP. It is important, however, to recognize that the uncertainties associated with these results could be quite large. The predictions of fission product releases has been shown to be sensitive to accident thermal-hydraulics as well as to the mechanisms of fission product release and transport. It should also be recognized that the prediction of the course and consequences of the low probability hypothetical situations considered here is inherently uncertain; at best, the small number of accident scenarios considered here can only be representative of a wide spectrum of possible outcomes in the event of an accident.

2. INTRODUCTION

The possibility of radioactive material being released to the environment from LWRs has long been the impetus for considerable concern and research. Most reactors in the United States were designed, and their sites were chosen, on the basis of research report TID-14844.(2.1) Published in 1962, TID-14844 makes certain assumptions about the release of fission products (radioactive material produced during reactor operations) to the reactor containment area during a hypothetical severe accident. Although these assumptions are representative of the state of knowledge at the time, the behavior of fission products has become better understood in the intervening years. Accordingly, the Nuclear Regulatory Commission conducted the Reactor Safety Study to reassess the accident risks in U.S. commercial nuclear power plants. The report of that study, known as WASH-1400,(2.2) was published in 1975 and provided a more comprehensive and physically accurate description of fission product behavior. The amount of fission product release (the "source term") estimated in WASH-1400 has since been used extensively in planning and evaluating reactor operations.

The WASH-1400 source term to the environment for accident sequences has had broad implications for operating LWRs--in licensing, emergency planning, safety goals, and indemnification policy. However, additional research continued to provide even better methods for estimating fission product release and transport. In 1981, the Nuclear Regulatory Commission issued the report "Technical Bases for Estimating Fission Product Behavior During LWR Accidents",(2.3) a review of the state of knowledge at the time. As part of the Technical Bases report, the assumptions, analytical procedures, and available data were evaluated, and new estimates were made. One advantage of the new estimates was that they took into account the fact that some radioactive material would be deposited inside the reactor during an accident and would therefore not escape from the reactor core to the environment. On the other hand, because of the limitations of the computer codes available at that time, the new estimates could not follow the transport of fission products along their flow path from the core to the environment by applying the various codes sequentially. This resulted in piecemeal, parametric estimates of release.

The research results reported here are intended to provide this systematic, sequential application of the codes as well as to present analyses performed with computational procedures improved since the "Technical Bases" report. It is to be recognized that in this study, an analytical approach was developed for estimating radionuclide transport and deposition which incorporates individual physical and chemical processes or mechanisms. This approach is being evaluated for use in predicting fission product source terms for release to the environment for specific reactors and accident sequences. When verified, predictions made with the approach used here are expected to replace the generic tabular release fractions such as those in Table 6, Appendix V of WASH-1400, where release fractions are given for broad classes of accidents.

The purpose of this report is then to:

(1) Develop analytical procedures and use them to predict updated release-from-plant fission product source terms for four types of nuclear power plants and for accident sequences giving a range of conditions. The estimated source terms are to be based on consistent step-by-step analyses using improved computational tools for predicting radionuclide release from the fuel and radionuclide transport and deposition.

(2) Determine the effects on fission product releases associated with major differences in plant design and accident sequences.

(3) Provide in-plant time- and location-dependent distributions of fission product mass for use in equipment qualification.

It is not necessarily the intent of this work to produce an all-encompassing definition of source terms, but rather to make best estimates of source terms for a range of typical plants and several risk-significant sequences covering a wide range of conditions. These analyses are to be made with the best available techniques, in a consistent manner, following along release pathways for fission products, and at a level of detail consistent with current knowledge of pertinent physical processes. Based on state-of-the-art techniques, these best-estimate analyses should provide an indication of the conservatisms inherent in current source term assumptions and guidance for the development of new source terms. The analytical methods and

corresponding predictions presented here are based on currently available information and are subject to revision and improvement as better analytical procedures are developed and as a more extensive experimental base evolves. The preparation of this report, therefore, is an evolutionary process which will be carried out over a period of time, with verification and possibly revision of the procedures continuing over several years.

2.1 References

(2.1) DiNunno, J. J., et al, "Calculation of Distance Factors for Power and Test Reactors Sites", TID-14844 (March 23, 1962).

(2.2) "Reactor Safety Study--An Assessment of Accident Risks in U.S. Commercial Nuclear Power Plants", WASH-1400, NUREG-75/014 (October, 1975).

(2.3) "Technical Bases for Estimating Fission Product Behavior During LWR Accidents", NUREG-0772 (June, 1981).

3. GENERAL APPROACH

The general philosophy behind this study is that mechanistic predictions of radionuclide release and transport are possible if proper modeling is performed to represent the physical and chemical processes occurring during LWR accidents. The study, then, represents an attempt to describe in a reasonably complete but tractable fashion the processes influencing radionuclide release to the environment for selected plants and accident conditions.

The objectives of this study originally called for a consistent analysis of radionuclide behavior by following fission product transport along flow paths, starting with release into the core region and ending with final release to the environment. To meet these objectives, numerous decisions and assumptions were required for the analyses: selection of plants and sequences for consideration; choice of analytical tools to be used or upgraded; evaluation and incorporation of experimental data; and determination of major physical effects which would be considered on a parametric variation basis to determine the sensitivity of calculations to such variations. Some of the major considerations will be reviewed and discussed in this section.

The general approach in this study was to select specific plants and accident sequences for consideration and then to use consistent and improved analyses of fission product release from fuel, transport, and deposition to predict fission product release to the environment for these specific cases. The approach consists of a series of steps performed in sequence such that in the combined analysis, the results are specific to an individual set of accident conditions, and each step is based on results from analyses of the previous step.

3.1 Plant Selection

The first major step in the process was the selection of types of nuclear power plant designs to be considered and a specific plant to represent each type. The types to be considered were: large, dry PWRs; Mark I BWRs; Mark III BWRs; and ice-condenser containment PWR designs. The specific plants chosen to represent each type, respectively, are the Surry and Zion, Peach Bottom, Grand Gulf, and Sequoyah plants. These selections were made on a

combined basis of typicality of design and availability of design details needed for analysis.

3.2 Selection of Accident Sequences

Accident sequences were chosen for each plant such that significant contributions to risk and a wide range of physical conditions were represented in the analyses. The selected plants and accident sequences are listed below:

PWR: Large Dry Containment (Surry-Volumes 1 and 5)	PWR: Large Dry Containment (Zion-Volume 6)	BWR: Mark I (Peach Bottom-Volume 2)
AB	TMLB'	TC
S_2D	S_2D	AE
V		TW
TMLB'		

BWR: Mark III (Grand Gulf-Volume 3)	PWR: Ice Condenser Containment (Sequoyah-Volume 4)
TPI	S_2HF
TQUV	TMLB'
TC	TML
S_2E	

The accident sequences for each plant are described in detail in Section 4.2 of the volume of the report dealing with that plant.

3.3 Computer Codes Used in the Study

Following the selection of plants and sequences, the required plant design data were collected and thermal-hydraulic analyses performed for each accident sequence. Overall thermal-hydraulic conditions on a time-dependent basis were estimated with the MARCH code,[3.1] and detailed thermal-hydraulic conditions for the primary system were estimated with the MERGE[3.2] code developed specifically for this program.

The time-dependent core temperatures were used as input to another code developed for this program, CORSOR[3.3], which predicts time- and temperature-dependent mass releases of radionuclides from the fuel within the pressure vessel. Releases during core-concrete interactions of radionuclides remaining with the melt were provided by Sandia National Laboratories using their newly developed model, VANESA[3.4].

Using the MARCH/MERGE-predicted thermal-hydraulic conditions and the CORSOR-predicted radionuclide release rates as input, a newly developed version of the TRAP-MELT code (TRAP-MELT 2)[3.5] was used to predict vapor and particulate transport in the primary coolant circuit.

Transport and deposition of radionuclides in the containment were calculated using the NAUA-4[3.6] code modified to include deposition within ice compartments.

The basic stepwise procedure described above is illustrated in Figure 3.1, which shows the relationships among the computational models. The calculations were of a "best estimate" type using input derived from experimental measurements whenever possible. Types of data employed in the analyses include vapor deposition velocities, aerosol deposition rates, aerosol agglomeration rates, fission product release rates from fuel, particle sizes formed from vaporizing/condensing fuel materials, engineering correlations for heat and mass transfer, and physical properties of various fuel, fission product and structural materials.

3.3.1 Assumptions

In preparation for performing calculations of thermal-hydraulic conditions and radionuclide transport and deposition. it was necessary to make a number of assumptions or to select conditions from among several options. Major assumptions used in this study of the Sequoyah plant are listed below in the categories of geometry, thermal hydraulics, and mechanisms.

Geometry

(1) Surfaces within the containment building available for radionuclide deposition include only the major geometrical features of the building.

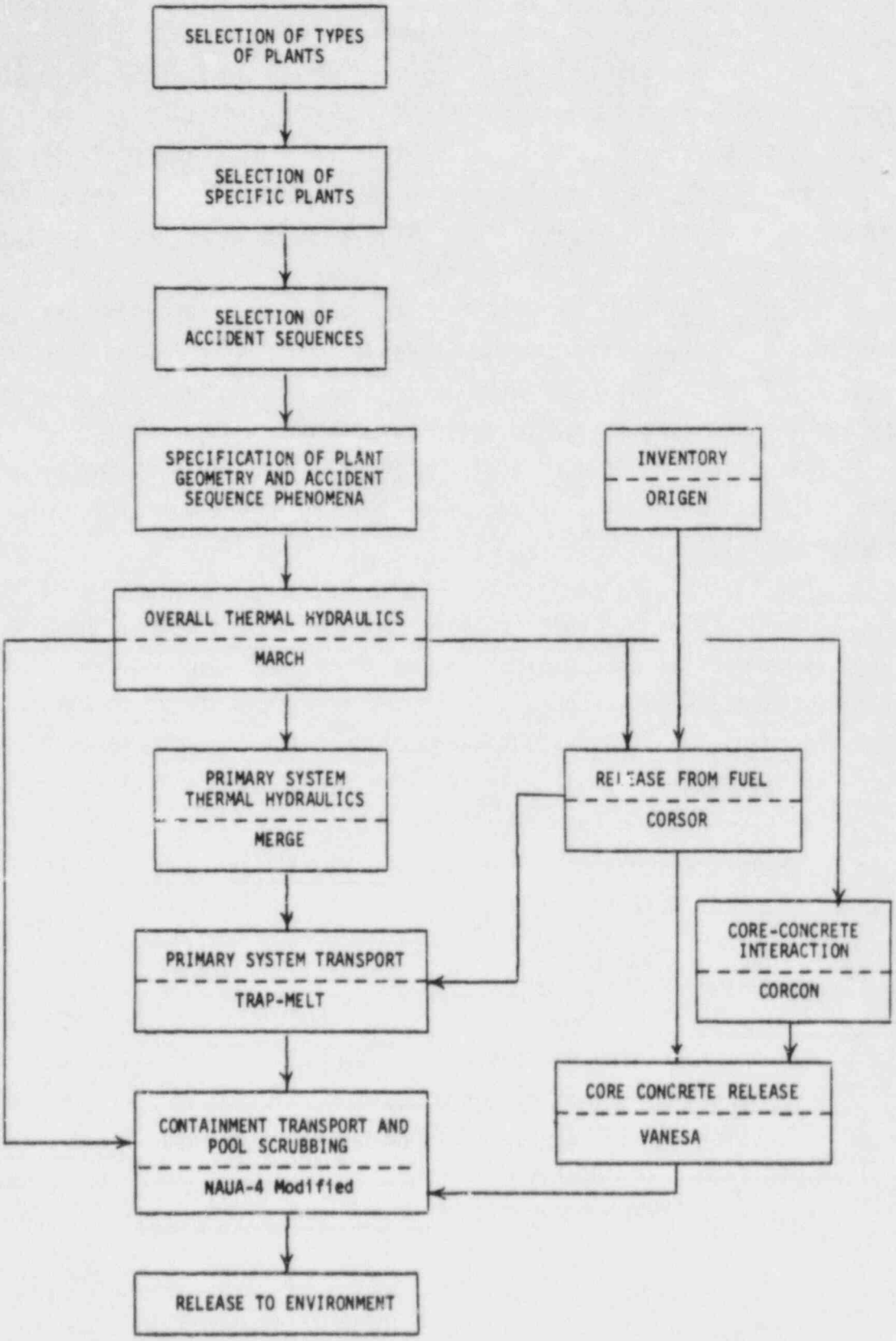

FIGURE 3.1. INFORMATION FLOW FOR RELEASE, TRANSPORT, AND DEPOSITION CALCULATION

(2) There is no attenuation of radionuclides as they pass through leak paths in the containment shell.

Thermal Hydraulics

(3) Before pressure vessel failure, flow in the primary coolant system is restricted to direct leak paths.

(4) The upper plenum geometry is modeled in terms of surface areas, steel thickness, and compartment heights rather than with exact geometries.

(5) Decay heating of surfaces by deposited fission products is neglected in the calculations.

(6) No operator intervention occurs that would lead to cooling of the steam generators.

Mechanisms

(7) Neither deposition nor resuspension of radionuclides occurs during rector coolant system depressurization at the time of pressure vessel melt-through.

(8) In the long term (after pressure vessel failure), deposited radionuclides remain in the primary system indefinitely.

(9) No change in fission product physical or chemical properties results from radioactive decay.

Some of the above assumptions have been relaxed or changed to accommodate best estimates of conditions and occurrences in specific cases. These are discussed in greater detail for each plant in Section 6.1 of the volume of the report dealing with that plant.

3.3.2 Uncertainty Considerations

The computation of radionuclide release and transport using mechanistic models is subject to many uncertainties of various magnitudes and importance. Quantitative estimates of uncertainties in individual parameters, and hence the overall importance of such uncertainties, has been outside the scope of

this study. Where practical, however, qualitative (and in some cases quantitative) estimates of uncertainties have been noted.

Some of the uncertainties in the analyses and procedures can be identified that are currently considered significant. The following is a list of some uncertainties that are believed significant and warrant further evaluation through more detailed analyses:

(1) The simplified fuel melting model in MARCH (i.e., a single melting temperature) could bias the predicted release of material from overheated fuel, particularly regarding the source of inert and low volatility fission product aerosols.

(2) The rate coefficients for the release of fission products from overheated fuel are empirical, rather than mechanistically based, and rely largely on scaled, simulant experiments.

(3) The model for the release of fission products and inert materials during the attack of concrete has a very limited experimental basis.

(4) The flow patterns in the reactor coolant system are uncertain. The adequacy of the simple thermal-hydraulic models used in this study will require experimental verification.

(5) Primary system transport models used in these analyses have not been validated against integral experiments.

(6) The mode and timing of containment failure in severe accident sequences can have a major influence on fission product behavior but are subject to large uncertainty.

(7) The calculation methods for water condensation in the containment are based on limited, small-scale experiments and require verification at larger scales.

(8) Deposition velocities for vapor species used in the TRAP-MELT calculations were taken as a mid-points in order-of-magnitude ranges of experimental data. More accurate data would reduce the uncertainty in these parameters and in the resulting rates for deposition by sorption.

3.4 References

(3.1) Wooton, R. O. and Avci, H. I., "MARCH (Meltdown Accident Response CHaracteristics) Code Description and User's Manual", NUREG/CR-1711, BMI-2064 (October, 1980).

(3.2) Freeman-Kelly, R. G. and Jung, R. G., "A User's Guide for MERGE" (February 10, 1984).

(3.3) CORSOR Manual.

(3.4) VANESA Manual.

(3.5) TRAP-MELT 2.1 User's Manual.

(3.6) Bunz, H., Koyro, M., and Schock, W., "A Code for Calculating Aerosol Behavior in LWR Core Melt Accidents Code Description and User's Manual".

4. PLANT AND ACCIDENT SEQUENCE SELECTION

4.1 Plant Description

The ice condenser containment plant selected for this study is the Sequoyah Unit No. 1 located near Chattanooga, Tennessee, owned and operated by the Tennessee Valley Authority. This is the same plant analyzed earlier as part of the Reactor Safety Study Methodology Applications Program (RSSMAP).[4.1] Sequoyah Unit No. 1 employs a four-loop pressurized water reactor (PWR) manufactured by the Westinghouse Electric Corporation. It is designed to generate 1148 MW(e) with a total thermal output of 3579 MW(t).

The ice condenser containment design of Sequoyah Unit No. 1 is illustrated in Figure 4.1. The primary containment is a cylindrical steel shell with a hemispherical dome and a flat bottom and is surrounded by a reinforced concrete shield structure. The thickness of the cylindrical portion varies, with circumferential stiffeners placed at axial locations where the wall thickness changes. The flat bottom is supported by a reinforced concrete foundation mat. The containment has been designed for a nominal internal pressure of 10.8 psig. A listing of the key parameters related to the design of the plant data is provided in Chapter 6.

In the RSSMAP study, an elastic-plastic analysis was used to determine the static strength of the primary containment structure. This analysis indicated that the structure would begin to yield at an internal pressure of 24 psig and approach its ultimate strength at 30 psig, where an unstable condition begins to develop. The location of the initial yielding is just below the containment springline, about midway between circumferential stiffeners, in the thinnest section of the cylindrical wall. Based on these analyses, a nominal failure pressure of 30 $\pm$3 psig (45 $\pm$3 psia) was utilized in RSSMAP. Somewhat higher failure pressures have been suggested for similar containments analyzed subsequently. It is not clear, however, that consistent interpretations of failure or failure pressure are always utilized. In order to compensate for possible conservatisms associated with the RSSMAP analyses, a failure pressure of 60 psia has been utilized in the present study.

The ice condenser serves as a large passive heat sink to condense steam and reduce containment temperature and pressure in the event of an accident. Ice is stored in a closed compartment between the upper and lower

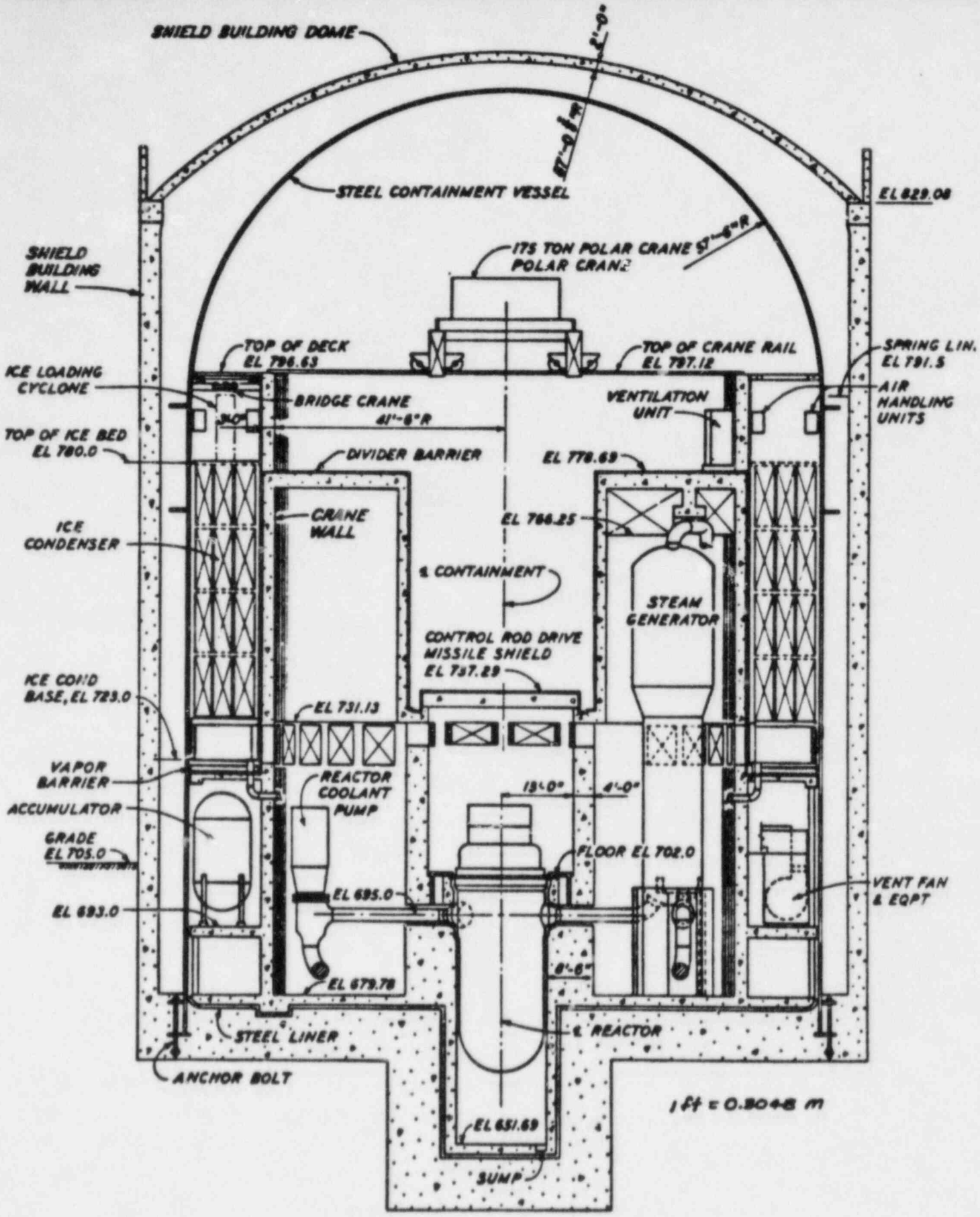

FIGURE 4.1 ICE CONDENSER CONTAINMENT

volumes of the containment. If primary coolant were released at high pressure and temperature, as would occur in a loss-of-coolant-accident (LOCA), the doors to the ice condenser compartment, which are normally closed, would open due to the increased containment pressure and allow the steam to flow through. Air Return Fans circulate air between the upper and lower containment volumes, and hence through the ice bed, enhance condensation by providing a recirculating flow.

The large passive heat sink permits a smaller volume and lower pressure containment design than would otherwise be possible. The design basis accident for the containment, however, is a large break LOCA with successful emergency core cooling system operation which does not consider phenomena that may be associated with accidents leading to severe core damage.

Another feature of ice condensers PWR's, though not associated with the containment design, is the addition of the Upper Head Injection (UHI) system. The UHI is a high-pressure accumulator which automatically provides an initial high flow of emergency cooling water into the top of the reactor vessel. The UHI operates at a higher pressure and thus supplements the water injection provided by the normal accumulators included as part of the PWR ECCS design.

As a result of the TMI-2 accident and subsequent NRC rulemaking activities, substantial attention has been given to the questions of hydrogen burning and possible effects on containment integrity during reactor accidents. In order to mitigate effects of such burning, the Sequoyah plant now includes igniters to burn hydrogen before it accumulates to hazardous levels. The operation of these igniters has been included in the present analyses, as appropriate.

4.2 Accident Sequence Selection

Three accident sequences have been selected for detailed investigation for the Sequoyah plant: TMLB', TML, and S_2HF. (Table 4.1 relates the letters used to identify the accident sequences with the systems that fail during the accident.) The TMLB' sequence involves a transient with complete loss of electric power, leading to the unavailability of the power conversion and auxiliary feedwater systems as well as the unavailability of active emergency core cooling and containment safety systems. The TML sequence includes loss of the power conversion system, the auxiliary feedwater systems,

TABLE 4.1. KEY TO PWR ACCIDENT SEQUENCE SYMBOLS

A - Intermediate to large loss of coolant accident (LOCA).

B - Failure of electric power to engineered safety features (ESF).

B' - Failure to recover either onsite or offsite electric power within about 1 to 3 hours following an initiating transient which is a loss of offsite AC power.

C - Failure of the containment spray injection system.

D - Failure of the emergency core cooling injection system.

F - Failure of the containment spray recirculation system.

G - Failure of the containment heat removal system.

H - Failure of the emergency core cooling recirculation system.

K - Failure of the reactor protection system.

L - Failure of the secondary system steam relief valves and the auxiliary feedwater system.

M - Failure of the secondary system steam relief valves and the power conversion system.

Q - Failure of the primary system safety relief valves to reclose after opening.

R - Massive rupture of the reactor vessel.

S_1 - A small LOCA with an equivalent diameter of about 2 to 6 inches.

S_2 - A small LOCA with an equivalent diameter of about 1/2 to 2 inches.

T - Transient event.

V - Low pressure injection system check value failure.

Containment Failure Modes:

α = steam explosion

β = containment isolation failure

γ = overpressurization due to hydrogen combustion

δ_e = early overpressure failure due to steam and noncondensible gases

δ_l = delayed overpressure failure due to steam and noncondensible gases

ϵ = basemat melt-through

and the all coolant makeup to the primary system; in this sequence, however, containment safety features are available. The S_2HF sequence is initiated by a small break in the reactor coolant system; the emergency core cooling and containment spray systems function in the injection mode but fail during recirculation due to a common-cause failure.

These sequences were among the dominant ones identified in RSSMAP and are consistent with the important accident sequences identified in ASEP.[4.2] Further discussion of these sequences and the fission product flow paths associated with them are given below.

4.2.1 Sequence TMLB' (Transient, Loss of Core Cooling and Containment Cooling)

In this sequence, the complete loss of electric power leads to the failure of the power conversion and auxiliary feedwater systems, loss of coolant makeup to the primary system, and loss of active containment engineered systems. Following reactor shutdown as a result of the transient, the water in the secondary side of the steam generators boils off due to decay heat in the core. After dryout of the steam generators, the primary coolant inventory heats up and the primary system pressure increases to the pressurizer relief valve setting. Primary coolant then boils off through the pressurizer relief valve, eventually leading to core uncovery and melting. If the primary system pressure falls below the upper head injection (UHI) or accumulator setpoints, the UHI or accumulator discharges and may temporarily arrest core heatup. As the core heats up and melts, fission products are released from the fuel, and they flow with steam and hydrogen through the upper plenum of the reactor vessel, through the hot leg to the pressurizer, and to the pressurizer relief tank.

Since the pressurizer relief tank has a limited capacity, continued release of the primary coolant raises the tank pressure to the burst disc setting, releasing primary coolant to the lower volume of the ice condenser containment. The resulting containment pressure increase opens the ice condenser doors. Steam is forced into the ice condenser and condenses. The effluent from the ice condenser is released to the upper containment volume. Because of the loss of electric power, neither the air return fans nor the hydrogen igniters are operable in this sequence. The fission products released to the containment flow with the gases and vapors through the ice condenser into the upper volume, with some removal of the fission products by the ice beds. As

long as ice is available, it is very effective in condensing steam that flows through it. After the ice has melted, the steam pressure in the containment may continue to build up. The ice will reduce the temperature of the noncondensibles passing through it but otherwise have no effect on them.

As hydrogen builds up in the containment atmosphere, there is the possibility of burning. The effect of potential hydrogen burns would be sensitive to their timing, location, and magnitude. Burns occurring in the lower compartment and passing through the ice bed may lead to only minor overall pressure increase; burns initiated in the upper compartment would tend to lead to greater pressure increases. Hydrogen burns propagating to both the upper and lower volumes would generally present more severe challenges to the containment integrity.

Following the failure of the bottom head of the reactor vessel, the core debris would be released to the reactor cavity. Any airborne fission products within the primary system would be released to the lower containment volume. Fission products released from the attack of the concrete by the hot core debris would be released into the reactor cavity and hence into the lower part of the containment.

If containment pressures high enough to lead to failure are reached, the failure would be expected to take place in the upper part of the cylindrical shell where the wall is thinnest.

Figure 4.2 illustrates schematically the fission product flow paths for the TMLB' sequence in the ice condenser containment.

4.2.2 Sequence TML (Transient, Loss of Core Cooling)

This sequence involves the loss of normal and emergency means of adding water to the secondary side of the steam generators and the loss of primary system coolant makeup capability. As a result, the steam generators boil dry, the primary system pressure increases to the pressurizer relief valve setpoint, and the primary system coolant inventory boils off, eventually leading to core melting. The primary system response for this sequence would be identical to that for the TMLB' sequence described above.

In the TML sequence all the containment safety features are available. Thus, after the steam generator dries out and the pressurizer relief valve is

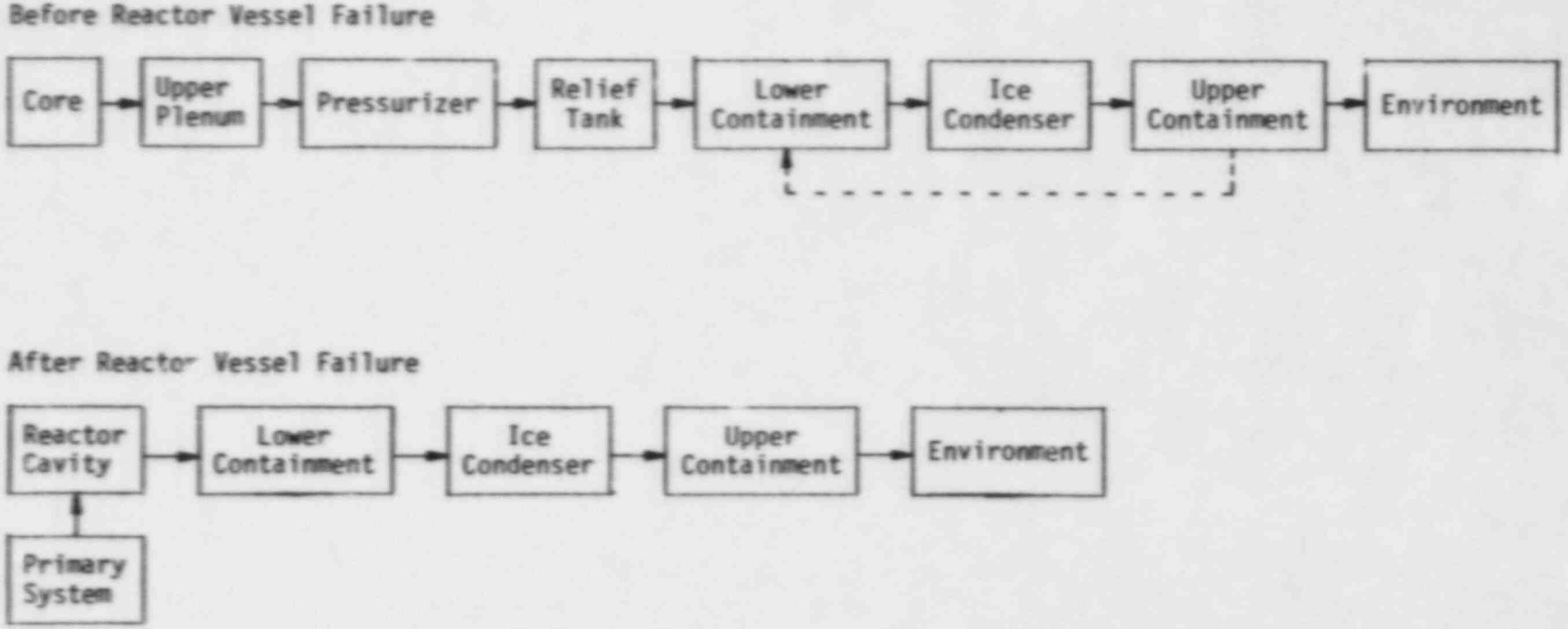

FIGURE 4.2 FISSION PRODUCT FLOW PATHS FOR ICE CONDENSER SEQUENCE TMLB'

actuated, the air return fans, containment sprays, and hydrogen igniters would be available to mitigate the consequences of the accident. The air return fans promote circulation of the containment atmosphere through the ice condenser and tend to promote homogenization of the atmosphere composition. The containment sprays provide for steam condensation after the ice is melted and help to absorb the energy released from hydrogen burning. The hydrogen igniter system is designed to burn off the hydrogen generated from the Zircaloy-steam reaction before it can accumulate to dangerous levels.

With the containment safety features available, containment failure should be less likely, or at least delayed in time relative to sequences where they are not available. If the containment does fail, the failure will occur in the thin-walled section of the upper part of the cylindrical shell, as in the TMLB' sequence. Figure 4.3 summarizes schematically the fission product transport paths for this sequence.

4.2.3 Sequence S_2HF (Small Pipe Break, Failure of ECCS and CSRS)

This sequence consists of a small break LOCA as the initiator, followed by a delayed failure of both the emergency core cooling (ECCS) and containment spray recirculation (CSRS) systems. Both the air return fans and the hydrogen igniters are available.

In the RSSMAP analyses, failures of the ECCS and the CSRS were found to be dominated by common-mode contributions. The upper and lower compartments in the ice condenser containment are connected by two drains which must be closed during refueling operations. The ECCS and CSRS draw water from the sump in the lower containment. The water delivered by the spray system to the upper compartment must pass through the drains to return to the sump for further recirculation. Failure to reopen these drains after refueling would, in the event of an accident, lead to all the water eventually being transferred from the lower compartment sump to the upper compartment. Attempting to draw water from the dry sump would lead to pump failure in both systems. This is the situation assumed for the present analyses. An alternative failure mode for both systems is the failure to realign pump suction from the depleted refueling water storage tank to the containment sump, as required to switch from the injection to the recirculation mode of oepration.

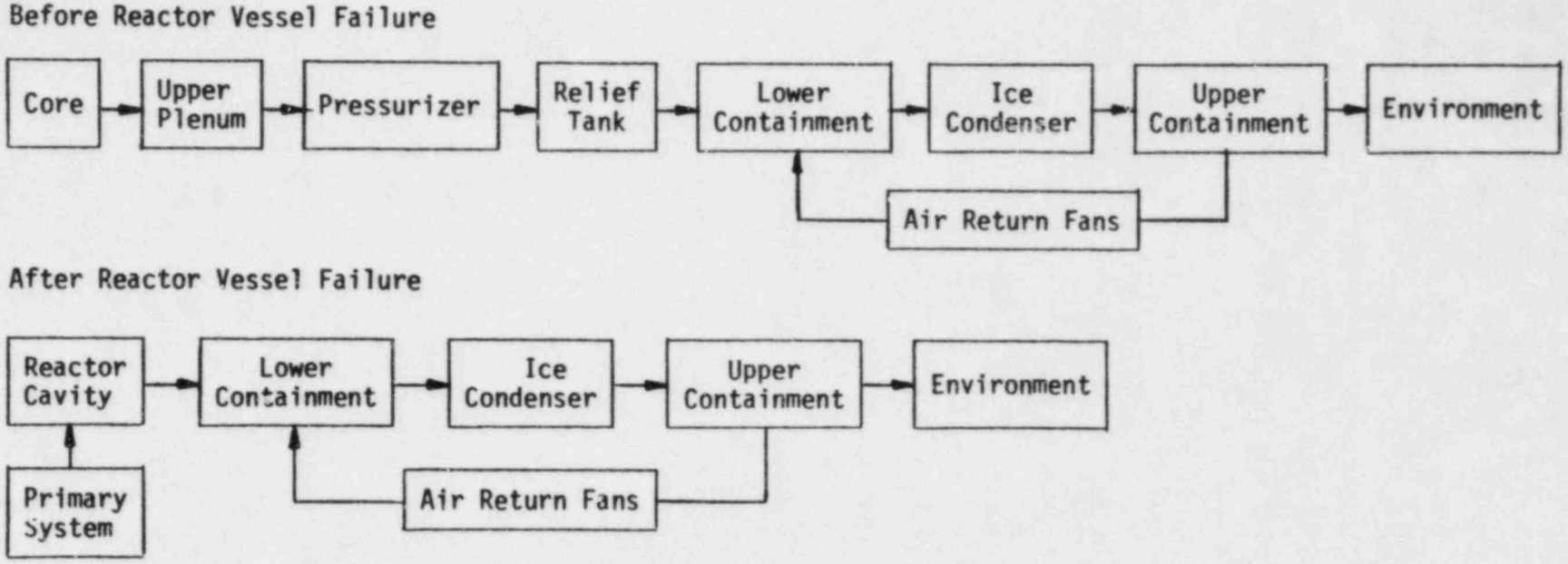

FIGURE 4.3 FISSION PRODUCT FLOW PATHS FOR ICE CONDENSER SEQUENCE TML

Since the ECCS operates successfully in response to the small break initiating this sequence, the core is well cooled and water-covered at the time of emergency core cooling failure. The actual quantity of water in the primary system at the time of ECCS failure depends on the size and location of the break. As the core uncovers, heats up, and melts, fission products are released from the core and flow through the upper plenum to the hot leg piping and out the break. Some fission products could flow through the unbroken loops and the steam generators before exiting the primary system. The latter path could provide significantly greater retention of fission products within the primary system. The distribution of flows between the broken and unbroken loops would depend on the location of the break. Following failure of the reactor vessel bottom head, airborne fission products in the primary system are released to the lower containment volume. Any fission products released from the attack of the concrete by the core debris are released into the reactor cavity and thus the lower containment volume.

The fission products released to the lower volume, either from the primary system or from the reactor cavity, flow through the ice condenser into the upper containment. From there they are recirculated to the lower compartment by the air recirculation fans. After containment failure, the operability and effectiveness of the air return fans is questionable, and the fission products in the upper containment could be available for leakage to the environment.

Figure 4.4 summarizes the fission product flow paths for the various stages of the S_2HF sequence.

REFERENCES

(4.1) Carlson, D. D., et al, "Reactor Safety Study Methodology Applications Program: Sequoyah #1 Power Plant", NUREG/CR-1659/1 of 4 (February, 1981).

(4.2) Kolaczkowski, A. M., et al, "Interim Report on Accident Sequence Likelihood Reassessment (Accident Sequence Evaluation Program)", Sandia National Laboratories (August, 1983).

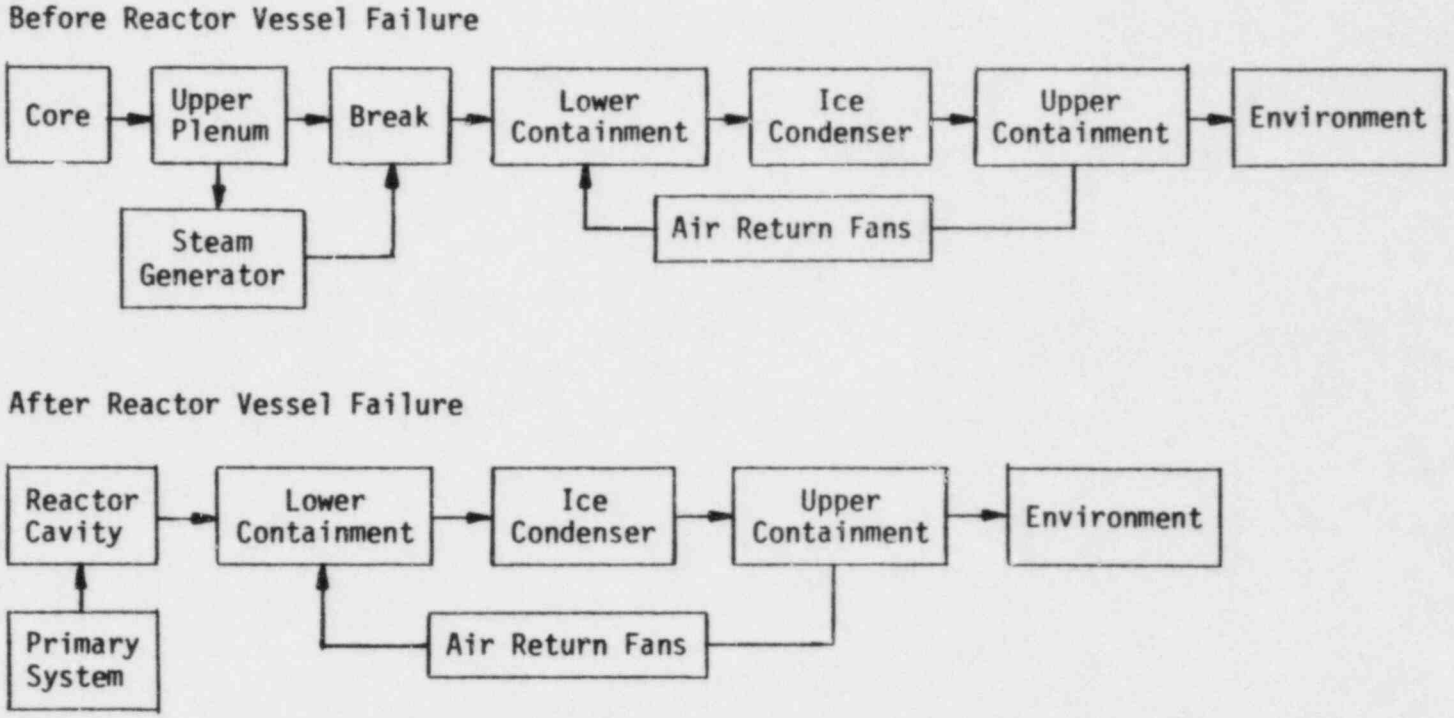

FIGURE 4.4 FISSION PRODUCT FLOW PATHS FOR ICE CONDENSER SEQUENCE S_2HF

5. ANALYTICAL METHODS

This section describes the analytical methods used in assessing the source term to the environment for the Sequoyah plant, a PWR with an ice condenser containment. The methods employed here differ significantly from those used to analyze the Surry plant, as described in Volume 1 of this report[5.1]. The Surry plant has been reevaluated using these revised methods; the results of the Surry reevaluation are reported in Volume 5[5.2].

The first major difference between the methods used here and those described in Volume 1 is that the MARCH 2 code is used here for the overall thermal-hydraulic calculations, replacing the MARCH 1.1 code used for Volume 1. MARCH 2 contains a number of changes in the treatment of accident phenomena from the earlier version of the code. The second major change is that in the present analysis, an accounting is made for the effect of the extent of Zircaloy cladding oxidation on the release rate for tellurium. Finally, a new code called ICEDF is used here to predict the removal of aerosols by the ice beds.

Some other, less significant changes have been made as well. These are discussed in the text.

5.1 Thermal Hydraulic Behavior

This section describes the computer code MARCH 2, which, along with the MERGE code, was used to analyze the thermal-hydraulic response of the reactor core, the primary coolant system, and the containment system for the selected accident sequences.

5.1.1 Overall System Thermal Hydraulics: MARCH 2

The MARCH 2[5.3] (Meltdown Accident Response CHaracteristics) computer code describes the physical processes involved in severe fuel-damage accidents in light water reactors. Version 2 of the code replaces Version 1.1.[5.4] The differences between the two versions include changes in models, code structure, and programming language. The new models in MARCH 2 were developed at a number of institutions, including Battelle, Sandia National Laboratories, Oak Ridge National Laboratories, Brookhaven National Laboratory, and the Tennessee

Valley Authority. In many cases, these models are provided as options to existing models. The changes in MARCH were largely undertaken to address recognized deficiencies in the early version related to modeling approximations, time-step control, and transportability of the code to other installations.

The MARCH 2 code was developed primarily for use in probabilistic risk assessment. The uncertainties in many of the MARCH 2 models are large, and in many cases the extent to which the models have been validated against experiments is limited. More mechanistic codes are being developed by the NRC, such as SCDAP and HECTR, but they were not available for use in this program.

The MARCH 2 code provides the capability to examine the behavior of a large variety of accident processes including depressurization or leakage from the reactor coolant system, core uncovery, core heatup, oxidation of Zircaloy cladding, fuel melting, fuel slumping, fuel-coolant interaction in the lower vessel head, vessel head failure, fuel-coolant interaction in the reactor cavity, debris bed coolability, core-concrete interactions, production of combustible gases, gas combustion in the containment, containment heat transfer, intercompartment flows, and the effect of engineered safety features on containment thermal hydraulic behavior. Some of the principal modeling improvements in Version 2 of the MARCH code are described below.

5.1.1.1 Containment Response. The containment response modeling in MARCH 2 includes the following principal changes: provision for expanded blowdown input via subroutine INITIAL, the ability to accept two input terms from the primary system, completely revised treatment of burning of combustibles, addition of a heat sink for radiation heat transfer from the debris in the reactor cavity, and removal of a number of restrictions in the earlier code.

The expanded blowdown table input capability is intended to facilitate the interfacing of the MARCH code with more detailed thermal-hydraulic codes that may be used to describe the initial portion of the accident sequence.

The containment response subroutine, MACE, has been changed to accommodate simultaneous break and relief/safety valve flows from the primary system. The two inputs can be directed to different compartments if desired, e.g., break flow to the drywell and relief/safety valve flow to the suppression pool of a BWR.

5.1.1.2 Primary System Response. The MARCH 2 treatment of the primary system includes both improvements in the treatment of initial (early) primary system response and the addition of several phenomenological models to treat the processes following core collapse into the bottom head. Included are changes in the steam generator model to remove some of the restrictions and limitations of the earlier version, improved break flow models, changes in the flashing model in response to primary system pressure changes, provisions for simultaneous break and relief/safety valve flow, changes in the treatment of heat transfer to structures, and consideration of the transport of fission products within the primary system.

5.1.1.3 Water and Steam Properties. The representation of the properties of water and steam has been improved in MARCH 2. This has included expansion of the property tables and correlations incorporated in the code as well as inclusion of additional properties required by the new phenomenological models. The input parameters are based on the ASME steam tables.

5.1.1.4 Decay Heat. MARCH 2 incorporates the current American National Standard[5.5] for evaluating fission product decay heating as a function of time after shutdown and time at power, including the contributions from heavy element decay. This replaces the earlier, simplified version incorporated in MARCH 1.1. Alternatively, decay heat as a function of time may be input in tabular form; this approach would be particularly appropriate for transients with failure to scram, where the power history would be provided by more detailed system codes.

5.1.1.5 Core Heat Transfer. MARCH 2 retains the basic model of the core as developed for the earlier version, but incorporates additional models for a more detailed treatment of heat transfer processes. Heat transfer between the fuel rods and the steam-hydrogen gas mixture is now calculated using either the full Dittus-Boelter correlation[5.6] for turbulent flow or a laminar flow correlation. A subroutine has also been added to approximate axial conduction heat transfer in the fuel rods using the Fourier law of heat conduction and the BOIL-calculated node temperatures. The effect of axial and radial thermal radiation heat transfer within the core, as well as between the core and surrounding structures and water surfaces, can now be calculated. The heatup

of the core support barrel by thermal radiation is included. Additional changes include corrections in the heat transfer analysis of partially covered core nodes and improvements in the metal-water reaction model.

5.1.1.6 Core Debris. A number of phenomenological models have been added for the treatment of the core debris in the reactor vessel bottom head. These include a flat plate critical heat flux model, a fragmented debris-to-water heat transfer correlation, and several options that consider formation of debris beds within the vessel head while water is still in the vessel. The bottom head heatup model utilizes a calculated heat transfer coefficient between the molten debris and the vessel head.

A major area of concern and controversy in the analysis of core meltdown accidents has been the behavior of core and structural debris upon contact with water in the reactor cavity. The highly simplified models of MARCH 1.1 have been supplemented with a flat plate critical heat flux model, a particulate heat transfer model with more mechanistic heat transfer coefficients, and several debris bed heat transfer correlations. If desired, the switchover from one model to another can be based on calculated conditions, e.g., debris temperature. The production of hydrogen from steel-water reactions has been incorporated into these models in addition to the zirconium-water reaction previously available. Also included are the heating of the evolved gases by the debris beds and the effect of hydrogen flow on bed flooding.

A heat sink has been provided for the thermal radiation from the top of the core debris as calculated by the INTER subroutine. The decomposition of concrete due to radiated heat flux is treated by an ablation-type model with the resulting gases added to the containment atmosphere. Also, the geometry of the corium-concrete mixture is fixed following solidification of the melt.

5.1.1.7 Burning in Containment. The treatment of combustible gases now includes consideration of the burning of hydrogen and carbon monoxide if their concentrations exceed flammability limits. Included are explicit considerations of inerting due to high steam concentrations and oxygen depletion, direction-dependent criteria for flame propagation between compartments, and burn velocities as functions of composition. Various options are available to

explore the effects of assumptions about the burning of hydrogen and carbon monoxide.

5.1.2 Primary System Thermal Hydraulics: MERGE

When the MERGE[5.7] code was written, the existing computer codes describing the thermal-hydraulic behavior of a core meltdown accident were not capable of analyzing the flow and temperatures in the individual volumes of the reactor coolant system downstream of the core in the pathway for release to the containment. The report "Technical Bases for Estimating Fission Product Behavior During LWR Accidents"[5.8], published by the NRC in 1981, indicated that in at least some accident sequences, the retention of fission products in the reactor coolant system (RCS) could be significant. To support more realistic analyses of fission product retention with the TRAP-MELT code discussed in Section 5.3.1, an effort was undertaken to write a simple stand-alone code, MERGE, to predict gas temperature, surface temperature, and flow within the reactor coolant system.

MERGE calculations are based on the output of MARCH, and the output of MERGE is input to the TRAP-MELT code. The MARCH results used by MERGE are: the primary system pressure, the flow rate of hydrogen leaving the core, the flow rate of steam leaving the core, and the average temperature of gases leaving the core. The MERGE analysis accounts for conservation of energy and conservation of mass by species. It is assumed that the gases within a volume are well mixed and have the same temperature, and that the pressure differential between volumes is negligible.

In MERGE, the equations are solved with an explicit time difference scheme. At a particular time step, conditions within the first volume downstream of the core are calculated first, and the solution proceeds from each volume to the next downstream volume. Knowing the initial and inlet flow conditions for each volume, MERGE solves for the value of the outlet flow from the volume that yields the known pressure. Heat transfer from the flowing gas to structures is considered. Forced laminar, forced turbulent, and natural convection heat transfer coefficients are utilized as appropriate, with a radiative term added to the coefficient. In addition, the MERGE-calculated

radiative heat transfer from the core to the first structure is calculated based on a MARCH-calculated radiative flux.

The MERGE code involves certain approximations and limitations. In the MERGE analysis, the flow of gases in the upper plenum is assumed to be one-dimensional; in reality, circulation patterns would more probably be established in this region due to the strong temperature gradients. Whether a more detailed analysis is required for this region must be determined by the results of sensitivity studies with the TRAP-MELT code. The need for validation experiments must also be evaluated.

5.2 Radionuclide Release from Fuel

5.2.1 Source Within Pressure Vessel: CORSOR

CORSOR[5.9] is a simple correlative code which estimates aerosol and fission product release rates from the core during the period of core heatup and melting in a light water reactor. Quantifying the aerosol and fission product release from the core region is an important first step in determining the radionuclide source term to the containment during a hypothetical severe core damage accident. The timing of the release of various materials influences their retention in the reactor coolant system because it determines which species emanating from the core will be able to interact. The timing also determines the residence time of the released materials and the temperatures in the reactor coolant system, since these are both dynamic parameters. Simplistic source terms, such as constant or linearly increasing release rates with concurrent releases for all radionuclides, may therefore lead to unrealistic estimates of radionuclide transport behavior.

The analysis presented in this volume includes two changes in CORSOR in comparison with the analyses presented in previous volumes of this report. One is a slight refinement of the calculation of tellurium release from fuel. The other is a method for calculating aerosol release from silver-indium-cadmium control rods.

For the present analysis, the core has been divided into 240 nodes, 10 radial and 24 axial, which have distinct temperatures as predicted by MARCH. The core inventory, determined from the program ORIGEN[5.10], has been divided

equally among the nodes. In an actual reactor, the distribution would vary both axially and radially and would change with time. Typically, fuel is shifted between three radial zones during its irradiation history. To flatten the power distribution across the core, the freshest fuel is placed in the outside zone of the core and the most highly burned-up fuel is placed in the central region. Thus, an abrupt change in the spatial distribution of radionuclides occurs at the time of refueling but then continues to shift during the cycle as the fissile inventory is preferentially depleted in the regions of higher flux.

Alternative distributions of fission products can be used in the CORSOR program, and the effect on fission product release rates of the "flat-flux" assumption can be quantitatively assessed by examining the results of parametric studies such as those described in Appendix B of Volume 1[5.1]. Uncertainties in the release rate coefficients are expected to have a more significant effect on release rates than will the assumptions regarding fission product distribution among core regions.

Temperatures at each of the nodes are obtained from the MARCH code for each of a number of time steps, beginning at the start of the accident and continuing to a user-specified time. An average temperature is computed over each time span during core heatup and melting, and if the temperature is less than 900 C for any node, no release will occur from that node. The average temperature for failure of the cladding of a fuel rod is taken to be 900 C.[5.8] The sensitivity of CORSOR release estimates to the temperature set for cladding failure was also discussed in Appendix B of Volume 1.[5.1] When any axial position in a fuel bundle achieves a temperature of 900 C, CORSOR calculates a gap release of certain volatile fission products for all fuel rods in that radial zone. This is intended to simulate the gap release accompanying the bursting of individual fuel rods. This release occurs because certain fission products accumulate in the fuel-cladding gap because of migration within the fuel. The amount of the gap release is taken to be 5 percent of the initial amount present for cesium, 1.7 percent for iodine, 3 percent for the noble fission gases, 0.01 percent for tellurium and antimony, and 0.0001 percent for barium and strontium. Since this emission is very small in comparison with the melt release, and is concurrent with the melt release, it is not treated separately in any of the transport analyses. Clearly, the gap release would

require more careful analysis if less severe hypothetical accident conditions were considered.

Subsequent mass release as the nodes progress toward melting is calculated on a nodal basis as the product of the amount of each species remaining, the release rate coefficient, and the time interval of integration. The mass released is then summed over all the nodes in the core for each species to give the total mass released during the time step. It should be noted that the MARCH code predictions for core temperatures do not take into account the heat of vaporization of materials released from the core.

The computation of the fractional release rate coefficients for fission products is based on empirical correlations derived from experiments performed by Lorenz, Parker, Albrecht, and others.[5.11-5.17] The data from these experiments were graphed and curves developed of the releases. A fractional release rate coefficient, K(T), is derived for species by fitting an equation of the form

$$K(T) = Ae^{BT}$$

to each of these curves. The resulting values of A and B for three different temperature regions of the graph are basically the same as those defined in Appendix B of the "Technical Bases Report"[5.8] but have, in many cases, been adjusted to account for updated evaluations.[5.18] It should be noted that the fractional release rate is a function of temperature and elemental species only, and any effects of pressure and specific surface area of the melt on the release rate are not considered. Additionally, details of complex phase interactions of various components within the melting core are, for the most part, not known quantitatively; hence the release rates are valid only to the extent that the experiments upon which the release rates are based adequately modeled a core meltdown situation.

The release rate coefficients used in CORSOR in the analyses presented in this volume are similar to those presented in Volumes 1-3, except that the method for calculating tellurium release from the fuel elements has been refined. Tellurium release is dependent on the extent of oxidation of the zirconium cladding.

In the equation shown above, depending upon the local extent of zirconium oxidation, different A values are used. For a node where zirconium oxidation is nearly complete, one A value is used, and for a node at which

zirconium oxidation is less than some specified fraction, the A value is lowered by a factor of 40. For the two-side oxidation of zirconium fuel-rod cladding, the extent of oxidation used as the delimiter between higher and lower release rates is 0.70 in CORSOR. For one-side oxidation this figure would be 0.96-1.0. It is recognized that this is a simplistic treatment of a complex process, but it is believed to be the best representative of the limited available information.

Several uncertainties associated with the CORSOR predictions must be mentioned. These uncertainties most strongly impact the predicted release rates for aerosols, rather than for the more volatile materials. One difficulty in predicting aerosol release is that as core melting progresses, the temperatures increase throughout the core until, eventually, a loss of geometry would be expected to occur.

The behavior of the control rods during core melting is still a source of uncertainty with respect to aerosol generation, as it was in the first three volumes of this report. In this analysis, however, a physical model for the release of control rod materials has been adopted, based on the recommendations of ORNL. The calculations proceed as follows: silver-indium-cadmium control rods in a radial zone are assumed to fail when, at any axial node within the radial zone a temperature of 1400 C is reached. At this time, 0.05 of the silver, 0.05 of the indium, and 0.50 of the cadmium are released from the control rods. The masses of these species released increases linearly (regardless of heating rate) so that when the melting point (2300 C) is reached, 0.50 of the silver, 0.15 of the indium, and 0.80 of the cadmium has been released. For temperatures greater than 2300 C, the mass released increases linearly with temperature, so that at 2800 C the balance of the local inventory has been released from the rod. While this release model is physical, there is no adequate set of experimental observations against which its predictions can be objectively assessed.

5.2.2 Source from Melt-Concrete Interactions: VANESA

The release of fission products and nonradioactive aerosols during the interaction of molten core materials with concrete plays an important role in determining the risk of severe reactor accidents and is modeled with the

VANESA code. Aerosol production and fission product release from core debris outside the reactor vessel can persist for many hours. The aerosols produced in this way do not usually have to traverse a convoluted pathway before they enter the reactor containment as do aerosols produced in the reactor vessel. The increased inventory of aerosols in the reactor containment brought on by ex-vessel core-debris interactions could lead to rapid agglomeration and settling of the condensed fission products released during the in-vessel phases of an accident. If containment failure is delayed, the primary source of radioactivity released to the environment would come from ex-vessel sources.

Release of fission products from core-concrete interactions can compensate for any inhibition in the release of volatile species during the in-vessel phase of an accident because gases from the thermal decomposition of concrete sparge through the melt and drive the release processes. Ex-vessel processes can also lead to the release of fission product elements that are ordinarily quite refractory. This, again, is because of the strong driving force produced by gas sparging and the unusual melt chemistry that arises during ex-vessel interactions of core debris with concrete.

Also of importance is the generation of aerosols from nonradioactive materials, such as concrete and steel, during ex-vessel interactions. The additional concentrations of suspended particulates in the containment brought on by these aerosols naturally mitigate the inventory of radioactivity released from the fuel that would then be available for release to the environment. This additional material, on the other hand, poses yet another threat to equipment in the containment whose performance is degraded by the presence of aerosols.

VANESA is a mechanistic model of fission product release and aerosol generation during core-concrete interactions. This model was based on observation from experiments involving high-temperature melts on concrete and information from analogous industrial processes. Two broad mechanisms of aerosol formation are considered in the model:vaporization of melt species accentuated by gas sparging, and mechanical formation of aerosols by violent agitation of the molten debris sparged with decomposition gases. Vaporization processes produce the most intense aerosol generation during ex-vessel core debris interactions, while mechanical processes provide a mechanism for aerosol formation that persists even when debris temperatures are so low that little vaporization of species in the debris can occur.

Input to this model includes melt temperature, concrete erosion rate, and gas generation rate predicted by the CORCON model of melt-concrete interactions. It computes the thermochemical limits of vaporization from the melt, and then compares the extent of vaporization recognizing kinetic barriers, such as mass transport, to the approach to the thermochemical limits for vaporization. Mechanical aerosol generation is estimated by analogy to experimental data with simulant systems.

More complete descriptions of the model are provided in the users' manual[5.20] and its uncertainties are discussed further in Appendix C of Volume 1.[5.1]

5.3 Radionuclide Transport and Deposition

5.3.1 Transport in Reactor Coolant System: TRAP-MELT

The TRAP-MELT code that was used for the primary system radionuclide transport analyses of this study was based on the published TRAP-MELT code[5.21] used for the "Technical Bases" report[5.8]. Major changes were made in the treatment of aerosol particle transport and behavior and in radionuclide condensation on and evaporation from particles. In addition, the internal data base of the code was increased to include physical property data for tellurium and cesium hydroxide. An outline of the code, highlighting these changes, is given below. A more detailed description is given in the TRAP-MELT Users' Manual[5.21]

The TRAP-MELT model is designed to treat radionuclide transport in an arbitrary flow system whose thermal-hydraulic conditions are given as functions of time. For this study, the data needed by TRAP-MELT to define the thermal-hydraulic conditions of the primary system were generated by MERGE. In addition, TRAP-MELT requires the definition of source terms for each radionuclide; these terms were developed by CORSOR.

Once the flow system is defined, it is subdivided into a series of control volumes that can, in principle, be arbitrary in number and flow connections and that are chosen on the basis of characteristic geometry, thermal-hydraulic conditions, and suspected significant radionuclide behavior such as change of phase, agglomeration, or deposition. Radionuclides in each control volume are assigned, with uniform distribution, to one of two carriers: the

wall surfaces and the gas phase. Each radionuclide is allowed to reside on these carriers in either particulate (liquid or solid) or vapor form so that by combining carrier with form in the concept of "state", the condition of a radionuclide in a given control volume is completely determined by its state. TRAP-MELT thus considers five states:

- Radionuclide vapor carried by gas
- Radionuclide particle carried by gas
- Radionuclide vapor carried on wall surface
- Radionuclide particle carried on wall surface
- Radionuclide vapor reacted with wall surface.

This list of states is not exhaustive (for instance, in two-phase flow, the carrier water must be considered) and the logic of the code has been chosen to accept an arbitrary number of states readily .

Radionuclide transport can occur among the five states of an individual control volume or between certain states of different control volumes are connected by fluid flow. The former types of transport are modeled or correlated in the code itself. The latter are assumed to occur in phase with the fluid flow (as developed by codes such as MERGE) and are imposed on the system. Sources of radionuclides to the system may occur in any volume and any state, and they must be input to the code as mass rate functions of time.

At present, the intravolume transport mechanisms contained in TRAP-MELT are:

- Competitive condensation on, or evaporation from, wall surfaces and particles of cesium iodide, cesium hydroxide, and tellurium
- Irreversible reaction of molecular iodine, cesium hydroxide, and tellurium with stainless steel surfaces
- Particle deposition on surfaces due to
  - Settling
  - Diffusion from laminar and turbulent flow
  - Inertial impaction from turbulent flow
  - Thermophoresis.

Particle transport (and evaporation or condensation from or on particles) depends on particle size. TRAP-MELT takes this into account by considering a discretized particle size distribution that is subject to change, in each volume, by the deposition processes themselves, by possible particle sources, by flow of particles from other volumes, by flow of particles out of the volume

in question, and by agglomeration. The last can be due to many mechanisms. TRAP-MELT considers the following agglomeration mechanisms:

- Brownian
- Gravitational
- Turbulent (shear and inertial).

Considerations of stiffness and linearity split the system of first-order differential equations resulting from the above-listed transport mechanisms into three classes. Most of the deposition mechanisms (transfer from gas to wall surface) are taken as first order in the concentration of radionuclide species on the carrier (gas, particle, or wall) from which the transfer occurs. They constitute the first class, whose transport scheme can be written in the form:

$$\frac{dC}{dt} = S + MC, \tag{5.1}$$

where C is the concentration vector of the species in question for each state and volume, S is the source rate vector for each state and volume, and M is the transport matrix between all states and volumes. Because the deposition terms are taken as first order, M is independent of C and depends, with S, on time only. It is thus possible to solve Equation (5.1) as a set of first-order differential equations with constant coefficients by standard techniques. This is done in TRAP-MELT for the class of linear mechanisms. Condensation and evaporation, which have a much shorter time constant than the linear processes, constitute the second class and are treated outside this framework but parallel to it, as is particle agglomeration, which constitutes the third class of mechanisms in the TRAP-MELT code.

The approach to this parallel treatment is as follows: Equation (5.1) is taken as the master time-translation operation of the radionuclide system. Time steps are adjusted so that S and M change little over a time step and so that the time step does not exceed one-third of the smallest flow residence time for any control volume. The latter assures that the system does not translate excessively between couplings to the other two classes of mechanisms. In addition, the characteristic coagulation time for the aerosol in each volume is evaluated and compared to the master time step. If the former is short compared to the latter, the master time step is appropriately reduced.

At the beginning of each time step, phase transitions of radionuclides are modeled by examining each control volume in turn and solving the molecular mass transport equations for vapor transport among the gas phase, particles, and wall surfaces. Because of the low heats of vaporization of the radionuclides in question, this transport is assumed to be isothermal. Transfer to the walls assumes the Dittus-Boelter correlation[5.4] for pipe flow and transfer to the particles occurs by diffusion based on the size distribution at the beginning of the time step. Redistribution of the vapor phase occurs in a time that is small compared to the master time step; therefore, this redistribution is essentially decoupled from the other processes considered which justifies the use of a time parallel solution treatment.

Once redistribution of the vapor phase has been effected, its effect on the existing particle size distribution (in the volume in question) is calculated by assuming that each size class gains (or loses) mass in proportion to the rate of vapor transfer to (or from) that size class. Conservation of number for each size class then dictates redistribution between, in general, two new contiguous size classes, the number in each size class being determined by mass conservation.

At the end of a time step, the particle size distribution in each volume is reevaluated over that time step to account for possible particle agglomeration, sources, and flow terms. The agglomeration algorithm has been excerpted from the QUICK aerosol behavior code[5.22], which is based on a size discretization scheme.

The approximations inherent in this parallel treatment are minimized by relegating mass redistribution and conservation to the master Equation (5.1), except for redistribution due to radionuclide phase change. Agglomeration and particle evaporation/condensation serve only to modify the particle size distribution and therefore affect particle deposition indirectly through mass-distribution-averaged deposition velocities. Thus the aerosol aspect is solved (over a master time step) completely in parallel to Equation (5.1), using all sources, flow terms, and particle removal terms evaluated for each size class considered. The resultant distribution is used to evaluate average particle deposition terms for use in the master equation only. Similarly, reevaluation of the particle size distribution due to radionuclide phase change affects these average deposition terms only.

In addition to the time-dependent thermal-hydraulic conditions and mass input rates by species, the TRAP-MELT code requires input information on the initial particle size distribution of the source, the control volume geometry, and the physical properties of species (including deposition velocities on surface materials). The code provides output in terms of time- and location-dependent mass by species and state, as well as size distribution of suspended particulate material.

There are a number of uncertainties which affect the TRAP-MELT code predictions of primary system retention of materials. Any errors or imprecisions in the input to the code will clearly affect the quality of the results, both for the primary system thermal-hydraulics provided by MERGE and for the core release rates determined by CORSOR. The extent of interaction among the materials released from the melting core is determined largely by the timing of their releases, and this represents a less straightforward, but no less important, potential effect on the code's results due to input inaccuracies.

The experimentally determined vapor deposition velocities for Te, CsOH and I_2 on hot surfaces may not represent an accurate description of the process as it occurs in the reactor coolant system (RCS) because of the imprecision in the available data and because the experimental systems may differ from the actual RCS conditions. Nevertheless, what data are available have been incorporated, since these analyses are intended to reflect the state of the art. Additional uncertainties affecting vapor and aerosol deposition arise from possibly inadequate specifications of primary system geometry and flow patterns.

The disposition of materials suspended in the coolant system at the time of core slumping or at depressurization of the pressure vessel can have significant impact on retention calculated for some of the sequences analyzed. This is because some fission products and aerosols emitted from the core have not escaped the RCS at the time of core slumping and are still available for injection into the containment. The large burst of steam which accompanies core slumping or depressurization when the pressure vessel fails will rapidly sweep out the coolant system, and the very short transit time to the containment is expected to lead to minimal retention of these materials. Thus, in the analyses in this document, the material suspended in the RCS at the time of core slump or pressure vessel failure is assumed to be injected into the

containment as a "puff" release, with no further retention in the primary system.

The analyses in the main body of this document are subject to some uncertainties which may overpredict retention in the primary system. One mechanism not included in the current analysis is the structure heatup due to decay heat from the deposited fission products. Heatup of surfaces where species of intermediate volatility (e.g., CsI and CsOH) are deposited would lead to reevolution and transport of the previously deposited materials through the reactor coolant system to regions of lower surface temperature or to the containment. Thus, the deposition of these species may be self-limiting to some extent. This effect is analyzed in the Appendix to this volume.

5.3.2 Transport in Containment: NAUA 4

The NAUA code was developed at the Kernforschungszentrum Karlsruhe, West Germany, for calculating aerosol behavior in LWR core melt accidents.[5.24] It is based on mechanistic modeling of aerosol agglomeration and deposition within a containment vessel where a condensing steam atmosphere may exist. The model for steam condensation on particles was validated by small-scale experimental measurements[5.25], and larger-scale validation is being planned.

The NAUA code calculates physical processes, excluding chemical changes and radioactive decay. The removal processes considered include gravitational settling and diffusional plateout. Interactive processes include Brownian and gravitational agglomeration and steam condensation. Aerosol sources and leakage are also included. Compositional changes resulting from time-dependent compositions for the input aerosol are tracked by the code.

The particle size distribution is defined by a number of monodisperse fractions. In this approach, the governing integro-differential equation is transformed into a system of coupled first-order differential equations. In effect, the particle size fractions interact and deposit according to the included mechanisms, generating a time-dependent distribution of mass among the various size fractions. Steam condensation is handled in a separate integration. Output from the code includes mass concentrations of condensed water and dry aerosol materials (airborne and on surfaces), as well as particle size distributions at various times throughout the calculation.

Since the original version of the NAUA code has no provision for engineered safeguards, calculations were made to account for removal of aerosol particles by sprays, as follows:

$$\frac{dn}{dt} = -\varepsilon\pi R^2 N\,(V_g - v_g)n, \tag{5.2}$$

where

n is the aerosol particle concentration,

ε is the collision efficiency,

V_g and v_g are settling velocities of the spray drops and aerosol particles, respectively,

R is the radius of the spray drop, and

N is the water drop concentration.

Due to hydrodynamic interaction between a falling water drop and airborne particles, only a small fraction of the particles within the cross-sectional area of the water drop is removed by spraying. To account for this hydrodynamic effect, the collision mechanisms due to inertial impaction, interception, and Brownian diffusion of aerosol particles were used by defining ε in Equation (5.2) as:

$$\varepsilon = \varepsilon_I + \varepsilon_R + \varepsilon_D, \tag{5.3}$$

where ε_I, ε_R and ε_D are the collision efficiencies due to intertial impaction, interception, and Brownian diffusion, respectively. The following collision efficiency models were utilized for the three mechanisms:

$$\varepsilon_I = \frac{Stk^2}{(Stk + 0.35)2} \tag{5.4}$$

$$\varepsilon_R = \frac{1.5(r/R)^2}{(1+r/R)^{1/3}} \tag{5.5}$$

$$\varepsilon_D = 3.5\ Pe^{-2/3}, \tag{5.6}$$

where Stk is the Stokes number for aerosol particles based on a characteristic length of water drop with radius R; r is the particle radius; and Pe is the Peclet number. The Stokes number and the Peclet number are defined as

$$Stk = \frac{2 r^2 \rho_p V_g C}{9 \mu R} \text{ and} \qquad (5.7)$$

$$Pe = \frac{2 V_g R}{\bar{D}} \qquad (5.8)$$

where $\bar{D}$ is the diffusion coefficient of aerosol particle

v_g is the settling velocity of water drop

C is the Cunningham slip correction factor

ρ_p is the particle density

μ is the gas viscosity.

In general, for relatively large particles, the inertial effects on the overall collision efficiency are larger than the interception term because the water drops are much larger than the aerosol particles. As particle size becomes smaller, the Brownian diffusion term will become increasingly important. It should also be mentioned that Equation (5.4) is given by Hetsroni[5.26] and Equations (5.5) and (5.6) are based on the work of Lee and Gieseke[5.27, 5.28].

Another particle deposition mechanism, diffusiophoresis, was added to the NAUA code. Diffusiophoresis results from steam condensation onto containment walls and involves two mechanisms: a net flow of gas toward the wall surface (known as Stephan flow), and a molecular weight gradient caused by the steam concentration gradient. In general, the effects of Stephan flow are much larger than those of the molecular weight gradient and result in deposition of particles on the wall surface. The condensation rate toward wall surfaces calculated by the MARCH code has been used to calculate deposition due to diffusiophoresis.

In utilizing the NAUA computer code for calculating aerosol behavior during various accident sequences, it was noted that in certain cases the code requires a long computing time to calculate the rate of condensation of water vapor onto particles. This type of problem takes place when a large amount of condensible water vapor was used as an input. It was noted that a supersaturation ratio of much greater than 1.0 was frequently encountered even after the condensation calculation was completed.

Some literature suggests that pure water vapor at 20 C will spontaneously form water droplets in the absence of condensation nuclei when the

supersaturation ratio exceeds 3.5, and at 0 C a saturation ratio of 4.3 is required for homogeneous nucleation. This mechanism has been implemented in NAUA in addition to the existing condensation calculation. As the critical supersaturation for the homogeneous nucleation, the following correlation equation given by Green and Lane[5.29] was used:

$$S = \exp(0.557 \cdot (\sigma/T)^{3/2} \cdot M), \qquad (5.9)$$

where

S is the critical supersaturation

σ is surface tension

T is the temperature in °C

M is the molecular weight of water.

No nucleation or self-condensation rates are calculated in the code. Rather, if critical supersaturation is realized at a given time, the excess water vapor is assumed to form water particles of a uniform size spontaneously. Of course, these small pure water droplets are subsequently subject to NAUA's usual condensation and coagulation processes both among themselves and with other particles containing solids. Although the effects of this mechanism on the overall aerosol concentration change are insignificant, the computational time is reduced considerably by this implementation.

5.3.3 Transport in Containment: ICEDF

Particle removal in the Sequoyah ice compartments was predicted using another revised version of the NAUA 4 code; one which had been modified to include particle deposition mechanisms taken from the ICEDF code[5.]. The ICEDF code computes decontamination factors, DF's, as a function of time and particle size and a similar procedure was used except that the sedimentation deposition mechanism was not activated. For evaluating gas density, viscosity, and thermal properties, it was assumed that the flowing gas was air.

The mechanisms used in calculating DF's of the ice bed are as follow:

(1) Impaction and interception

$$K_I = V_I \cdot A_I \cdot E \tag{5.10}$$

where

V_I = gas velocity approaching the collector strips forming the ice baskets

A_I = projected area for impaction

E = impaction efficiency.

To include interception, E becomes

$$E = \frac{Stk^2}{(Stk + 0.5)^2} - 0.04 + 2\frac{d_p}{d_c}$$

where

d_p = particle diameter

d_c = the diameter of the collector

$$Stk = \frac{V_I \rho_p \cdot d_p^2 \cdot C}{9 \cdot \mu \cdot d_c \cdot \chi}$$

ρ_p = particle density

C = Cunningham correction factor

μ = viscosity of flowing gas

χ = dynamic shape factor of particles.

(2) Brownian diffusion

(i) for the surface of the strips,

$$K_{BD1} = V_I \cdot A_{BD} \cdot \varepsilon_{BD} \tag{5.11}$$

where

A_{BD} = projected area for diffusional deposition

ε_{BD} = diffusional capture efficiency

$$\varepsilon_{BD} = \frac{1}{Pe} + 1.727\frac{Re^{1/6}}{Pe^{2/3}}$$

$$Pe = \frac{d_c V_I}{D}$$

$$Re = \frac{\rho d_c V_I}{\mu}$$

D = particle diffusivity

ρ = gas density

(ii) for other parallel surfaces

$$K_{BD\Sigma} = \sum_i A_i K_i \tag{5.12}$$

where

$$\frac{K_i l}{D} = 0.13\,(Gr \cdot Sc)^{1/3}$$

$$Sc = \frac{\mu}{\rho D}$$

$$Gr = \frac{l^3 g}{(\mu/\rho)^2}\,\frac{\Delta\rho}{\rho}$$

l = length of surface in direction of flow

g = gravitational acceleration

$\Delta\rho$ = density difference in fluid-bulk compared to fluid at the surface.

(3) Diffusiophoresis

$$K_p = 0.9\,G_o\left(\frac{X_{2o}X_i}{X_{2i}} - X_o\right) \tag{5.13}$$

where

G_o = volume flow rate of gas at outlet of ice bed

X_{2o} = outlet mole fraction of air

X_{2i} = inlet mole fraction of air

X_o = outlet mole fraction of steam

X_i = inlet mole fraction of steam.

(4) Thermophoretic deposition

$$k_{th} = \frac{3}{2}\frac{\mu}{\rho}\,C\,\psi\cdot\frac{(A\,T_i - T_o)}{T_{AV}}\cdot\frac{G_o}{\alpha} \tag{5.14}$$

where

$$\psi = \frac{1}{1 + 3\,C_m\,Kn}\;\frac{\frac{kg}{kg} + C_t\,Kn}{1 + 2\,\frac{kg}{kp} + 2\,C_t \cdot Kn}$$

$$A = \rho_i\,G_i\,C_{p_i}/\rho_o\,G_o\,C_{p_o}$$

T_i = temperature of inlet gas

T_o = temperature of outlet gas

T_{AV} = average temperature of gas

α = thermal diffusivity of gas at outlet conditions

C_m, C_t = momentum and temperature accommodation coefficients

Kn = Knudsen number of the particle

kg/kp = ratio of the thermal conductivities of the gas and particle.

Integrating the above four mechanisms, DF is calculated as

$$DF = (1 + k_{th}/G_o)(1 + K_D/G_o)(1 + (K_I + K_{BD1} + K_{BD2})/G). \qquad (5.15)$$

References

(5.1) Gieseke, J. A., et al, "Radionuclide Release Under Specific LWR Accident Conditions, Volume 1", BMI-2104 (July, 1983).

(5.2) Gieseke, J. A., et al, "Radionuclide Release Under Specific LWR Accident Conditions, Volume 5", BMI-2104 (to be published).

(5.3) Wooton, R. O., et al, "MARCH 2 Code Description and Users' Manual", Draft (December, 1982).

(5.4) Wooton, R. O. and Avci, H. I., "MARCH (Meltdown Accident Response Characteristics) Code Description and Users' Manual", NUREG/CR-1711, BMI-2064 (October, 1980).

(5.5) "American National Standard for Decay Heat Power in Light Water Reactors", ANSI/ANS-5.1-1979.

(5.6) Geankoplis, C. J., "Mass Transport Phenomena", Holt, Rinehart, and Winston (1972).

(5.7) Freeman-Kelly, R., "A Users' Guide for MERGE", Battelle's Columbus Laboratories, October, 1982.

(5.8) "Technical Basis for Estimating Fission Product Behavior During LWR Accidents", NUREG-0772 (June, 1981).

(5.9) CORSOR Manual.

(5.10) Bell, M. J., "ORIGEN, The ORNL Isotope Generation and Depletion Code", ORNL-4628 (1973).

(5.11) Lorenz, R. A., et al, "Fission Product Release from Highly Irradiated LWR Fuel", NUREG/CR-0722 (1980).

(5.12) Lorenz, R. A., Collins, J. L., and Malinauskas, A. P., "Fission Product Source Terms for the LWR Loss-of-Coolant Accident", NUREG/CR-1288 (1980).

(5.13) Lorenz, R. A., et al, "Fission Product Release from Highly Irradiated LWR Fuel Heated to 1300-1600 C in Steam", NUREG/CR-1386 (1980).

(5.14) Lorenz, R. A., "Fission Product Release from BWR Fuel Under LOCA Conditions", NUREG/CR-1773 (1981).

(5.15) Parker, G. W., Martin, W. J., and Creek, G. E., "Effect of Time and Gas Velocity of Distribution of Fission Products from UO_2 Melted in a Tungsten Crucible in Helium", Nuclear Safety Program Semi-Annual Report for period ending June 30, 1963, ORNL-3483, 19-20 (1967).

(5.16) Albrecht, H., Matschoss, V., and Wild, H., "Experimental Investigation of Fission and Activation Product Release from LWR Fuel Rods at Temperatures Ranging from 1500-2800 C", proceedings of the Specialists' Meeting on the Behavior of Defected Zirconium Alloy Clad Ceramic Fuel in Water Cooled Reactors, 141-146 (September, 1979).

(5.17) Albrecht, H., Matschoss, V., and Wild, H., "Release of Fission and Activation Products During Light Water Reactor Core Meltdown", Nuclear Technology, 46, 559-565 (1979).

(5.18) Niemczyk, S. J. and McDowell-Boyer, L. M., "Technical Considerations Related to Interim Source Term Assumptions for Emergency Planning and Equipment Qualification", ORNL/TM-8275 (1982).

(5.19) Weast, Robert C., Ed., CRC Handbook of Chemistry and Physics, 59th Edition, (1978).

(5.20) VANESA Manual.

(5.21) Jordan, H., Gieseke, J. A., and Baybutt, P., "TRAP-MELT Users' Manual", NUREG/CR-0632, BMI-2017 (February, 1979).

(5.22) Jordan, H., Schumacher, P. M., and Gieseke, J. A., "QUICK Users' Manual", NUREG/CR-2105, BMI-2082 (April, 1981).

(5.23) Owczarski, P. C., Postma, A. K., and Schreck, R. I., "Technical Bases and Users' Manual for SPARC -- Suppression Pool Aerosol Removal Code", report to the U.S. NRC, NUREG/CR-3317 (May, 1983).

(5.24) Bunz, H., Koyro, M., and Schock, W., "A Code for Calculating Aerosol Behavior in LWR Core Melt Accidents Code Description and Users' Manual".

(5.25) Schock, W., Bunz, H., and Koyro, M., "Messungen der Wasserdampfkondensation an Aerosolen unter LWR-un-falltypischen Bedingungen", KfK 3153 (August, 1981).

(5.26) Hetsroni, G., "Handbook of Multiphase Systems", McGraw Hill Book Company and Hemisphere Pub. Co. (1982).

(5.27) Lee, K. W. and Gieseke, J. A., J. Aerosol Science, 11, 335 (1980).

(5.28) Lee, K. W. and Gieseke, J. A., Environ. Sci. & Technol., 13, 446 (1979).

(5.29) Green, H. L. and Lane, W. R., Particulate Clouds: Dust, Smokes and Mists, D. Van Nostrand Co., Princeton, New Jersey (1957).

6. BASES FOR TRANSPORT CALCULATIONS

6.1 Plant Modeling and Thermal Hydraulic Analyses

The MARCH 2 and MERGE codes were used to assess accident sequence progression and system thermal hydraulic conditions for each of the sequences considered. A summary of the reactor system characteristics, containment parameters, and MARCH modeling options is presented in Table 6.1.* Most of the data used to describe the plant were extracted from the Final Safety Analysis Report for Sequoyah Unit No. 1; the detailed description of the reactor vessel internals was provided by Westinghouse Electric Corporation. The latter are not presented because of their proprietary nature.

6.1.1 Sequence TMLB'

This sequence is characterized by the complete loss of all active engineered safety features. Reactor shutdown is followed by the boiloff of the steam generator secondary side water inventory. The loss of the steam generators heat sink leads to the heatup of the primary system and the increase of primary system pressure up to the pressurizer relief valve setting. The primary coolant is boiled off through the relief valve, leading to eventual core uncovery and melting. The timing of key events as predicted by MARCH is given in Table 6.2. Core and primary system conditions at key times during the sequence are given in Table 6.3. The temperature histories of selected core nodes as calculated by MARCH are given in Figure 6.1. In Figure 6.1 the notation ROD (X,Y) represents the core node at axial position X and radial region Y.

The flow path for fission product release from the primary system is illustrated in Figure 6.2. A schematic representation of the breakdown of control volumes used in the MERGE analysis is presented in Figure 6.3. The gas and structure temperatures of each control volume in the primary system as calculated by MERGE are given in Figures 6.4a-b. In the MERGE analyses Volume 2 represents the upper plenum of the reactor vessel; Structure 1 represents

*All tables in this section of the report have been placed at the end of the section.

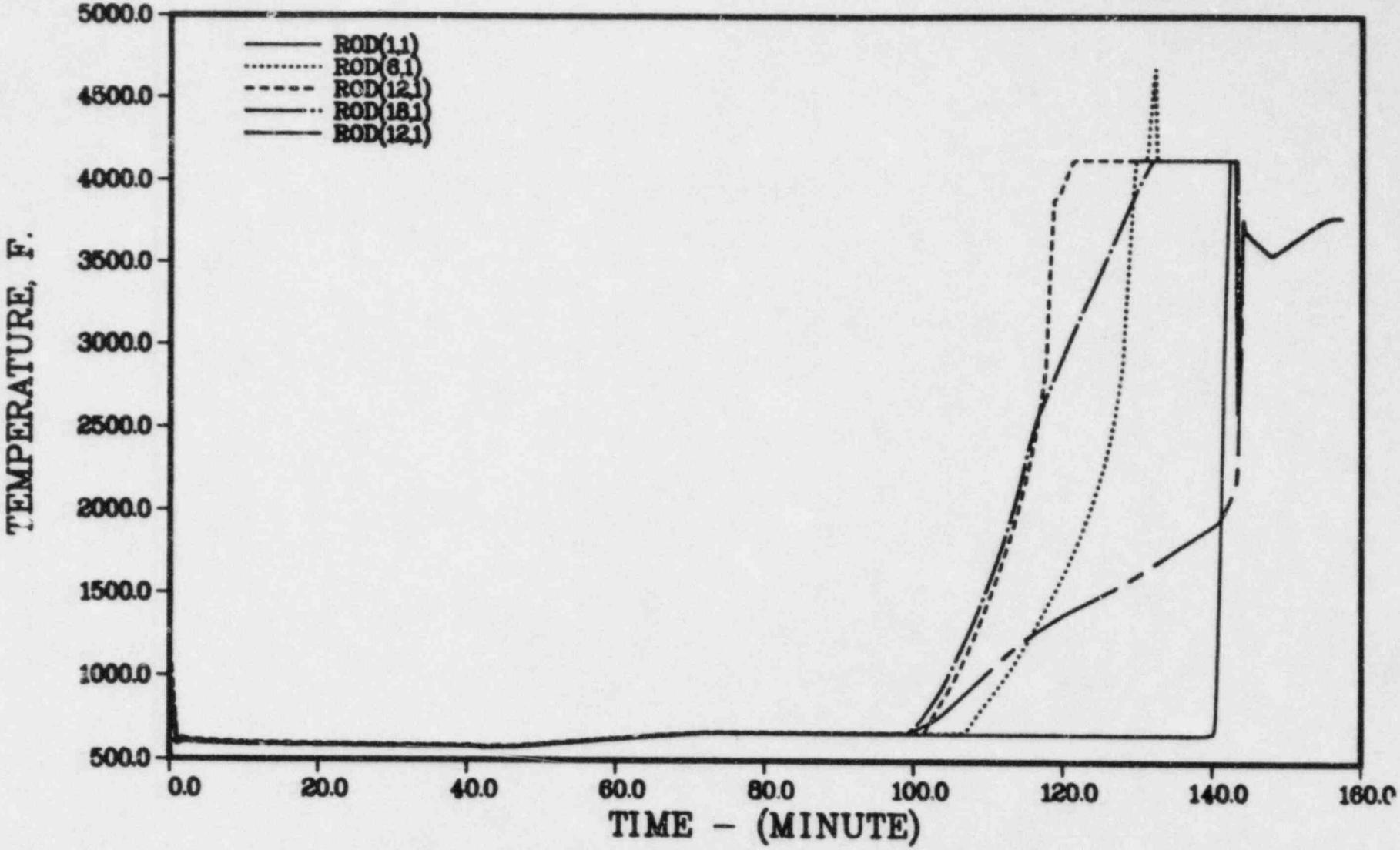

FIGURE 6.1a SELECTED CORE NODE TEMPERATURES FOR SEQUOYAH TMLB AND TML SEQUENCES

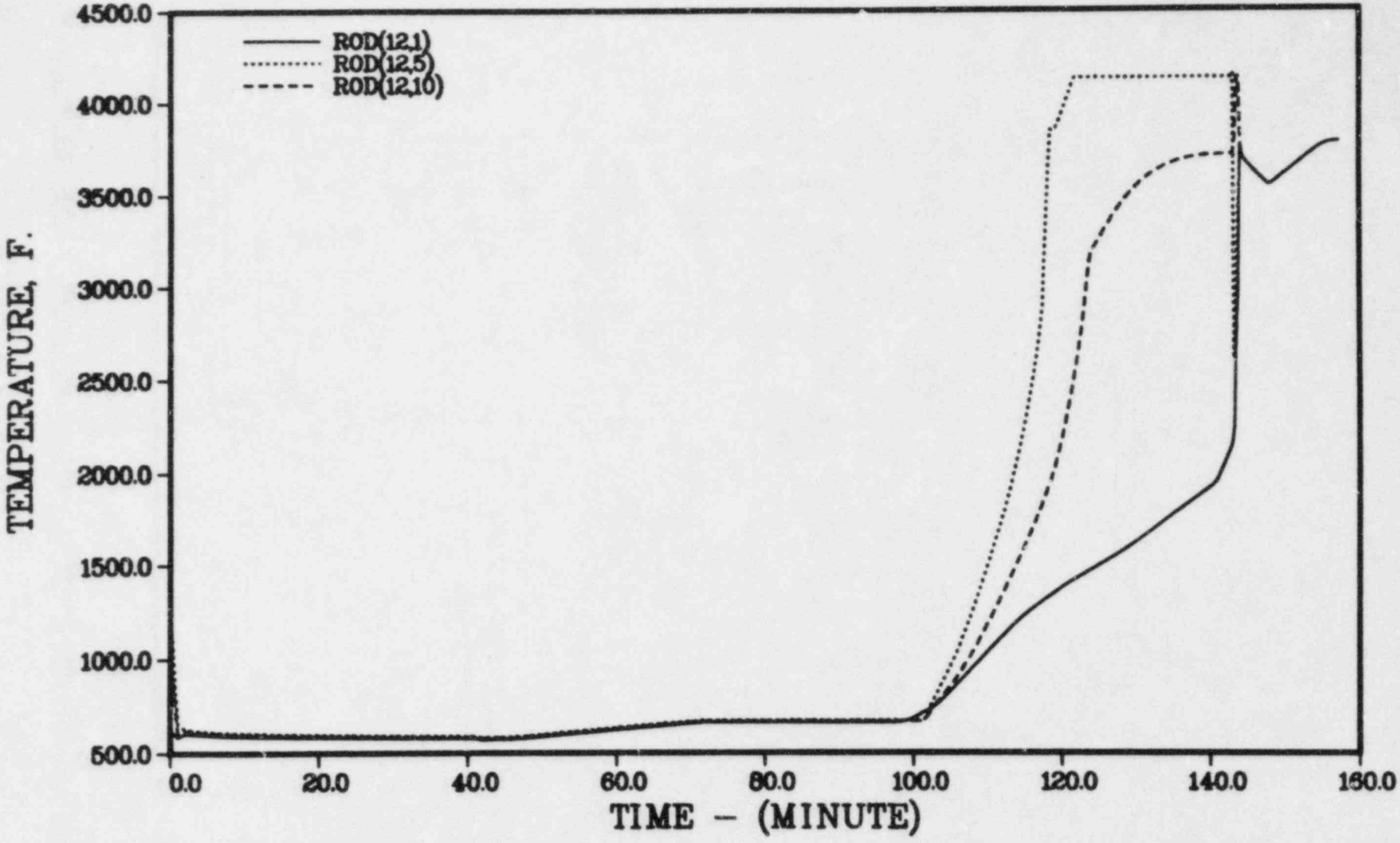

FIGURE 6.1b SELECTED CORE NODE TEMPERATURES FOR SEQUOYAH TMLB AND TML SEQUENCES

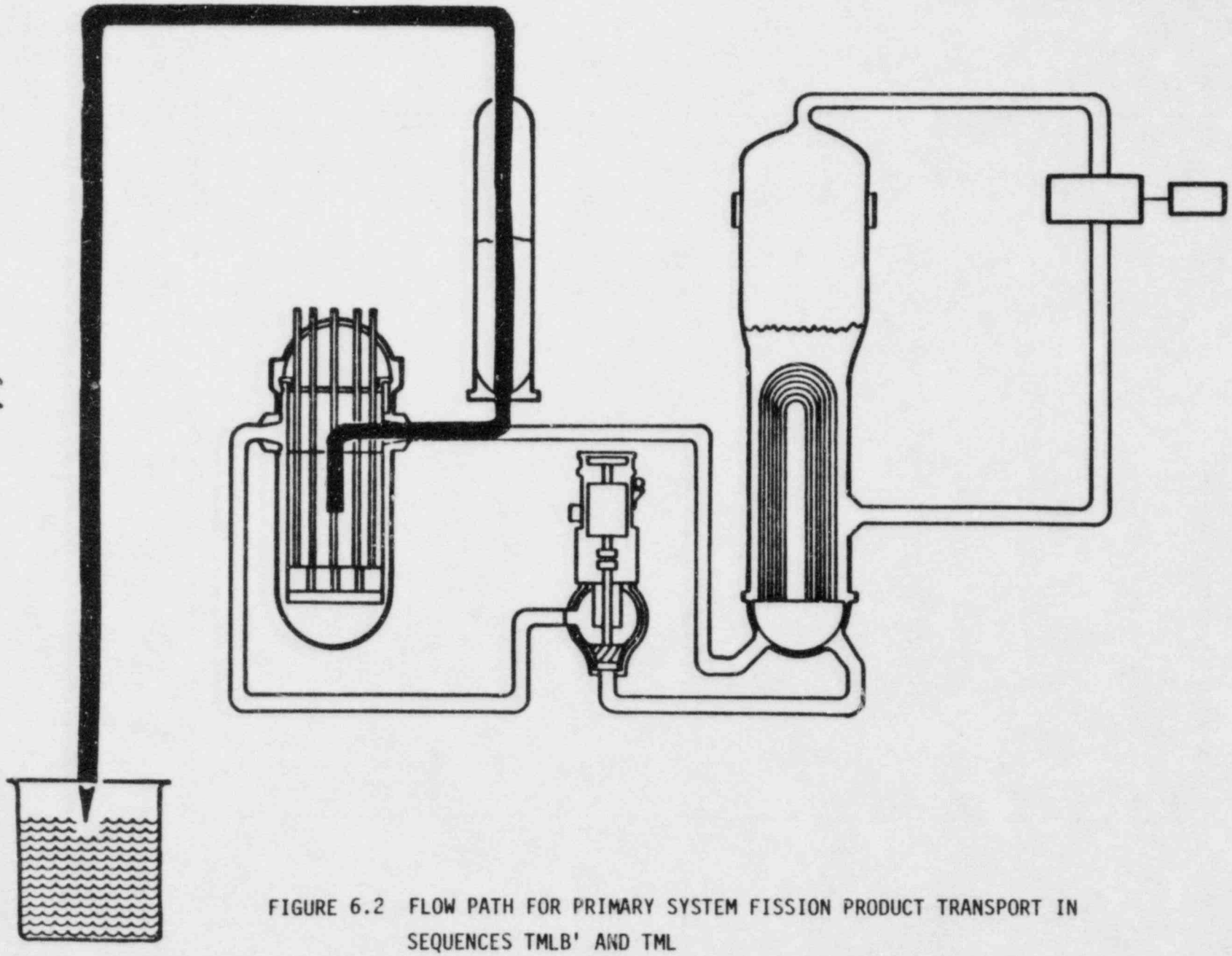

FIGURE 6.2 FLOW PATH FOR PRIMARY SYSTEM FISSION PRODUCT TRANSPORT IN SEQUENCES TMLB' AND TML

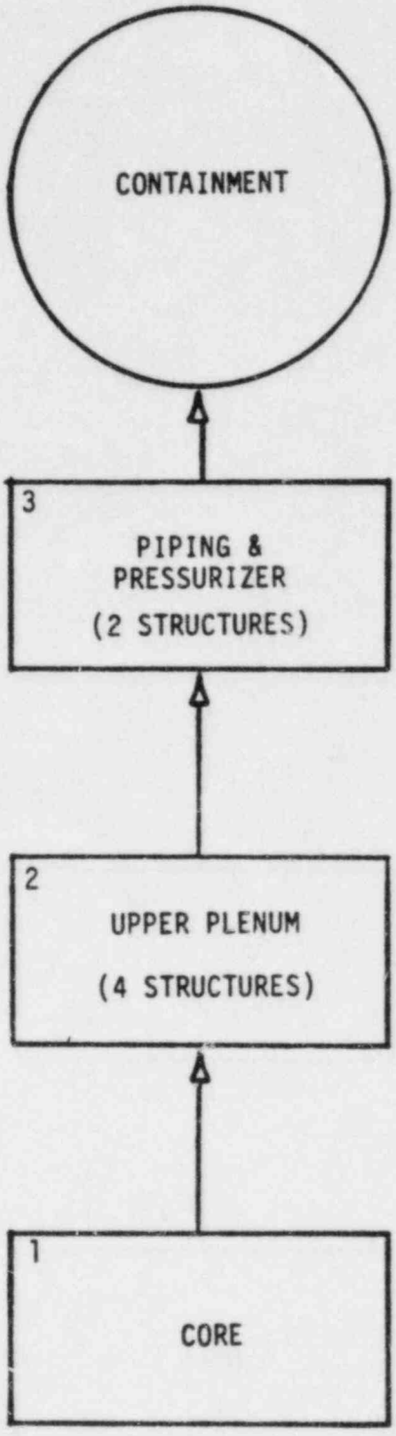

FIGURE 6.3 SCHEMATIC OF MERGE CONTROL VOLUMES FOR SEQUOYAH TMLB' AND TML SEQUENCES

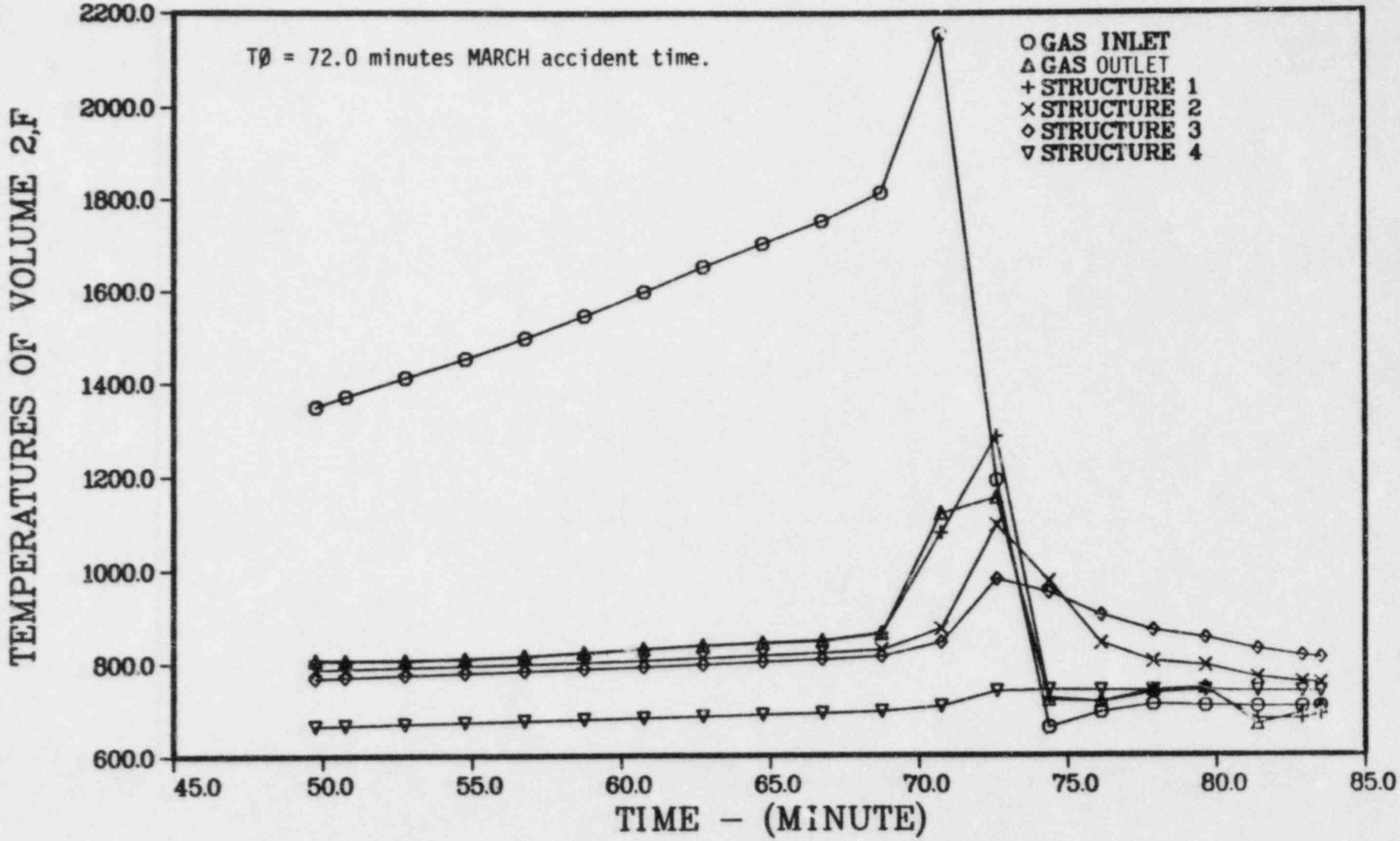

FIGURE 6.4a UPPER PLENUM GAS AND STRUCTURE TEMPERATURES FOR SEQUOYAH TMLB AND TML SEQUENCES

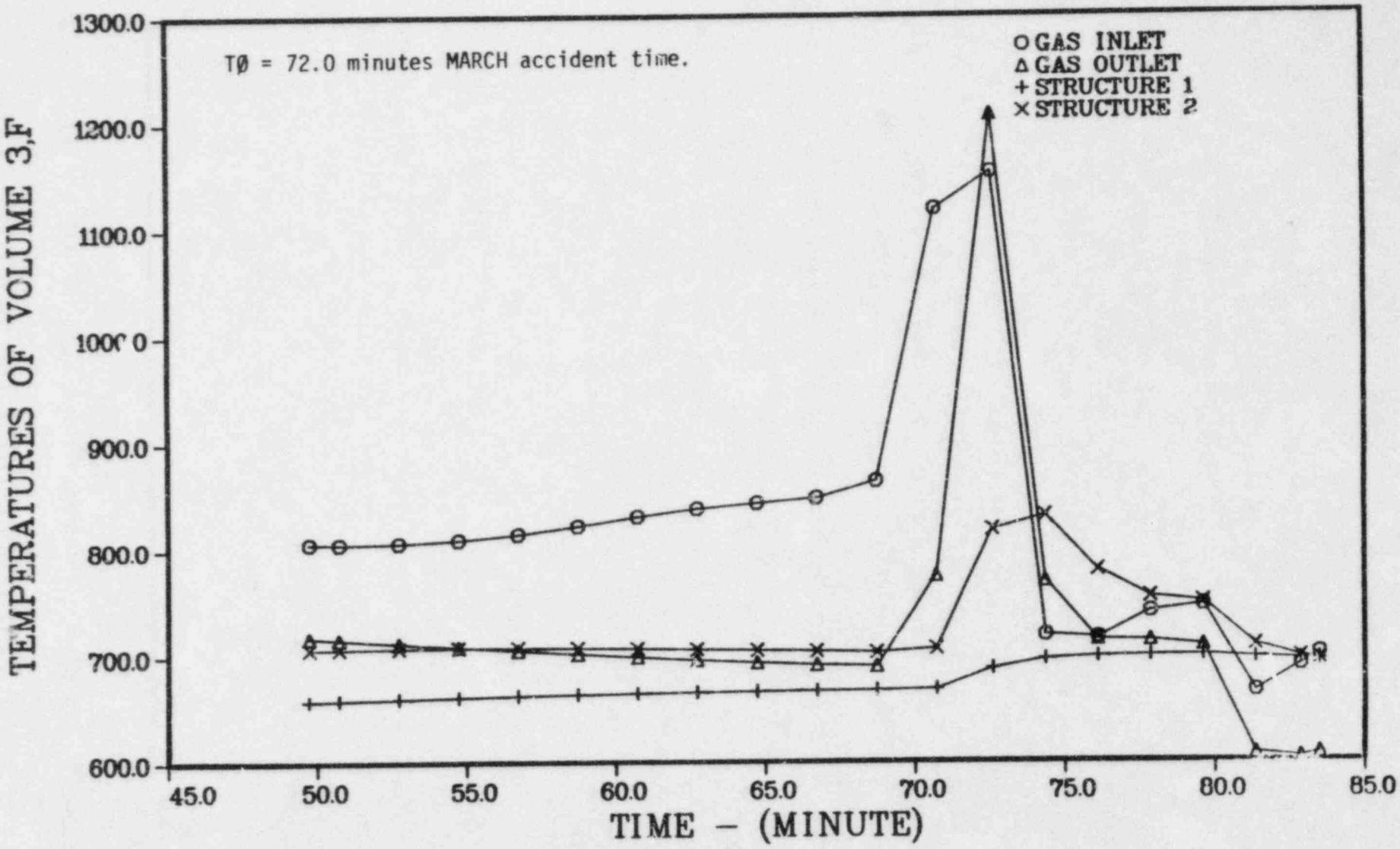

FIGURE 6.4b PRESSURIZER AND PIPING GAS AND STRUCTURE TEMPERATURES FOR SEQUOYAH TMLB AND TML SEQUENCES

the top core plate, Structure 2 represents the control rod guide tubes and support columns, Structure 3 is the upper support casting, and Structure 4 represents the core barrel. Volume 3 represents the pressurizer and piping, with Structure 1 being the pressurizer and Structure 2 being the piping.

The water, steam, hydrogen, and fission products released from the primary system enter the lower compartment of the containment. From there the gases, vapors, and airborne fission products may flow through the ice condenser and into the upper containment. Any radioactivity removed by the melting ice would wind up in the water in the containment sump. After containment failure the radioactivity in the upper compartment would be available for leakage to the environment. Figure 6.5 illustrates the fission product transport paths in the containment prior to failure; Figure 6.6 shows the paths after containment failure.

The MARCH modeling of the Sequoyah containment for the present analyses includes provision for sump water overflow into the reactor cavity if enough water accumulates on the containment floor. The volume of water on the floor before overflow into the cavity is 36,500 ft^3; the maximum volume of water in the cavity is 16,300 ft^3. These values were derived from the drawings in the FSAR for the Sequoyah plant. Just prior to the time of bottom head failure, the reactor cavity is predicted to be dry for the TMLB' sequence. Failure of the vessel bottom head leads to the discharge of the upper head injection and accumulator water into the reactor cavity. Continued melting of the ice will lead to overflow into and the eventual filling of the reactor cavity. The course of events following vessel bottom head will be dependent on the nature of the interaction between the core debris and the water in the reactor cavity. If the core debris fragment upon interaction with the water in the reactor cavity and form a coolable bed, a very long time would be required to evaporate all the water in the cavity. After the water is evaporated the debris would reheat and attack the concrete. If the fragmentation of the debris leads to an uncoolable bed, attack of the concrete would still take place even with water on top; in this case the overlaying water could provide significant fission product removal capability. However, in the absence of intervention to change the accident sequence, the water would eventually be evaporated with the possible reevolution of the previously trapped radioactivity. Whether or not the debris bed is predicted to be coolable is a function of the assumed particle size, bed porosity, area of the bed, and the condition

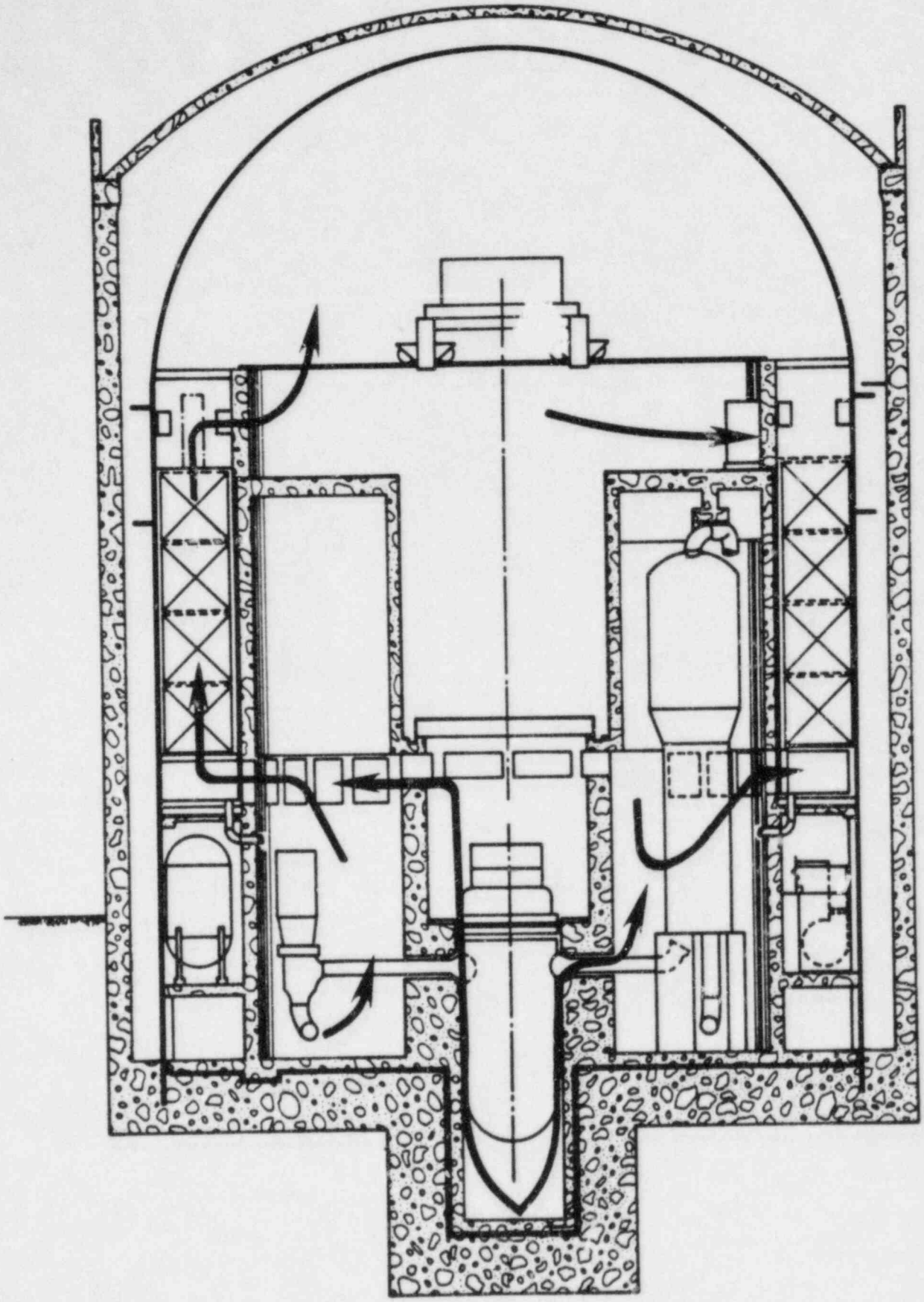

FIGURE 6.5. FISSION PRODUCT TRANSPORT PATHS BEFORE CONTAINMENT FAILURE

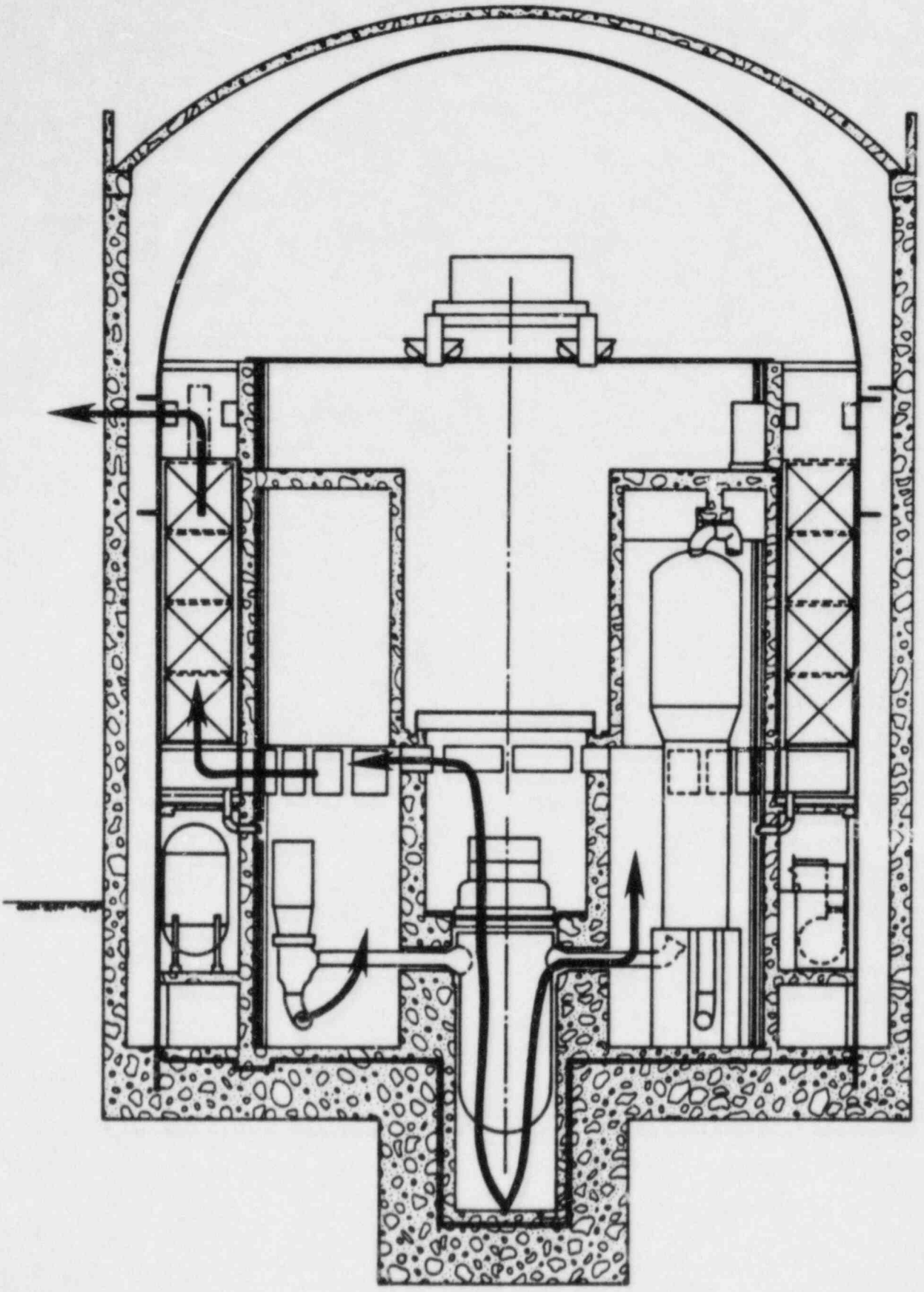

FIGURE 6.6. FISSION PRODUCT TRANSPORT PATHS AFTER CONTAINMENT FAILURE

(temperature) of the debris at the time of bed formation. The MARCH code permits the investigation of the effect of these variables, but there is little basis for specifying with any degree of confidence the actual conditions that could result. It is also possible that the debris could be ejected from the cavity as a result of the interaction with water. In such a case the debris would probably be quenched by the water in the containment. If the debris are ejected from the cavity, there is some likelihood of direct heating of the containment atmosphere by finely dispersed core debris. The possible effects of direct interaction between the core debris and the containment atmosphere have not been considered in this study.

The possible course of events could also be affected by assumptions regarding hydrogen burning. Prior to the time of vessel failure the containment atmosphere is predicted to be nonflammable in the present analyses. The failure of the bottom head results in the release of large quantities of steam and hydrogen to the lower compartment of the containment. Due to the high concentration of steam, the lower compartment atmosphere is not flammable. The effect of the ice condenser in removing steam from the gas flow leads to flammable conditions in the upper compartment shortly after head failure. In the TMLB' sequence the hydrogen igniters would not be operable; if, however, ignition takes place due to some other source, there could be significant likelihood of containment failure.

Within the scope of the present study it has not been possible to investigate in detail the many possible combinations of hydrogen burning and debris-water interaction events that can be postulated. For the purposes of the fission product analyses, two variations of the TMLB' sequence have been treated. In TMLB'-γ, hydrogen ignition is assumed when the containment atmosphere becomes flammable; the latter occurs shortly after the failure of the vessel head. The burning of the hydrogen is predicted to lead to containment failure. In the TMLB'-γ sequence the core debris are assumed to fragment upon interaction with the water in the reactor cavity, but the debris bed is not cooled effectively and heats up, leading to the attack of the concrete. It is recognized that another possibility would be a coolable bed which would delay the onset of concrete attack for this sequence. In the TMLB'-δ sequence ignition of the hydrogen is not assumed, but the fragmentation of the debris upon interaction with water in the cavity is assumed as in the previous case. In

the absence of hydrogen burning, but with the debris uncoolable, the containment is predicted to fail due to the buildup of noncondensibles.

Table 6.4 presents the containment conditions at key times during the accident sequence as calculated by MARCH for the two variations of the sequence discussed above. Figures 6.7 and 6.8 give the containment pressure and temperature histories for TMLB'-γ in which it was assumed that ignition of hydrogen took place following reactor vessel failure; this led in turn to the prediction of containment failure as a result of the burn. If the hydrogen does not burn, as is assumed in TMLB'-δ, the time of containment failure will be considerably different; Figures 6.9 and 6.10 illustrate the containment pressure and temperature histories for these assumptions.

It is noteworthy that the present analysis indicates that ice will be present through the time of core melting and after containment failure. The ice will contribute to fission product removal from the gas and vapor flowing through it. In these analyses it has been assumed that containment failure would not lead to bypass of the ice bed, e.g., by failure of the divider barrier between the upper and lower compartments in the containment.

The rate of ice depletion is proportional to the rate of steam flow through the ice condenser. The present analyses are based on the assumption that water will be forced out the pressurizer relief valve until the pressurizer surge line is uncovered; after that the flow out of the relief line is in the form of steam. These assumptions are consistent with the current understanding of expected behavior in such a transient. The flow of water out of the relief valve leads to earlier core uncovery than would be the case if all the water would have to be vaporized. Since only a part of this water will flash to steam upon release to the containment, a relatively low rate of ice depletion takes place during liquid flow out of the relief valve.

Table 6.5 summarizes the containment leak rate and flow information for the various cases as derived from the MARCH results and used in the evaluation of fission product behavior in and release from the containment.

6.1.2 Sequence TML

The TML sequence involves the loss of both normal and emergency means of adding water to the secondary side of the steam generators as well as the loss of primary system coolant makeup capability. As a result, the steam

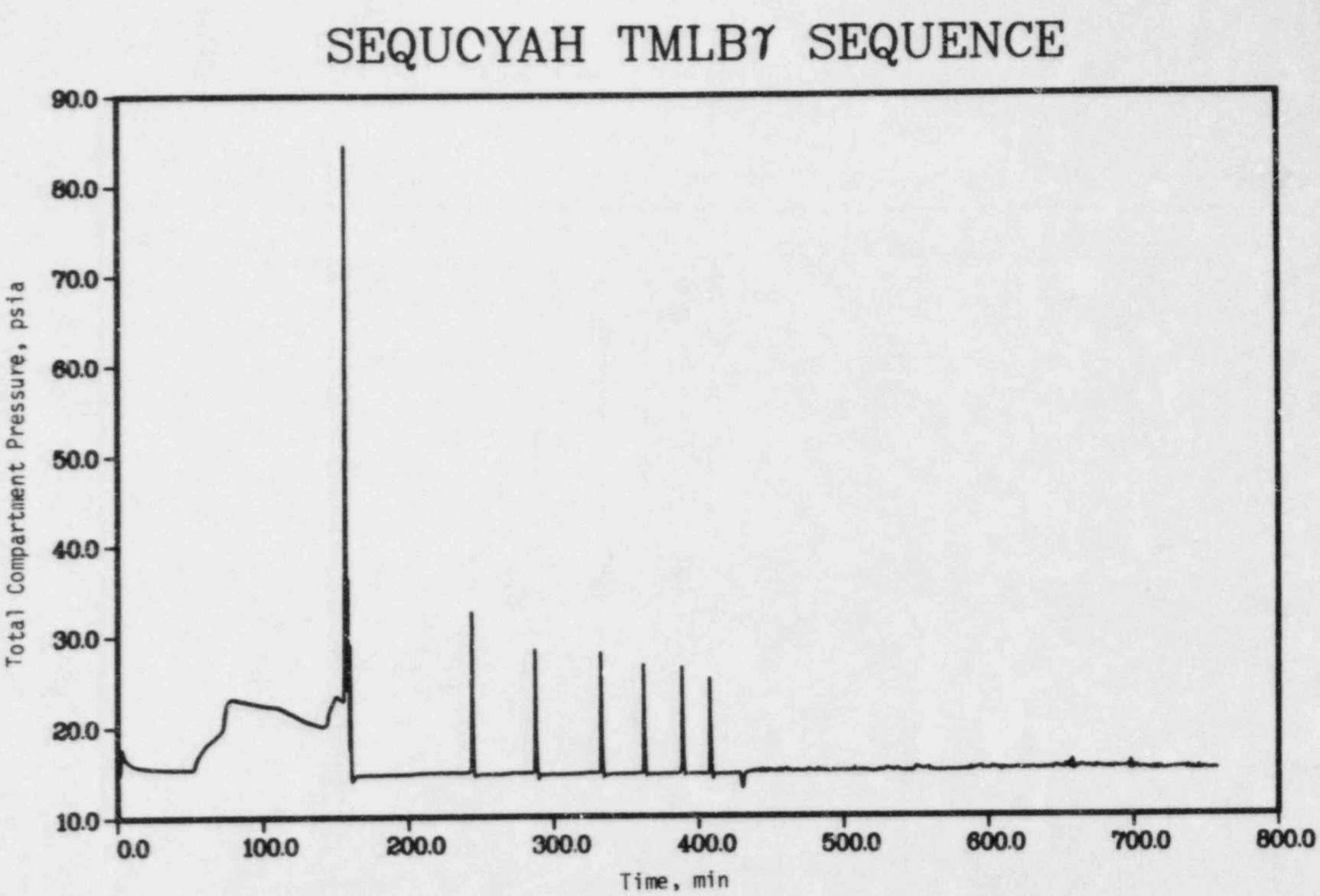

FIGURE 6.7 CONTAINMENT PRESSURE RESPONSE DURING SEQUOYAH TMLB'-γ SEQUENCE

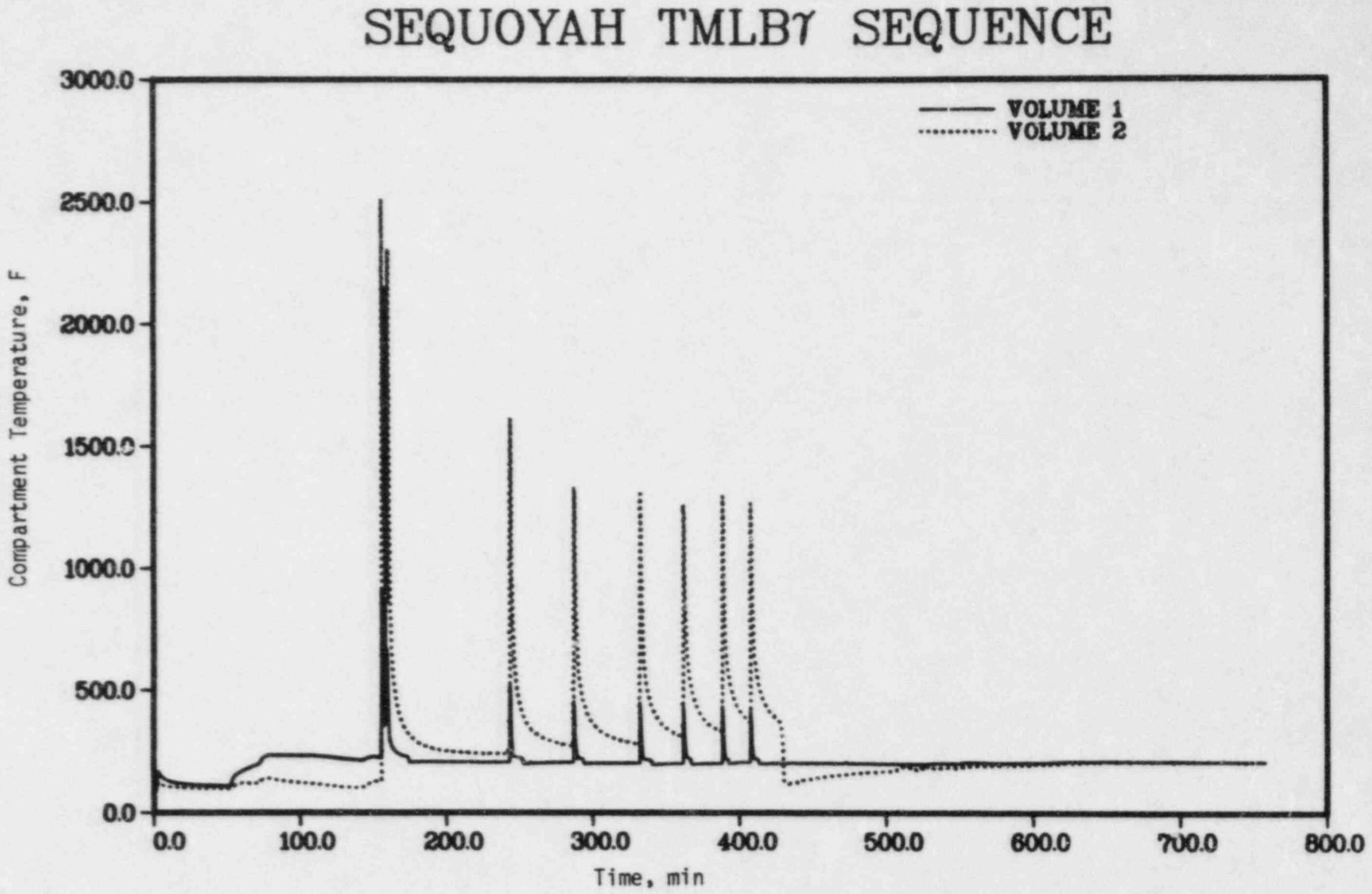

FIGURE 6.8 CONTAINMENT TEMPERATURE RESPONSE DURING SEQUOYAH TMLB'-Y SEQUENCE

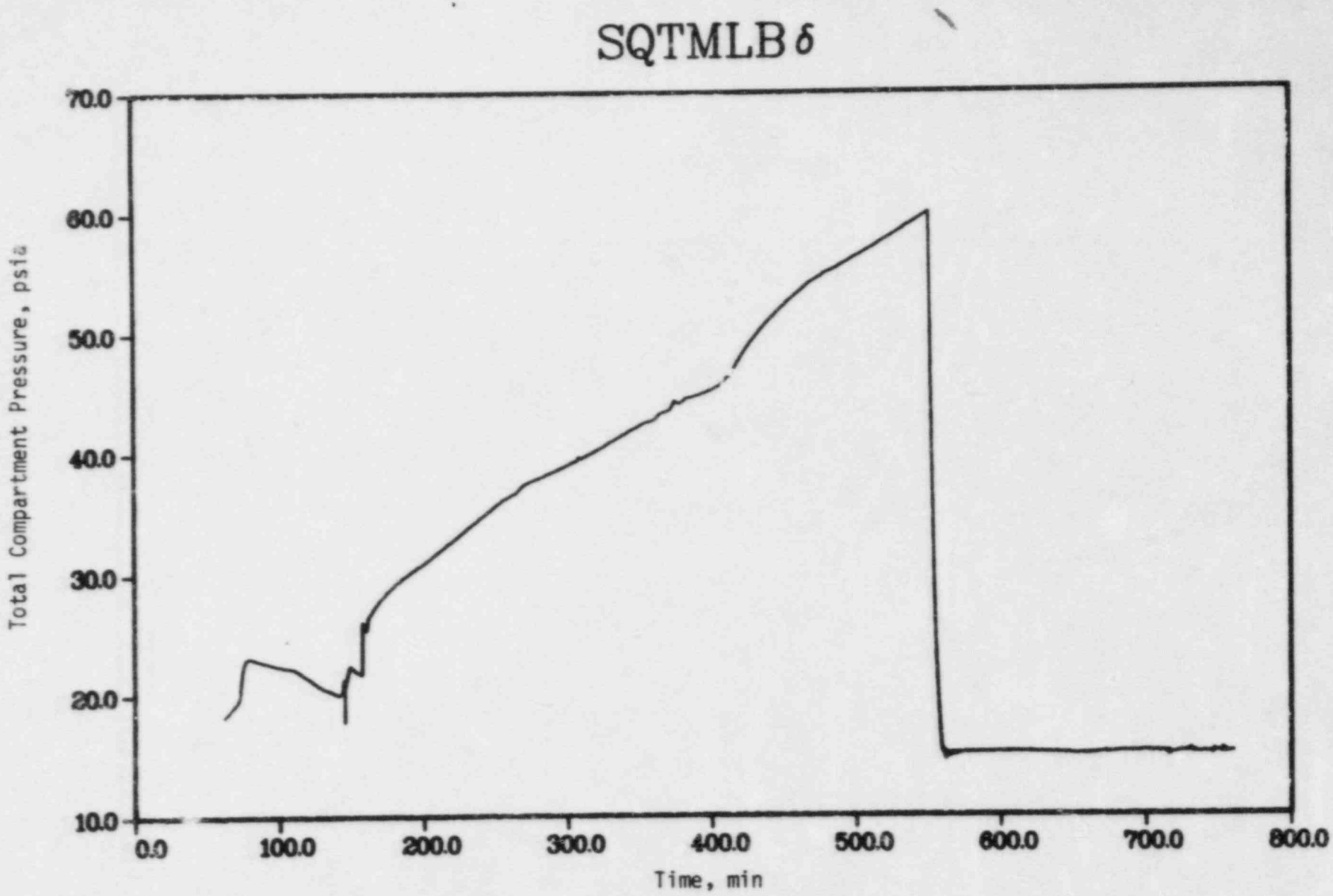

FIGURE 6.9 CONTAINMENT PRESSURE RESPONSE DURING SEQUOYAH TMLB'-δ SEQUENCE

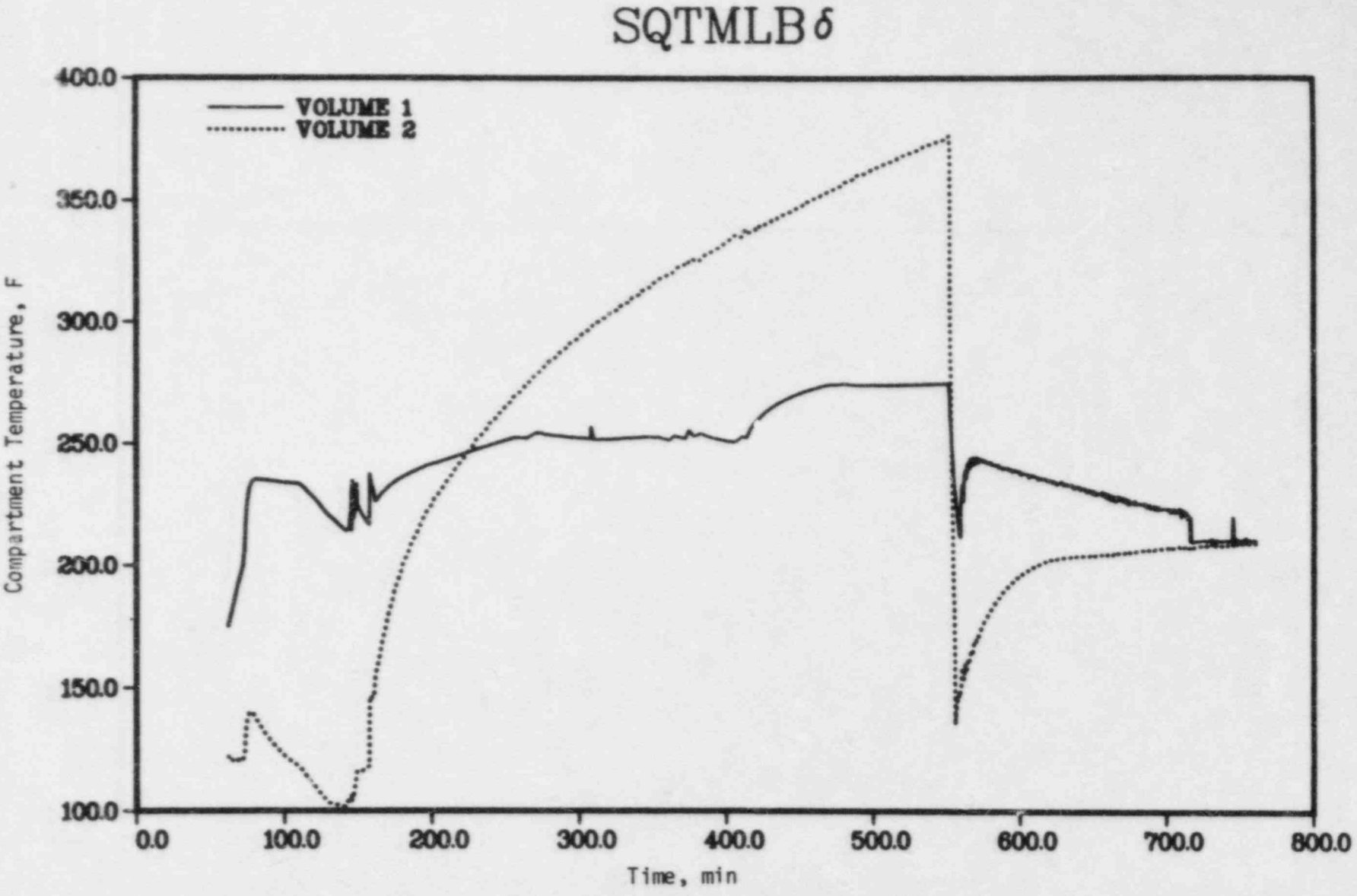

FIGURE 6.10 CONTAINMENT TEMPERATURE RESPONSE DURING SEQUOYAH TMLB'-δ SEQUENCE

generators would boil dry, the primary system pressure would rise to the pressurizer relief valve set point, and the primary coolant inventory would be boiled off, leading to eventual core melting. The primary system flow paths and response for this sequence would be identical to that for the TMLB' sequence discussed above.

In the TML sequence the active containment safety features, including air return fans, sprays, and hydrogen igniters, are available to mitigate the consequences of the accident. During the boiloff of the primary coolant and core melting phases of the accident, the containment pressures and temperatures are maintained at low levels, primarily due to the ice condenser and air return fans. Up to the time of reactor vessel bottom head failure the hydrogen concentrations in the containment remain below eight (8) volume percent hydrogen, the assumed hydrogen concentration for ignition. The failure of the bottom head leads to the release of the high pressure steam and hydrogen from the primary system into the lower compartment. The large amount of steam released at head failure is predicted to inert the lower compartment, but results in the prediction of hydrogen burning in the upper compartment. Such an upper compartment hydrogen burn would lead to a pressure above the assumed failure level of 60 psia under the modeling assumptions utilized in this study.

The evaluation of hydrogen burning, particularly in multivolume containments, can be sensitive to the ignition limits assumed, the rate of hydrogen release to the containment, containment compartmentalization, etc. In order to gain some insight on the sensitivity of the predicted pressures on containment compartmentalization and ignition limits assumed, a number of alternate MARCH calculations were performed as discussed below.

For the reference MARCH analyses discussed here, the ice condenser containment was modeled as a two compartment system with the ice condenser treated in the junction between the two compartments. The free volume associated with the ice condenser itself was included in the upper compartment. In the reference cases a threshold of eight (8) volume percent hydrogen was utilized for the start of burning by the hydrogen igniters. The latter is, of course, subject to the availability of oxygen and consideration of inerting by steam and carbon dioxide. Under the above assumption, a peak pressure of 66 psia was predicted for the TML sequence for a burn in the upper compartment which was predicted to take place after head failure. With the same compartmentalization but an assumed ignition threshold of six (6) volume percent

hydrogen, a peak pressure of 52 psia was predicted. It is interesting to note that with the lower threshold a smaller burn was predicted to take place just prior to head failure, followed by the larger burn leading to the 52 psia pressure.

Further MARCH runs were performed in which the containment was renodalized into four compartments. The lower part of the containment was broken up into a dead end volume and the main lower volume; the upper compartment was broken up in to the volume immediately above the operating floor and the volume of the hemispherical dome. With this type of compartmentalization and an ignition threshold of eight (8) volume percent hydrogen, peak hydrogen burn pressures of 48 psia predicted.

Additional runs were performed which explicitly modeled the upper plenum of the ice condenser, with the upper contai ment treated as a single volume and the lower volume broken up into two compartments as before. These runs gave peak pressures of 49 and 40 psia for ignition thresholds of eight (8) and six (6) volume percent hydrogen, respectively. It should be noted that the timing of the burns and the number of burns varied with the compartmentalization as well as ignition thresholds.

As was expected, the above calculations indicated that predicted peak pressures from hydrogen burning decreased with finer compartmentalization and lower ignition thresholds. Relatively high pressures were obtained in some cases because propagation of burning from one compartment to another was predicted for the set of assumptions utilized. In all the cases considered, peak pressures several times the nominal design pressure of the containment were predicted.

The failure of the vessel bottom head will release the core debris to the reactor cavity. As before, the subsequent course of events will be sensitive to the assumptions regarding debris water interactions. In the TML sequence the cavity would be full of water at the time of head failure, with water continuously resupplied due to the operation of the containment sprays. If the interaction of the debris with this water leads to the formation of a coolable bed, the accident would be effectively terminated at this point. If the debris are not coolable, attack of the concrete would ensue; however, the products of concrete decomposition as well as released activity would be scrubbed by the overlaying water pool. Attack of the concrete by the core debris could eventually lead to containment overpressurization due to the

buildup of noncondensibles. It is possible also that melt-through of the basemat could precede containment overpressure failure.

From the above it is clear that a wide variety of outcomes are possible for the TML sequence, depending on the actual course of hydrogen burning and the behavior of the debris in the reactor cavity. For purposes of the fission product release and transport analyses, two variations of the TML sequence were selected; these are described below. In the TML-γ sequence the failure of the reactor vessel bottom head is followed by a hydrogen burn which leads to early containment failure. No representation is made as to the likelihood of such a failure. Based on the analyses that have been performed, as described above, the possibility of significant containment pressurization as a result of such burns cannot be dismissed. The core and structural debris that enter the reactor cavity will encounter a large quantity of cold water, with water being continually added to the cavity. In the TML-γ sequence a coolable debris bed has been assumed to form, thus precluding further evolution of fission products. In the TML-δ sequence the containment is assumed to accommodate the series of hydrogen burns that take place. The debris entering the reactor cavity are not coolable and attack the concrete basemat leading to the eventual overpressurization of the containment from the buildup of the noncondensibles. It is also possible that melt-through of the basemat could take place prior to containment overpressurization. The continued attack of the concrete in the presence of a large overlaying pool of water would imply that the debris do not break up but remain in a slab-type configuration. If the containment successfully accommodates the series of hydrogen burns initiated by the igniters and if the debris fragment in the reactor cavity to form a coolable configuration, this accident sequence would be terminated without containment failure.

Table 6.4 gives the containment conditions at key times during the accident sequence for the two variations of the TML sequence. Figures 6.11 and 6.12 give the containment pressure and temperature histories for TML-γ; Figures 6.13 and 6.14 give the corresponding histories for TML-δ.

Table 6.5 summarizes the containment flows and leakages derived from the MARCH results that were used in the calculations of fission product behavior in and leakage from the containment.

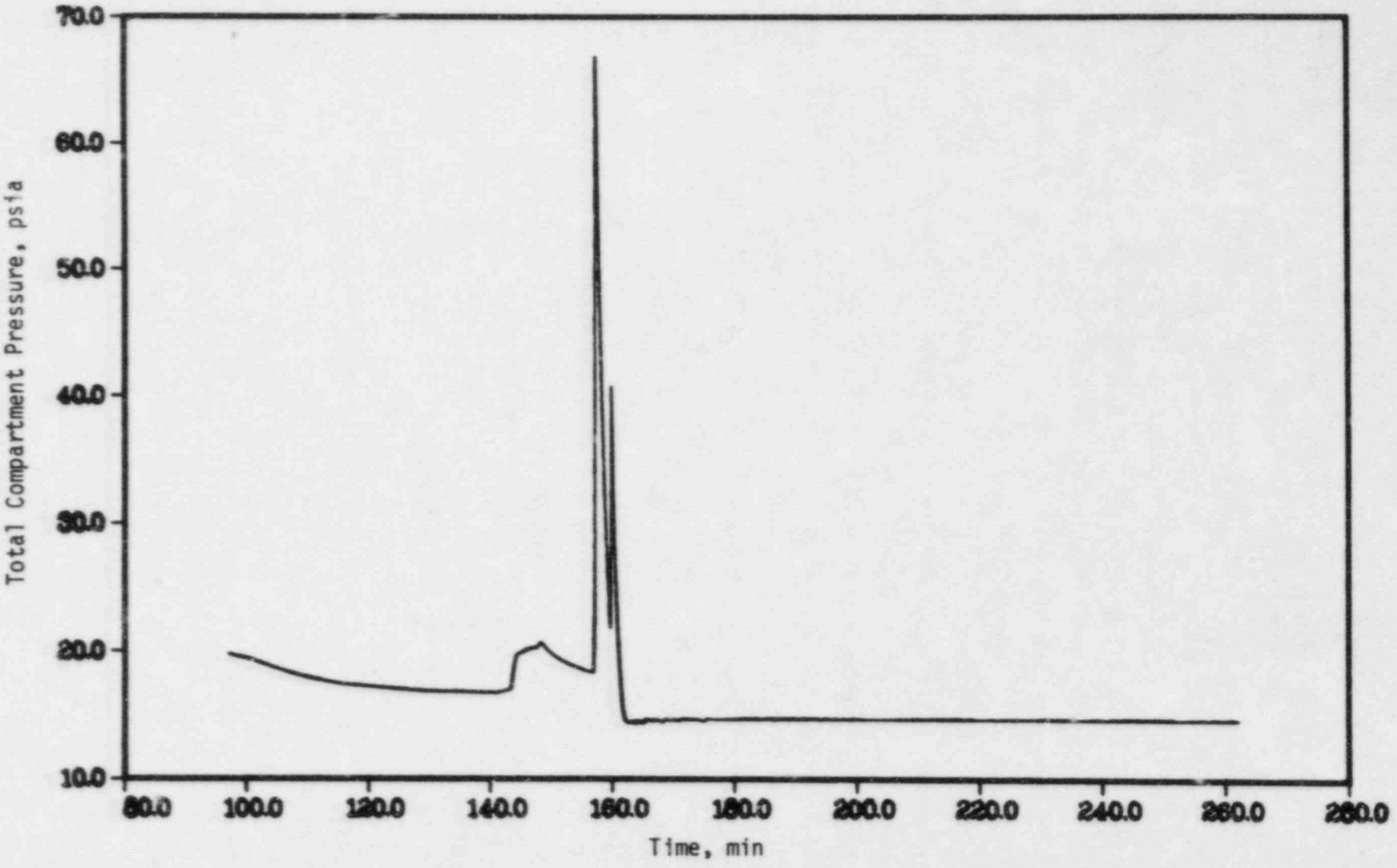

FIGURE 6.11. CONTAINMENT PRESSURE RESPONSE DURING SEQUOYAH SEQUENCE TML -Y

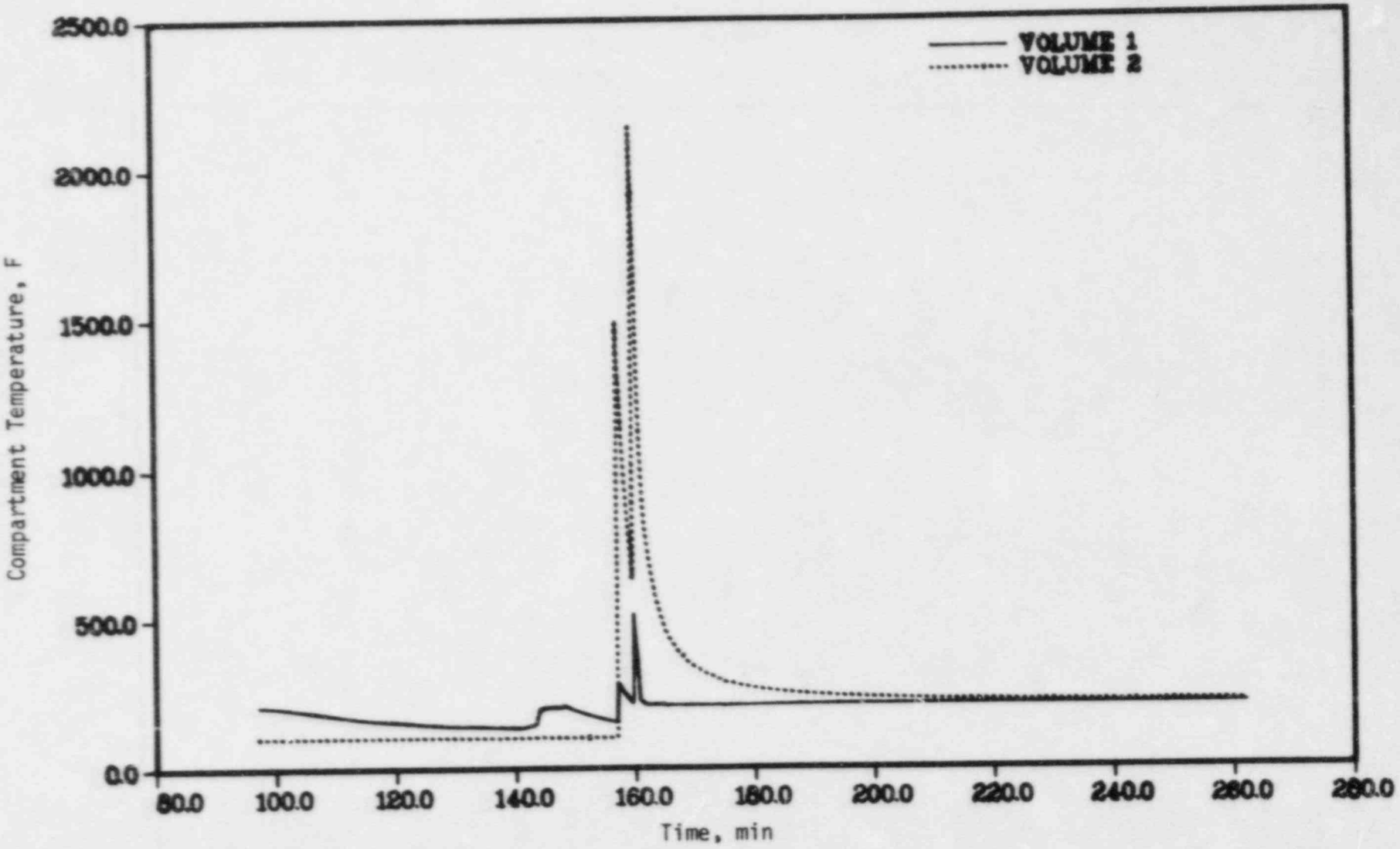

FIGURE 6.12. CONTAINMENT TEMPERATURE RESPONSE DURING SEQUOYAH SEQUENCE TML

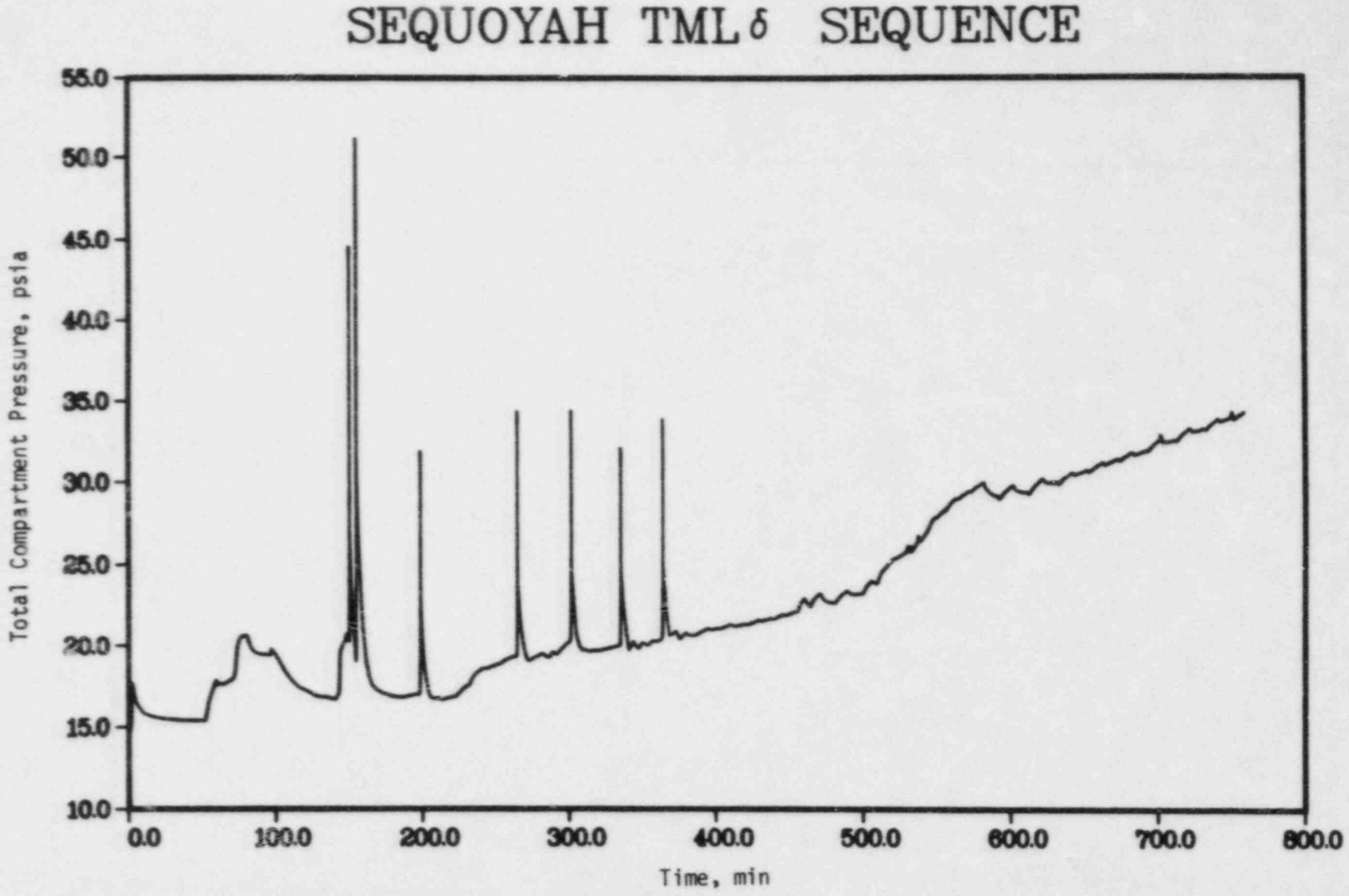

FIGURE 6.13 CONTAINMENT PRESSURE RESPONSE DURING SEQUOYAH TML-δ SEQUENCE

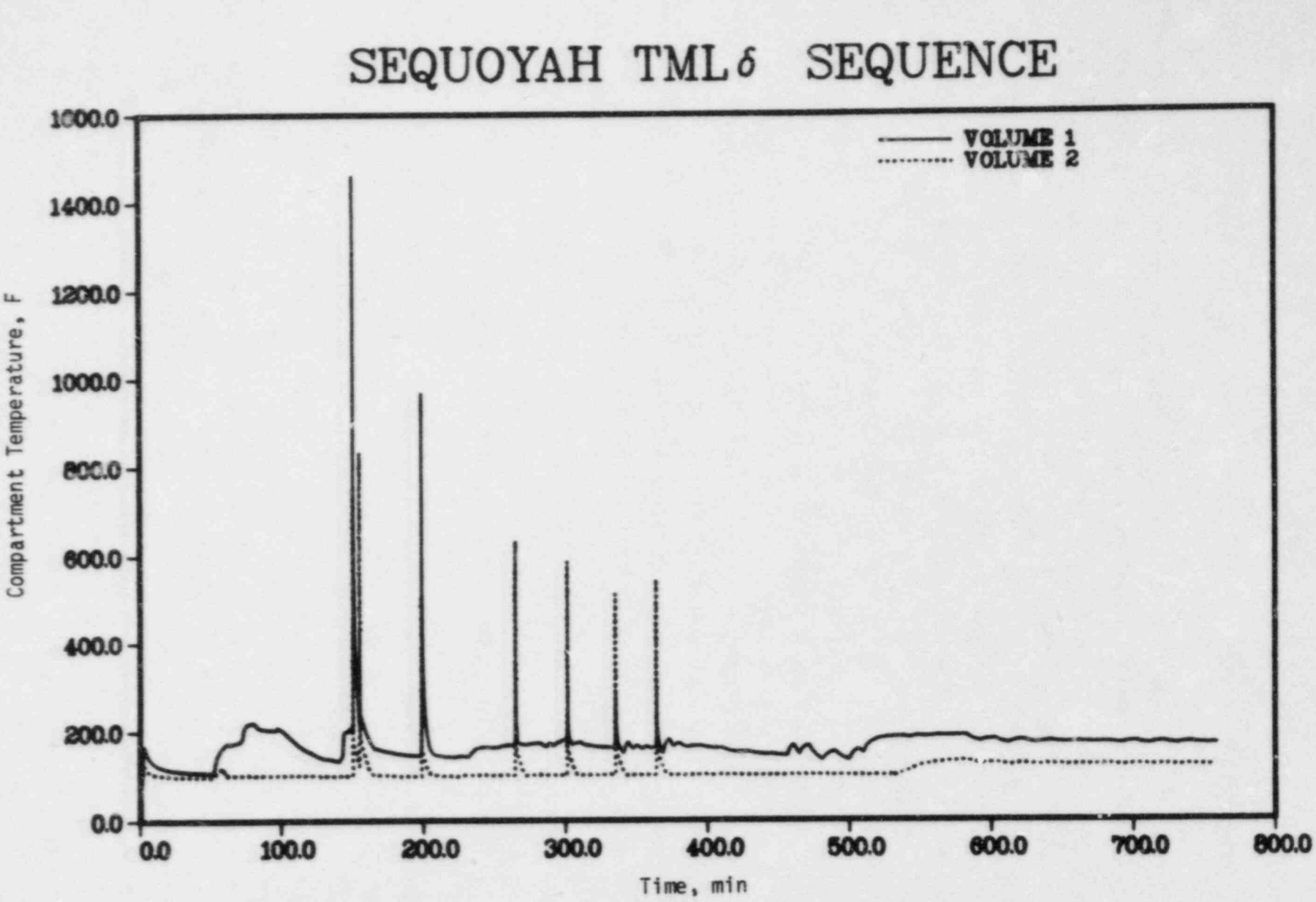

FIGURE 6.14 CONTAINMENT TEMPERATURE RESPONSE DURING SEQUOYAH TML-δ SEQUENCE

6.1.3 Sequence S_2HF

The S_2HF sequence is initiated by a small break in the primary system with all engineered safety systems operating initially. As discussed previously, the emergency core cooling system and the containment spray system both fail in the recirculation mode due to a common cause in this sequence. At the time of the emergency core cooling system failure, the core is water covered and well cooled; continued depressurization and boiloff of the water leads to core uncovery and melting. The timing of the key events for the S_2HF sequence as predicted by the MARCH code is given in Table 6.2. Core and primary system conditions at key times during the sequence are given in Table 6.3. The temperature histories of selected core nodes are illustrated in Figure 6.15.

Figure 6.16 illustrates the fission product flow path within the primary system for this sequence. A schematic representation of the breakdown of the control volumes used in the MERGE analysis is shown in Figure 6.17. The gas and structure temperatures of each control volume in the primary system as calculated by MERGE are given in Figure 6.18a-c. In the MERGE analyses Volume 2 represents the upper plenum of the reactor vessel; Structure 1 is the top core plate, Structure 2 represents the control rod guide tubes and support columns, Structure 3 is the upper support casting, and Structure 4 represents the core barrel. Volume 3 represents the hot leg piping with a single structure. Volume 4 represents the steam generator with a single structure.

At the time of core uncovery and melting in the S_2HF sequence as considered here the containment sprays have failed, but the air return fans and hydrogen igniters are available. The ice has melted at about the time that the core starts to melt; thus natural deposition within the containment is the principal mechanism for fission product attenuation. The hydrogen released to the containment during core melting undergoes a series of relatively small burns due to the action of the igniters, with resulting pressures below the assumed failure level. Following vessel failure and after some attack of the concrete basemat by the hot debris, a burn is initiated in the lower compartment which propagates into the upper compartment. The resulting pressure exceeds the failure level. This burn includes substantial combustion of carbon monoxide as well as hydrogen. The carbon monoxide is produced by the decomposition of concrete by the core debris.

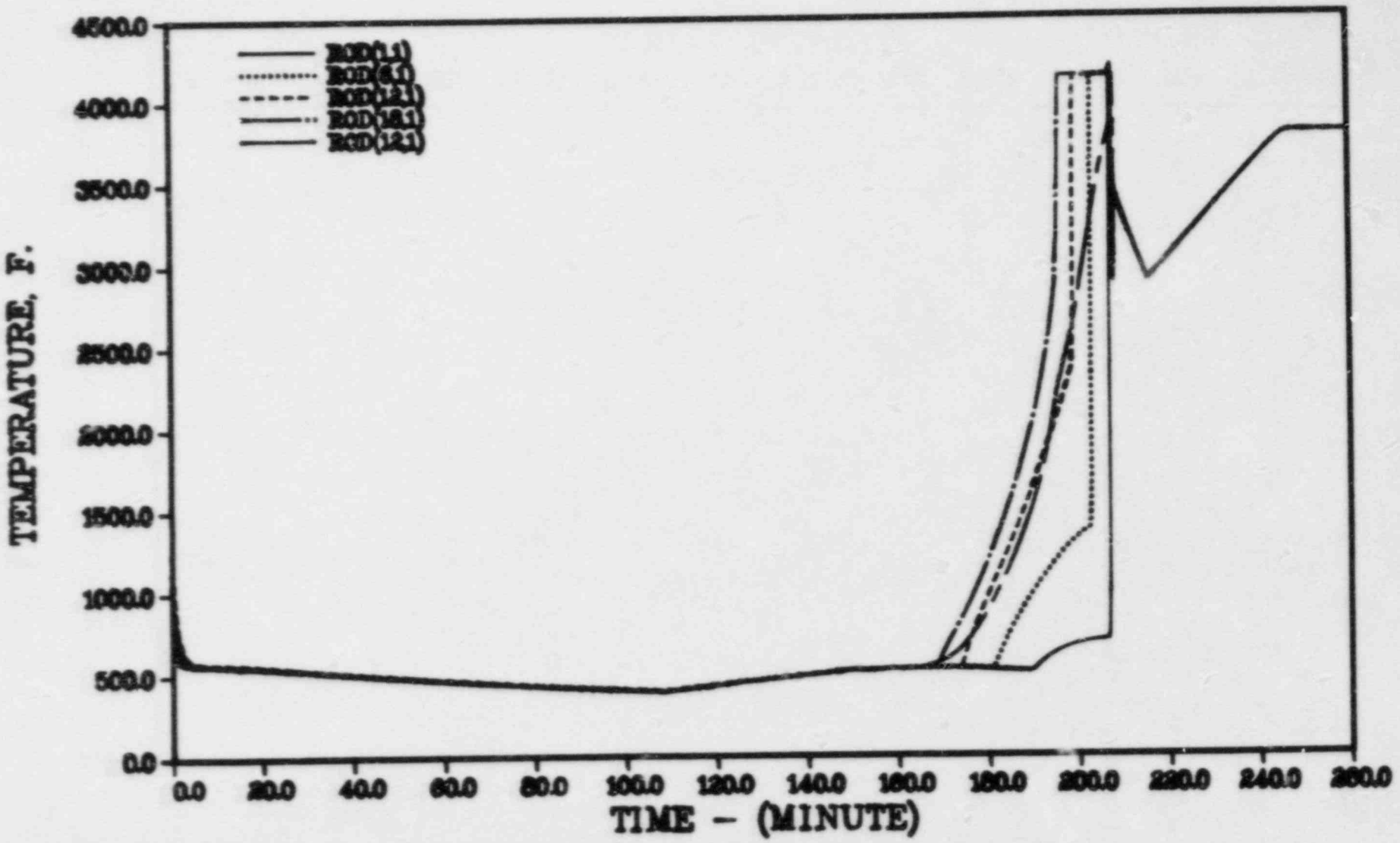

FIGURE 6.15a SELECTED CORE NODE TEMPERATURES FOR SEQUOYAH S_2HF SEQUENCE

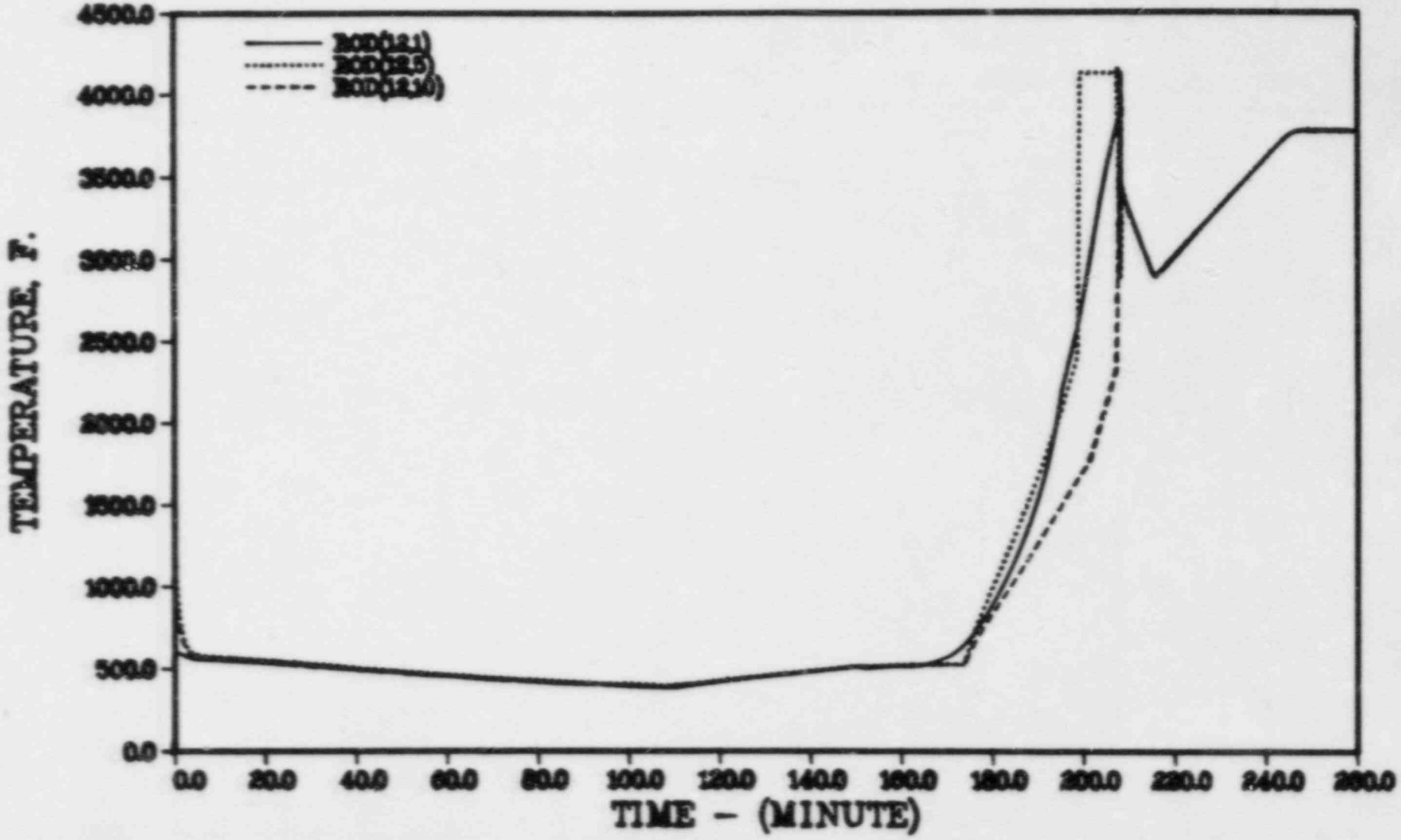

FIGURE 6.15b SELECTED CORE NODE TEMPERATURES FOR SEQUOYAH S_2HF SEQUENCE

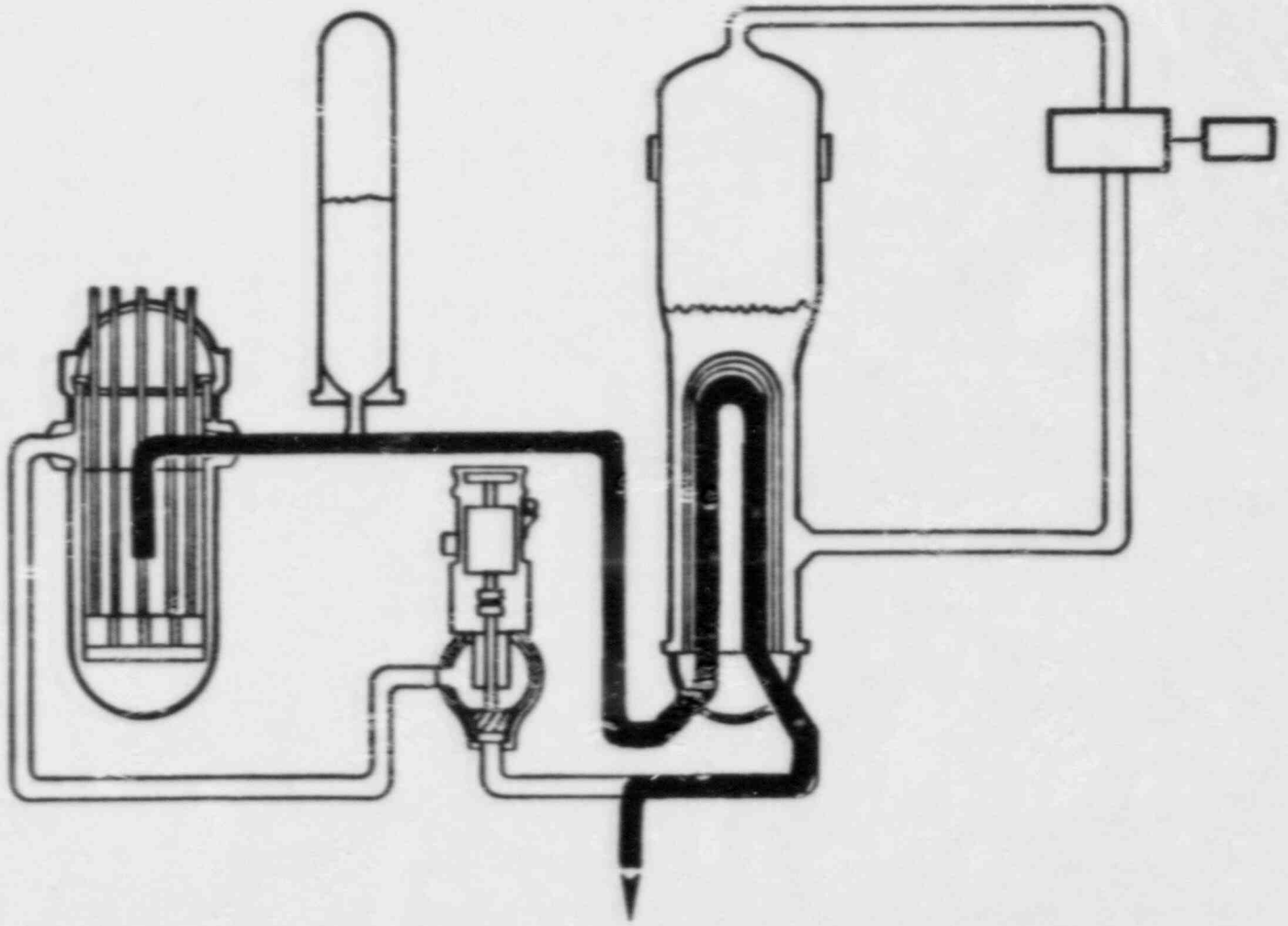

FIGURE 6.16. FLOW PATH FOR PRIMARY SYSTEM FISSION PRODUCT TRANSPORT IN SEQUENCE S_2HF

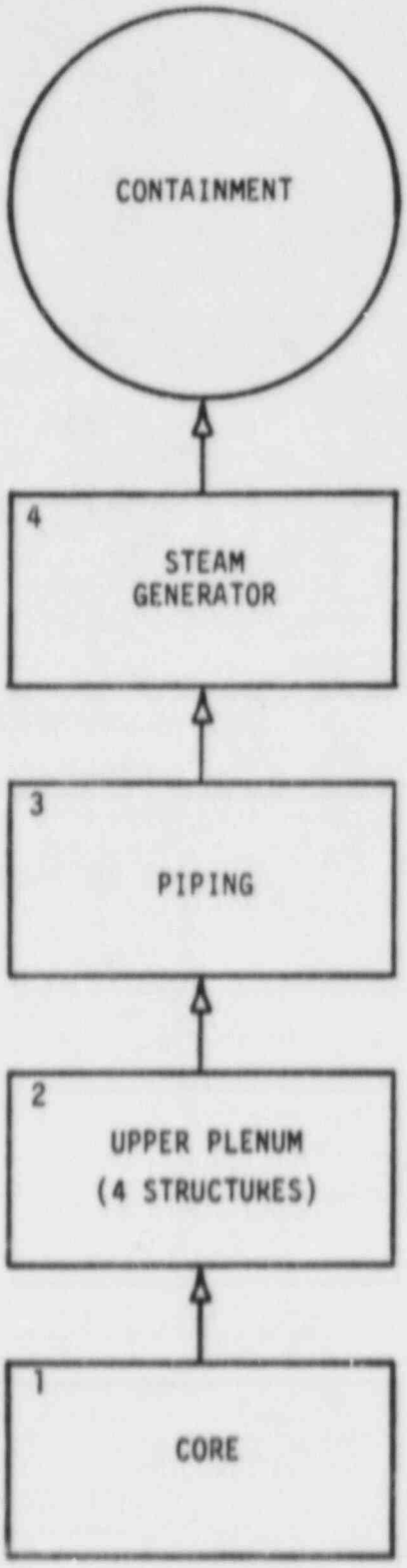

FIGURE 6.17 SCHEMATIC OF MERGE CONTROL VOLUMES FOR SEQUOYAH S_2HF SEQUENCE

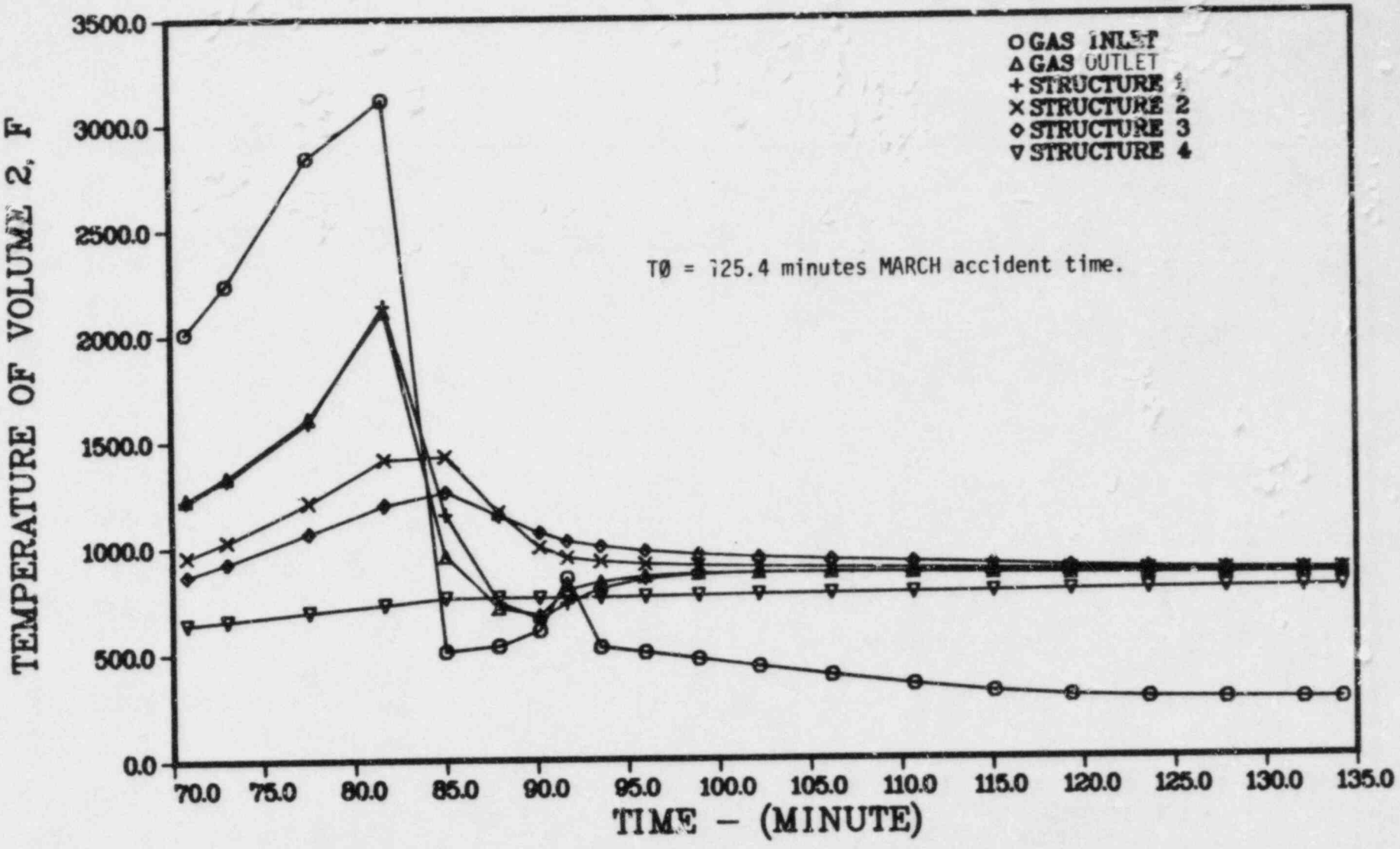

FIGURE 6.18a UPPER PLENUM GAS AND STRUCTURE TEMPERATURES FOR SEQUOYAH S_2HF SEQUENCE

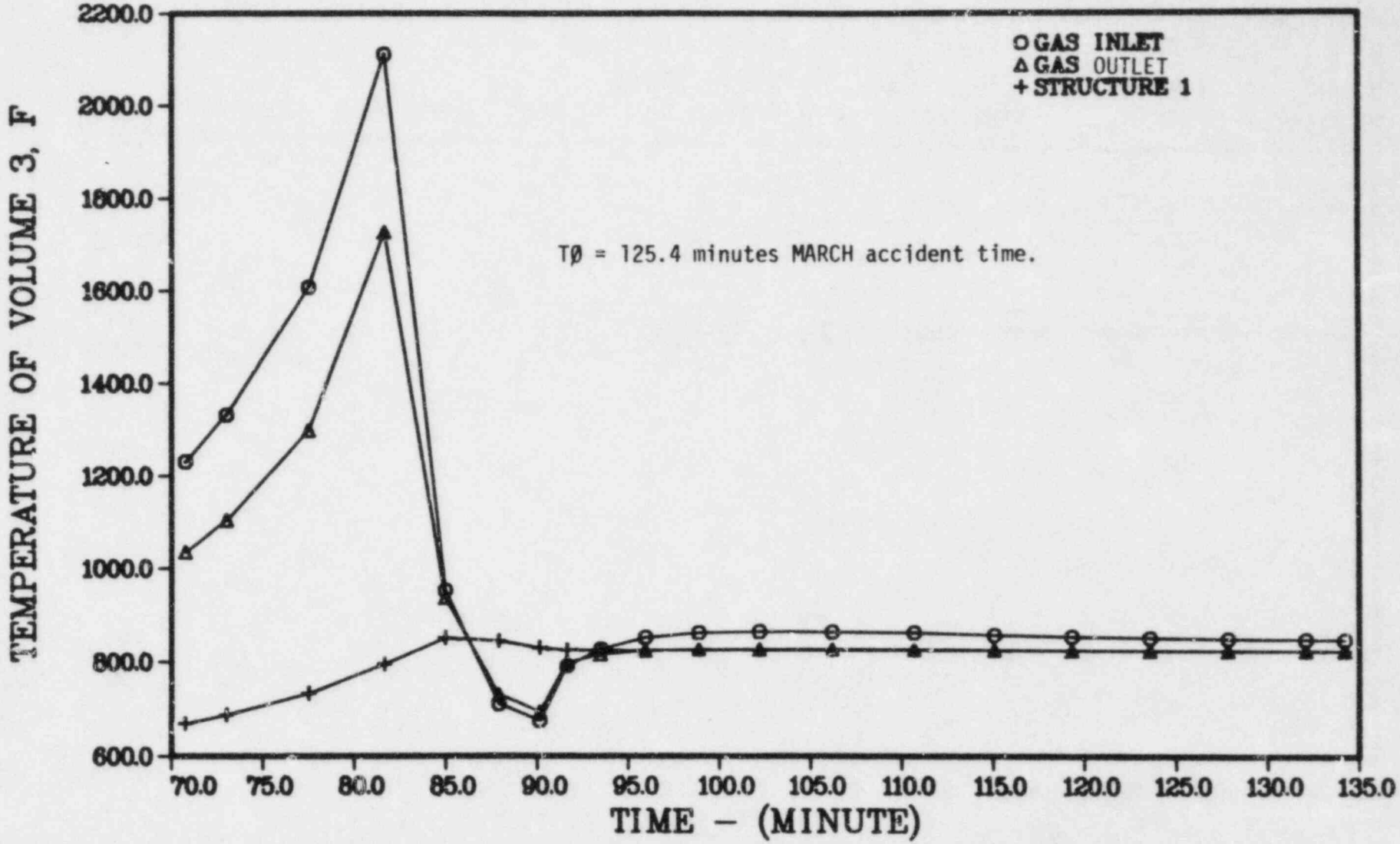

FIGURE 6.18b HOT LET PIPING GAS AND STRUCTURE TEMPERATURES FOR SEQUOYAH S_2HF SEQUENCE

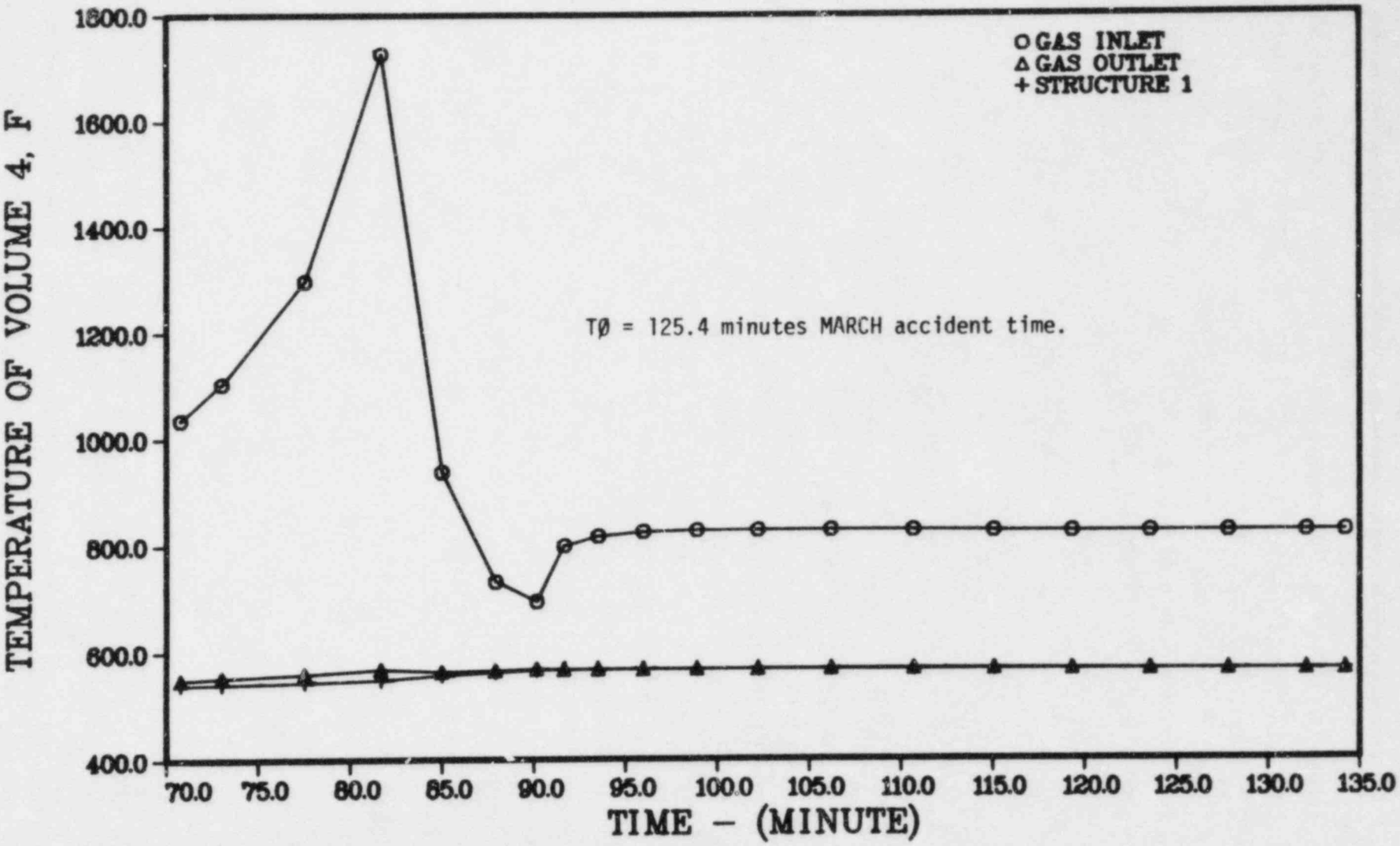

FIGURE 6.18c STEAM GENERATOR GAS AND STRUCTURE TEMPERATURES FOR SEQUOYAH S_2HF SEQUENCE

Table 6.4 gives the containment conditions at key times during the accident sequence. Figures 6.19 and 6.20 give the containment pressure and temperature histories for this sequence.

Table 6.5 summarizes the containment flows and leakages derived from the MARCH results that were used in the calculations of fission product behavior in and leakage from the containment.

6.2 Radionuclide Sources

6.2.1 Source Within Pressure Vessel

Inventory

The reactor fission product inventory which was used in the sequences considered in this report is based upon ORIGEN calculations for the Surry plant with a three region model with the maximum burnup corresponding to 33,000 MW days/ton. These fission product masses were then scaled up by the ratio of the mass of fuel in the Sequoyah plant to that in Surry to attempt to account for the variation in core size and are presented in Table 6.6. The inventory of structural materials and control rods was based on information specific to the Sequoyah plant, and assuming a control rod composition of 81 mol percent Ag, 14 mol percent In, and 4.9 mol percent Cd.

The distribution of the fission product inventory among the nodes of the core was made according to the power peaking factors for the radial and axial nodes listed in Table 6.7. The distribution of the structural and control rod materials was assumed to be homogeneous axially and distributed radially in proportion to the volume contained in each radial node, also listed in Table 6.7.

Release from Fuel

The rates of release of the various species from the melting core were calculated using the CORSOR code and the temperature profiles predicted by MARCH for the TMLB and S_2HF sequences. (The TML and TMLB sequences are identical during the in-vessel portion of the accident.) The CORSOR code has been described in previous reports, and includes certain changes from previous

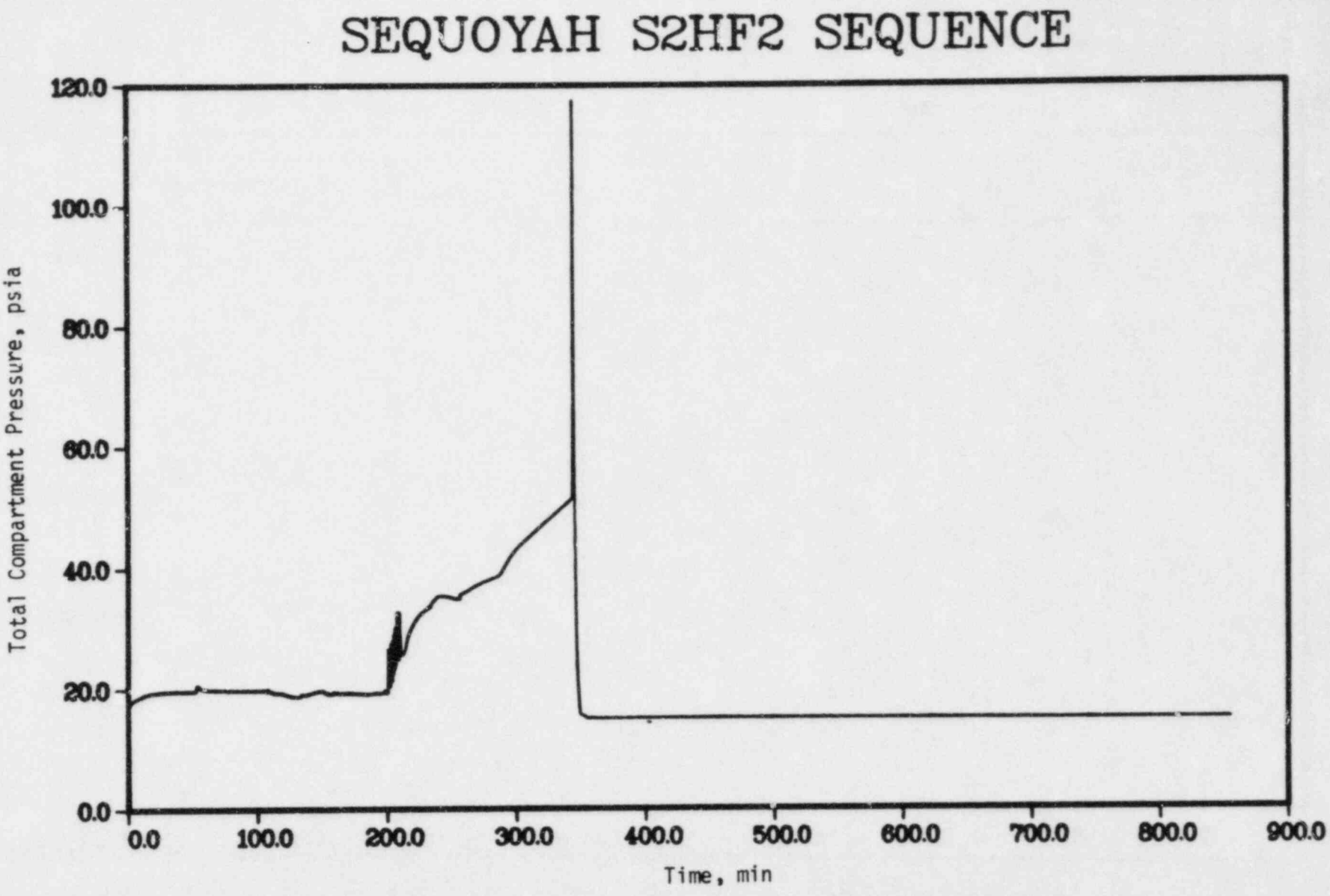

FIGURE 6.19 CONTAINMENT PRESSURE RESPONSE DURING SEQUOYAH S2HF-Y SEQUENCE

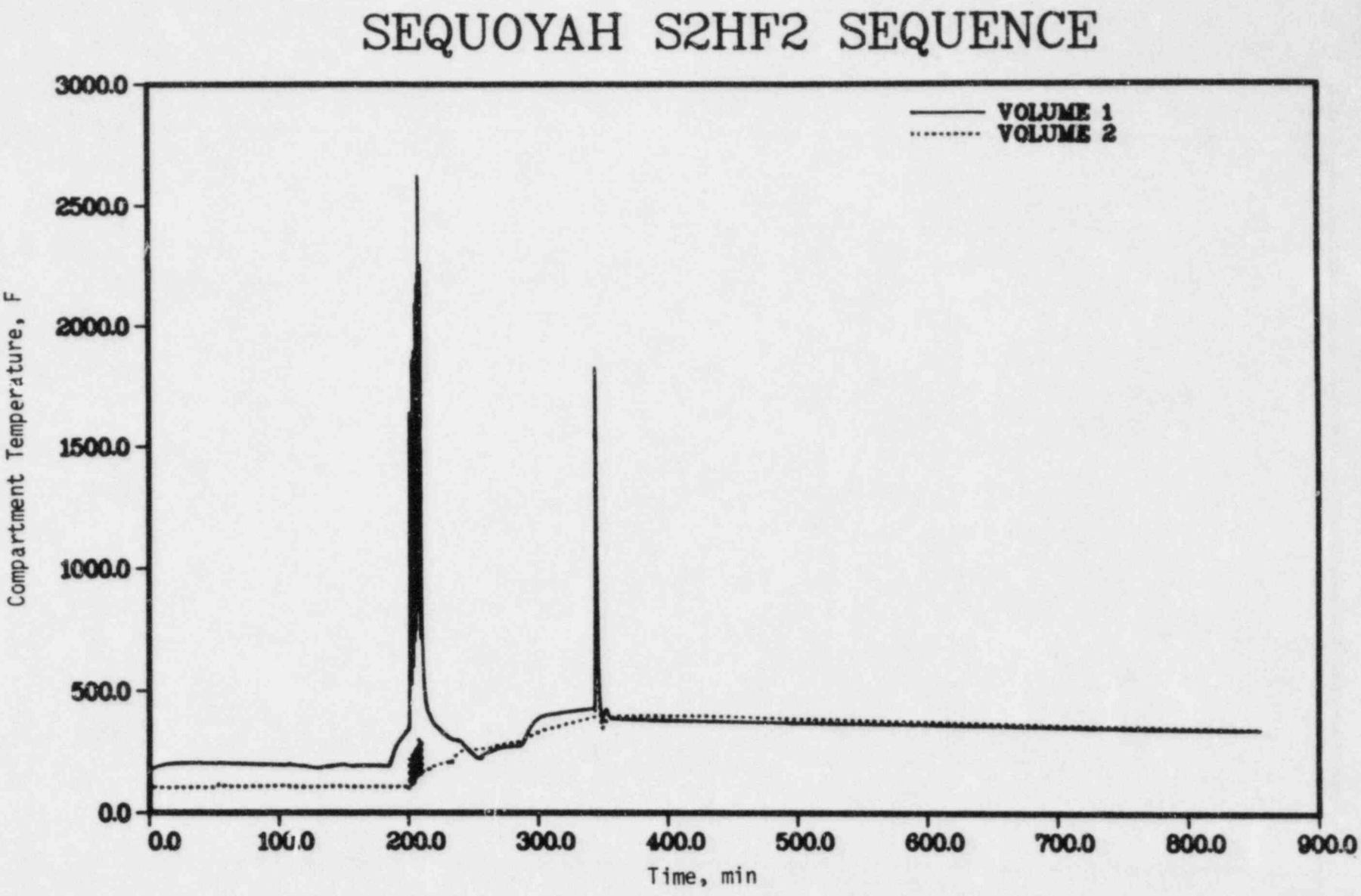

FIGURE 6.20 CONTAINMENT TEMPERATURE RESPONSE DURING SEQUOYAH S2HF-γ SEQUENCE

versions as detailed in Chapter 5 of this report. The results of the CORSOR code are presented in Figures 6.21 and 6.22 which illustrate the masses of each of the species released as functions of time.

As a result of the emissions from the core during the in-vessel phase of the accident, the inventory available for release during the core-concrete interaction which follows bottom head failure is reduced. This reduction differs from species to species depending chiefly upon their emission rates, and the inventory available for release during the core-concrete interaction is given in Table 6.8 and 6.9 for the TMLB and S_2HF sequences.

Regrouping of Released Species

In order to track the Reactor Safety Study groups independently, an additional CORSOR run was performed for the S_2HF sequence which produced release rates for all groups. A description of the makeup and methodology for calculating the release of each group follows.

- Group 1 (Xe, Kr) -- Xe and Kr releases were summed and a release rate computed. This group was not previously computed.

- Group 2 (I, Br) -- Br release was not considered due to an absence of data concerning Br release and its small inventory relative to I (1:16).

- Group 3 (Cs, Rb) -- Thermodynamic and physical properties of Rb justify treating it identically to Cs. As a result, the Rb inventory was lumped into the Cs inventory for treatment by CORSOR. Releases for I and Cs were combined to produce release rates for CsI and CsOH which were the forms assumed to be transporting through the primary system. This assumption is based on the predicted temperatures and gas compositions combined with consideration of the likely chemical thermodynamic equilibrium states.(6.1,6.2)

- Group 4 (Te, Se, Sb) -- Se and Sb were not considered based on their small inventory and lack of data concerning their behavior. Their inclusion in this group would be further complicated by the dependence of Te release on the extent of Zircaloy oxidation.

- Group 5 (Ba, Sr) -- Ba and Sr were released separately and their releases summed to form the

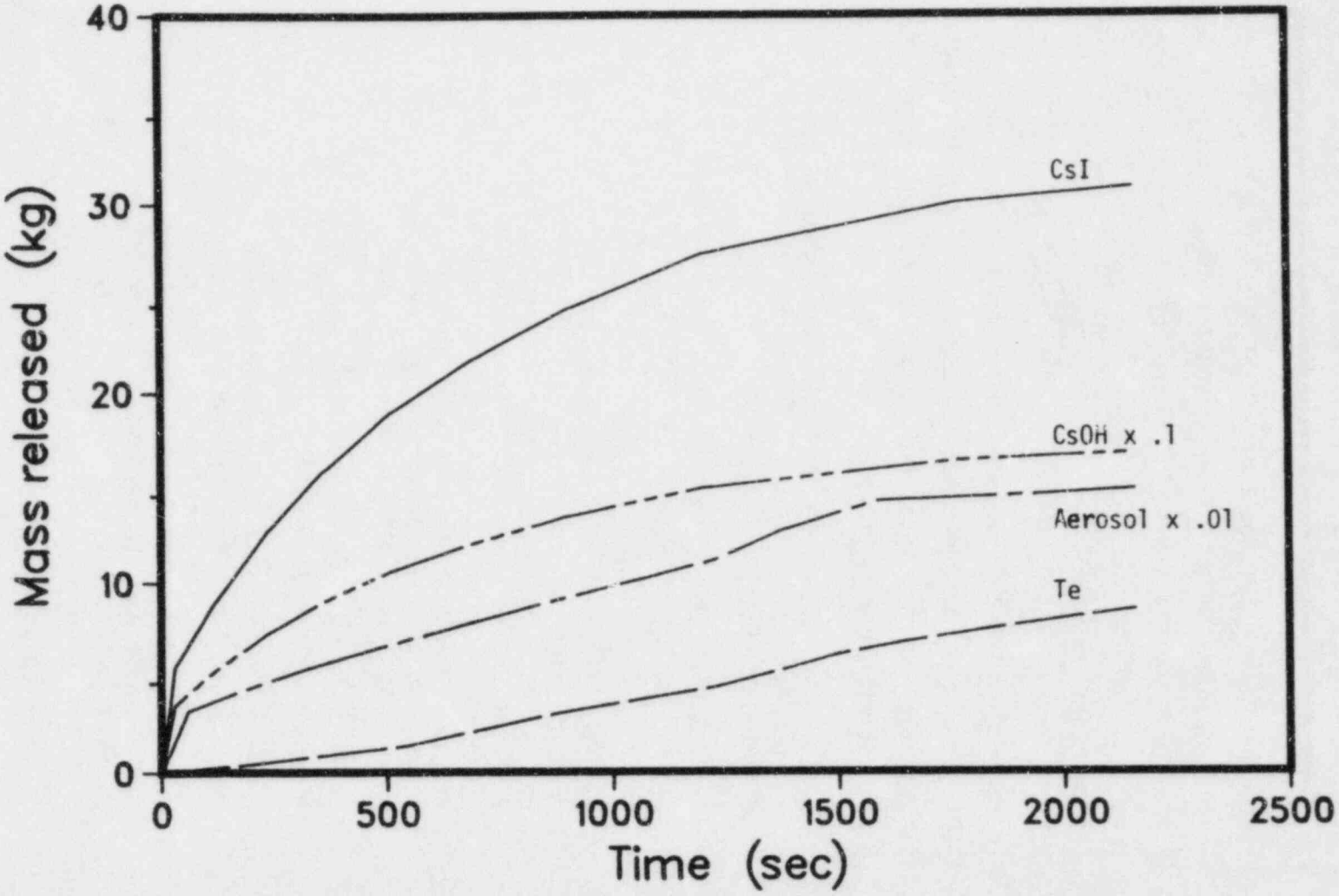

FIGURE 6.21. CORSOR PREDICTIONS OF SPECIES MASS RELEASED FROM THE CORE DURING THE TMLB SEQUENCE FOR THE SEQUOYAH PLANT (Time Measured from Start of Core Melt)

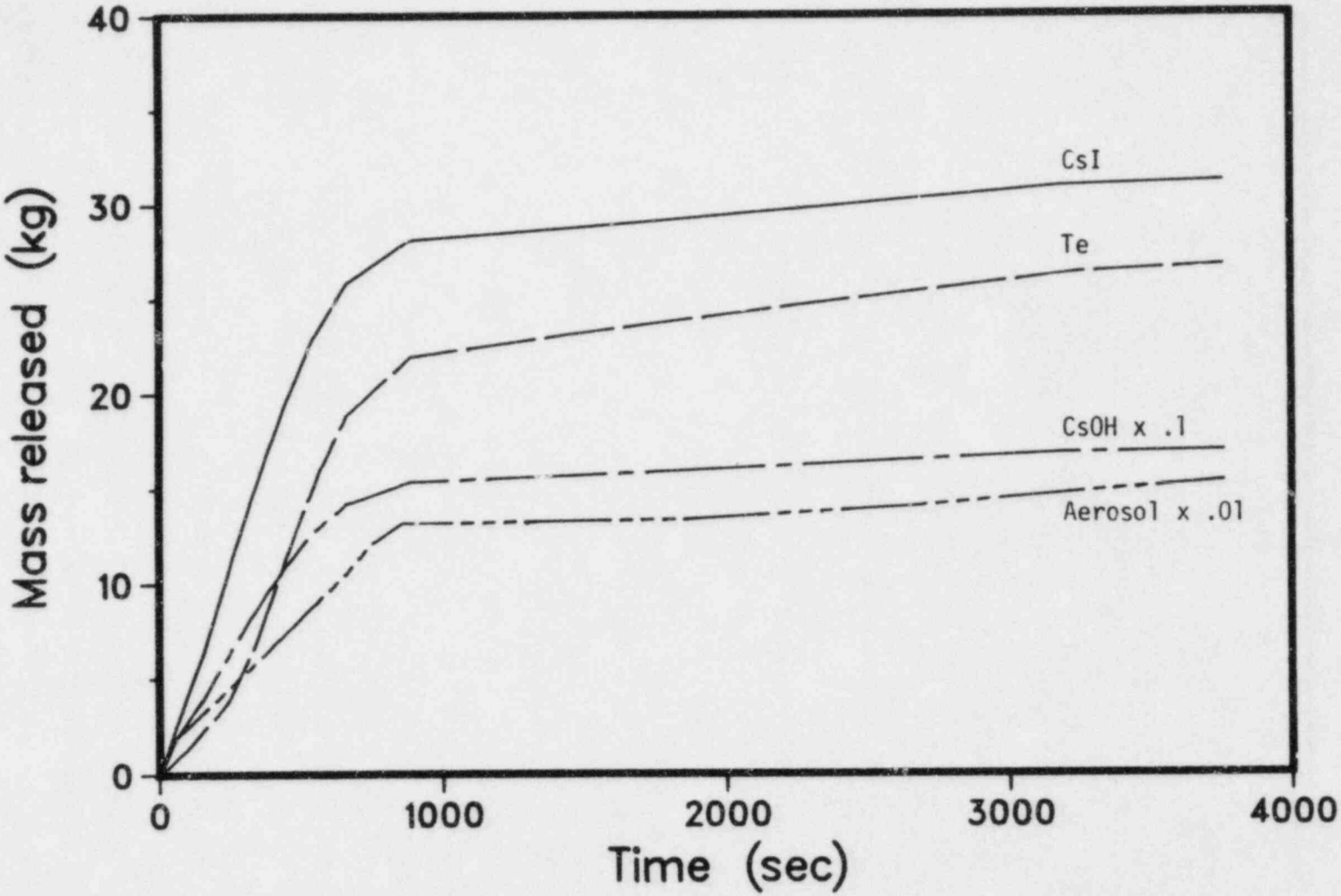

FIGURE 6.22. CORSOR PREDICTIONS OF SPECIES MASS RELEASED FROM THE CORE DURING THE S_2HF SEQUENCE FOR THE SEQUOYAH PLANT (Time Measured from Start of Core Melt)

release rate for this group. Further, their releases were not included in the aerosol materials sum.

- Group 6 (Rh, Pd, Tc, Ru, Mo) -- Rh, Pd, and Tc inventories were added to the Ru inventory for purposes of release calculations. The releases of Ru and Mo were then summed to produce release rates for this group. The aerosol materials sum does not include these releases.

- Group 7 (La, Y, Eu, Nd, Np, Sm, Pm, Pu, Zr, Ce, Nb, Pr) -- All members of Reactor Safety Study Group 7 with the exception of Zr were treated identically for purposes of release, using UO_2 release rate coefficients. Their release and the release of Zr were summed to produce release rates for this group. Table 6.6b lists initial inventories of Group 7 members not included in Table 6.8.

- Aerosol Materials (Fe, UO_2, Zr (cladding), Sn, control rod: Ag, Cd, In) -- The release rate for this group includes only nonfission products.

Table 6.6c lists initial inventories and final CORSOR releases for the Reactor Safety Study groups.

It is necessary to select an initial particle size for those materials forming the aerosol species. It has been shown[6.3] that when significant agglomeration occurs, the initial aerosol size has a negligible effect on subsequent aerosol behavior after agglomeration has proceeded for a very short time. Nevertheless, initial particle sizes were chosen to correspond to the best available information. Numerous reviews of experimental mean aerosol sizes from vaporizing and condensing fuel indicate that the sizes will be from slightly below 0.01 μm to about 0.1 μm with the most likely size being about 0.05 μm.[6.4,6.5] A number median radius of 0.05 μm and a geometric standard deviation of 1.7 were assumed for the primary particles in the current analyses, and a bulk density of 3 g/cc was assumed for the particles.

6.2.2 Sources Within the Containment

Radionuclides enter the containment as they are transported through the primary system; on melt-through of the reactor pressure vessel that material still suspended in the RCS is released into the containment as the RPV and

containment pressures are equalized. The final source considered is that material released during the core-concrete interaction. Because of a lack of release information or even more generally a lack of evidence that they are of potential importance, sources sometimes postulated as arising from steam explosions (oxidation release) or from jet emission of hot, molten corium on RPV failure were not included in these analyses.

Release from Primary System

The source to the containment of material penetrating the primary system is defined in mass input rate by species of interest and on a time-dependent basis by the output from the TRAP-MELT calculations. Also provided in the TRAP-MELT output is the size distribution of the particulate material. This calculated information is included in the subsequent report section on results.

Volatile metals, leaving the primary system are assumed to be condensed as they enter the containment to particles having the same size distribution as the particles otherwise predicted to be released from the primary system.

Release from Core-Concrete Interaction

The VANESA code (Sandia model described in Volume 1) was used to make predictions of aerosol and gas release rates and compositions as a function of time. Composition of the core materials contacting the concrete was as determined with the CORSOR code to be the materials remaining in the melt at the time of head melt-through. These compositions for the various sequences are given in Table 6.8. The concrete was taken to be a limestone concrete and the initial temperature of the molten material was as calculated with the MARCH code. The total release rates and compositions of the release are given in Tables 6.10, 6.11, and 6.12. These rates and compositions define the source to the containment after vessel head failure.

Source Term for Volatile Iodides

In a previous section it was noted that the thermodynamics of the cesium-iodine-hydrogen-oxygen system indicate that iodine will be present primarily as a nonvolatile iodide in the primary coolant system. After release from the primary system, a small fraction of the iodine inventory in the containment is believed to be present as volatile iodides.[6.1] The presence of volatile iodide species in containment-type systems has been observed in experiments[6.6] and in the TMI-2 post-accident containment atmosphere.[6.7] At present, the mechanisms responsible for the generation of these volatile iodides are not well understood. Since a theoretical model is not available, an empirical approach has been selected for the formulation of a source term for volatile iodides. This source term consists of two components. One component represents the fraction of the containment iodine inventory which is present as volatile iodides before containment failure. The second component represents a generation rate for volatile iodides after containment failure. The containment inventory of volatile iodides present prior to containment failure was estimated from levels observed in TMI-2[6.7] and from estimates of the probable detection limits in relevant experiments.[6.8] The volatile iodide generation rate was estimated from a conservative evaluation of the measurements of the airborne iodine levels in the TMI-2 containment over the time period from 100-2000 hours after reactor trip. Based on these estimates it has been assumed for this study that 0.05 percent of the containment iodine inventory will be present as volatile iodides prior to containment failure and after containment failure, additional volatile iodides will be generated at a rate of 2×10^{-7} fraction/hour of the containment iodine inventory.

Of this volatile iodine source, it is believed that a fraction of the iodine inventory in a reactor containment will be present as volatile organic iodides (predominantly CH_3I).[6.1] (Other volatile species may also be present.) Therefore, in the analysis of reactor accidents involving a radionuclide release from the reactor system and containment failure, formation in the containment and subsequent release of organic iodides should be considered. Unfortunately, the mechanism responsible for the generation of organic iodides has not yet been elucidated. As a result, it is not yet possible to establish a definitive source of organic iodides. Early estimates of the organic iodine source terms were based on a conservative interpretation of

experimental systems studies.[6.6,6.9] Early thermodynamic studies predicted that organic iodides should be present in much smaller concentrations than observed in experiments.[6.10] These calculations predicted that CH_3I would comprise only 10^{-4} percent of the total gaseous iodine inventory modeled. Experimental data[6.6] and "chemical species specific" measurements of the TMI-2 airborne iodine inventory[6.7] imply that the concentration of organic iodides present in a reactor containment during and following an accident may be higher than the concentrations predicted by thermodynamic calculations for an equilibrium system. Additionally, observations of the airborne iodine behavior at TMI-2[6.7] imply the presence of competing sources and sinks for volatile iodine species. In light of these data, a kinetic description may be required to adequately quantify the time dependence of the organic iodide concentration in reactor containments during and following reactor accidents. Pending results of studies, such as those which are currently under way,[6.2] use of a general source term for volatile iodides rather than separate source terms for CH_3I, I_2, etc., has been assumed as noted above.

References

(6.1) Technical Base for Estimating Fission Product Behavior During LWR Accidents, NUREG-0772, (June, 1981).

(6.2) Torgerson, D. F., et al., Fission Product Chemistry Under Reactor Accident Conditions, presented at the International Meeting on Thermal Nuclear Reactor Safety, Chicago, Illinois, U.S.A. (September, 1982).

(6.3) Jordan, H., Schumacher, P. M., and Gieseke, J. A., "Comparison of QUICK Predictions with Results of Selected, Recent Aerosol Behavior Experiments", NUREG/CR-2922, BMI-2089 (September, 1982).

(6.4) Gieseke, J. A., et al, "Aerosol Source Term for Fast Reactor Safety Analysis", BMI-X-637 (August 11, 1972).

(6.5) Nuclear Aerosols in Reactor Safety, CSNI/SOAR No. 1 (June, 1979).

(6.6) Postma, A. K. and Zavodoski, R. W., Review of Organic Iodide Formation Under Accident Conditions in Water-Cooled Reactors, WASH-1233 (1972).

(6.7) Pelletier, C. A., et al., Preliminary Radioiodine Source Term and Inventory Assessment for TMI-2, SAI-139-82-12-RV (September, 1982).

(6.8) Lin, C. C., Chemical Effects of Gamma Radiation on Iodine in Aqueous Solutions, J. Inorg. Nuc Chem., 42, pp. 1101-1107 (1980).

(6.9) Reactor Safety Study: An Assessment of Accident Risks in U.S. Commercial Nuclear Power Plants, WASH-1400 (1974).

(6.10) Barnes, R. H., Kircher, J. F., and Townley, C. W., Chemical Equilibrium Studies of Organic Iodide Formation Under Nuclear Reactor Accident Conditions, BMI-1816 (1966).

TABLE 6.1 REACTOR CHARACTERISTICS, CONTAINMENT PARAMETERS, AND MARCH OPTIONS FOR SEQUOYAH ICE CONDENSER PWR ANALYSIS

Reactor Power	3570 MWt
Operating Pressure	2265 psia (15.6 MPa)
Operating Temperature	580 F (304 C)
Primary System Volume	13,195 ft^3 (373.6 m^3)
Primary System Water Inventory	547,400 lb (248,520 kg)
Active Core Height	12 ft (3.66 m)
Core Flow Area	51.5 ft^2 (4.78 m^2)
Total Vessel Water Area	107.0 ft^2 (9.94 m^2)
Pressurizer Relief Valve Setpoint	2350 psia (16.2 MPa)
Pressurizer Relief Valve Capacity	21,000 lb/min (159 kg/s)
Steam Generator Water Inventory	350,000 lb (158,900 kg)
Steam Generator Relief Valve Setpoint	1,100 psig (7.6 MPa)
Zircaloy in Core	50,913 lb (23,115 kg)
Misc Metal in Core	19,158 lb (8,698 kg)
UO_2 in Core	222,739 lb (101,124 kg)
Weight of Grids Included in Debris	95,000 lb (43,130 kg)
Bottom Head Diameter	14.4 ft (4.39 m)
Bottom Head Thickness	0.469 ft (0.14 m)
Core Lattice Positions	55,777
Fuel Rods in Core	50,952
Rod Diameter	0.374 in (0.0095 m)
Fuel Diameter	0.3226 in (0.0092 m)
Clad Thickness	0.025 in (0.0006 m)
Containment parameters	
Total Free Volume	1,285,580 ft^3 (36,404 m^3)
Upper Compartment	897,880 ft^3 (25,425 m^3)
Lower Compartment	387,700 ft^3 (10,979 m^3)
Initial Temperature	100 F (37.8 C)
Initial pressure	14.7 psia (0.1 MPa)
Weight of Ice	2.45 x 10^6 lb (1.11 x 10^6 kg)
Ice Temperature	20 F (-6.7 C)

TABLE 6.1. (CONTINUED)

Material	Thermal Conductivity Btu/hr Ft F	W/cm C	Heat Capacity Btu/lb F	J/kg K	Density lb/ft^3	kg/m^3
Iron	25	0.4325	0.113	473.1	487	7801.7
Concrete	0.8	0.1384	0.238	996.5	158	2531.2

Slab	Iron Thickness,ft	Concrete Thickness,ft	Initial Temperature,F	Area in U.C.,ft^2	Area in I.C.,ft^2
U.C. shell	0.049	0	100	27396	0
Divider	C.02 each face	4.28	100	13305	13305
L.C. shell	0.072	0	100	0	12945
L.C. Conc.	0	3.01	100	0	78,080
Baskets*	0.026	0	20	286,000	0

Steel/concrete interface coefficient: 100 Btu/hr ft^2 F (0.0568 W/cm^2/C)

Concrete composition:

Weight fraction $CaCO_3$:	0.80
Weight fraction $Ca(OH)_2$:	0.15
Weight fraction SiO_2:	0.01
Weight fraction Al_2O_3:	0.01
Weight fraction free H_2O:	0.03
Gm rebar per gm concrete:	0.135

Engineered safety systems

ECC Pump	Maximum Flow GPM (ℓ/sec)	Shut off Pressure psig (MPa)
High head	1100 (69)	2530 (17.4)
Safety injection	1300 (82)	1520 (10.5)
Low head	6000 (378)	210 (1.4)

*The ice basket area is not used until all the ice is melted.

TABLE 6.1. (CONTINUED)

Containment spray pump: 4750 gpm (300)

Heat exchanger rated conditions

	ECR HX	Spray HX
Capacity, Btu/hr (W)	3.74×10^7 (1.09×10^7)	9.5×10^7 (2.78×10^7)
Primary flow, lb/min (kg/s)	37,260 (282)	39,333 (297)
Secondary flow, lb/min (kg/s)	41,400 (313)	49,910 (377)
Primary inlet, F (C)	137 (58)	146 (63)
Secondary inlet, F (C)	91 (33)	83 (28)

ECC storage and injection tanks

	Upper head Injection	Accumulator	RWST
Weight of water, lb (kg)	93000 (42,222)	230,000 (104,420)	2.90×10^6 (1.3×10^6)
Initial pressure, psia (MPa)	1326 (9.1)	600 (4.1)	14.7 (0.1)
Temperature, F (C)	100 (38)	100 (38)	100

Fractional value of RWST to start ECC recirculation: 0.293
Fractional value of RWST to start spray recirculation: 0.139

Calculated model input

Core heatup section:

Number of radial zones: 10
Number of axial zones: 24
Meltdown model: BOIL model A
Core melting temperature: 4130 F (2277 C)

Core slumping: Starts when lowest node in a zone has melted

Core collapse: Occurs when 75 percent of core has melted

Zircaloy - water reaction: Urbanic-Heidric reaction rate data, hydrogen blanketing, steam limited, continues for melted nodes, reaction of molten Zircaloy in the bottom head calculated.

TABLE 6.1. (CONTINUED)

Bottom head failure section:

Head melting temperature:	2800 F (1538 C)
Debris melting temperature:	4130 F (2277 C)
Heat loss from top of debris:	To water or core barrel
Debris thermal conductivity:	8 Btu/hr ft F (0.1384 w/cm/C)
Tensile strength of vessel:	σ = min (80,000, 1.49×10^{16} TEMP-3.9105), lb/in^2

Reactor cavity processes, debris fragmentation:

Particle diameter:	0.5 inch (1.27 cm)
Particle thermal conductivity:	2.0 Btu/hr ft F (0.0346 w/cm/C)

Reactor cavity processes, concrete decomposition:

Metal-concrete interface heat transfer coefficient: HIM = 0.01 w/cm^2 K

Oxide-concrete interface heat transfer coefficient: HIO = 0.01 w/cm^2 K

Top surface emissivity: E = 0.5

Heat to cover water: surface boiling plus 50 percent of area radiating at internal temperature of top layer.

Containment Section:

Atmosphere-wall heat transfer coefficient:

$h = h_c$ (TSAT-TWALL) + 0.19 (T-TWALL)$^{4/3}$/(T-TWALL)

h_c = 0 if TSAT TWALL

2.0 h_c = Uchida data 280 Btu/hr ft^2 F

Containment break area: 7.0 ft^2 for overpressure failure (0.65 m^2)

TABLE 6.2 ACCIDENT EVENT TIMES

Event	Time, minutes
	Sequoyah TMLB'-Y
Steam Generator Dry	62.0
Core Uncover	97.8
Start Melt	121.5
Start Slump	143.5
Core Collapse	145.0
Vessel Head Dry	149.2
Bottom Head Fail	157.8
Containment Fail	157.8
Concrete Attack	158.9
Ice Melt Complete	428.5
End Calculation	761.2
	Sequoyah TMLB'-δ
Steam Generator Dry	62.0
Core Uncover	97.8
Start Melt	121.5
Start Slump	143.5
Core Collapse	145.0
Vessel Head Dry	149.2
Bottom Head Fail	157.8
Concrete Attack	161.5
Containment Fail	552.5
Ice Melt Complete	556.0
End Calculation	761.6

TABLE 6.2 (Continued)

Event	Time, minutes
	Sequoyah TML-γ
Steam Generator Dry	62.0
Spray and Fan On	62.0
Core Uncover	97.2
Start Melt	121.0
Spray Recirculation On	126.0
Start Slump	143.0
Core Collapse	144.5
Vessel Head Dry	148.8
Bottom Head Fail	157.2
Hydrogen Burn	157.2
Containment Fail	157.2
Hydrogen Burn	159.7
End Calculation	263.1
	Sequoyah TML-δ/ε
Steam Generator Dry	62.0
Spray and Fan On	62.0
Core Uncover	97.2
Start Melt	121.0
Spray Recirculation On	126.0
Start Slump	143.0
Core Collapse	144.5
Vessel Head Dry	148.8
Hydrogen Burn	150.1
Hydrogen Burn	155.2
Bottom Head Fail	157.3
Concrete Attack	157.3
Hydrogen Burn	198.7
Hydrogen Burn	264.7

TABLE 6.2 (Continued)

Event	Time, minutes
Sequoyah TML-δ/ε (Continued)	
Hydrogen Burn	301.5
Hydrogen Burn	335.5
Hydrogen Burn	364.3
Ice Melted	531.1
End Calculation	760.4
Sequoyah S_2HF-Y	
Fan On	0.6
Spray On	1.1
ECCS Recirculation	40.9
Spray Recirculation	52.7
ECC and CS Fail	107.7
Core Uncover	162.9
Start Melt	195.9
Ice Melt Complete	197.7
Hydrogen Burn	201.7
Start Core Slump	207.9
Hydrogen Burn	208.1
Core Collapse	208.7
Hydrogen Burn	208.9
Vessel Head Dry	216.0
Bottom Head Fail	259.6
Concrete Attack	259.7
Hydrogen Burn	352.1
Containment Fail	352.2
End Calculation	860.3

TABLE 6.3 CORE AND PRIMARY SYSTEM RESPONSE

Accident Event	Time, minutes	Primary System Pressure, psia	Primary System Water Inventory, lbm	Average Core Temperature, F	Peak Core Temperature, F	Fraction Core Melted	Fraction Clad Reacted
			Sequoyah TMLB'				
Core Uncover	97.8	2378	9.8×10^4	666	670	0.	0.
Start Melt	121.5	2376	4.5×10^4	2094	4130	0.	0.06
Start Slump	143.5	2375	4.2×10^4	3464	4153	0.53	0.25
Core Collapse	145.0	2375	3.7×10^4	3546	4467	0.76	0.43
Vessel Head Dry	149.2	2377	0.	3545	---	---	0.49
Bottom Head Fail	157.8	2374	0.	3783	---	---	0.49
			Sequoyah S_2HF				
Core Uncover	162.9	789	1.1×10^5	521	524	0.	0.
Start Melt	195.9	591	5.0×10^4	1906	4130	0.	0.06
Start Slump	207.9	465	3.9×10^4	3447	4264	0.69	0.57
Core Collapse	208.7	648	3.7×10^4	3447	4130	0.81	0.65
Vessel Head Dry	216.0	1058	0.	2923	---	---	0.66
Bottom Head Fail	259.6	41	0.	3768	---	---	0.66

TABLE 6.4 CONTAINMENT RESPONSE

Accident Event	Time, minutes	Compartment Pressure, psia	Compartment Temperature, F		RWST or CST Water Mass, lbm	Ice Weight, lbm	Sump Water Mass, lbm	Sump Water Temp., F	Reactor Cavity Water Mass, lbm	Reactor Cavity Water Temp., F	Steam Cond. on Walls lbm/min
			1	2							
					Sequoyah TMLB'-Y						
Steam Gen. Dry	62.0	17.9	170	122	2.9×10^6		3.78×10^4	151	0.	---	1180/0 *
Core Uncover	97.8	22.4	234	122	2.9×10^6		1.16×10^6	146	0.	---	857/0
Start Melt	121.5	21.4	228	111	2.9×10^6		1.23×10^6	146	0.	---	546/0
Start Slump	143.5	20.3	215	105	2.9×10^6		1.24×10^6	147	0.	---	315/0
Core Collapse	145.0				2.9×10^6						
Vessel Head Dry	149.2	22.4	224	116	2.9×10^6		1.43×10^6	145	0.	---	0/0
Hydrogen Burn	157.6	26.1	237	145	2.9×10^6						
Hydrogen Burn	157.8	75.7	601	2264	2.9×10^6						
Bottom Head Fail	157.8				2.9×10^6				3.13×10^5	143	0/0
Containment Fail	157.8	27.1	239	176	2.9×10^6		1.87×10^6	143	3.13×10^5	143	0/0
Concrete Attack	160.5				2.9×10^6						
Hydrogen Burn	160.5	54.2	1961	2899	2.9×10^6						
Hydrogen Burn	244.1	31.2	486	1531	2.9×10^6						
Hydrogen Burn	288.4	26.4	406	1180	2.9×10^6						
Hydrogen Burn	333.3	26.6	418	1196	2.9×10^6						
Hydrogen Burn	362.5	24.9	381	1127	2.9×10^6						
Hydrogen Burn	391.3	25.0	405	1164	2.9×10^6						
Hydrogen Burn	421.8	25.2	399	1177	2.9×10^6						
Hydrogen Burn	430.7	23.2	381	1277	2.9×10^6						
Ice Melt Complete	456.9	14.7	204	120	2.9×10^6		2.32×10^6	185	9.75×10^5	212	249/294
End Calculation	761.2	15.4	211	212	2.9×10^6		2.16×10^6	213	8.51×10^5	213	0/0

* Volume 1/Volume 2

TABLE 6.4 CONTAINMENT RESPONSE

Accident Event	Time, minutes	Compartment Pressure, psia	Compartment Temperature, F		RWST or CST Water Mass, lbm	Ice Weight, lbm	Sump Water Mass, lbm	Sump Water Temp., F	Reactor Cavity Water Mass, lbm	Reactor Cavity Water Temp., F	Steam Cond. on Walls lbm/min
			1	2							
					Sequoyah TMLB'8						
Steam Gen. Dry	62.0	17.9	170	122	2.9×10^6		3.78×10^4	151	0.	---	1180/0*
Core Uncover	97.8	22.4	234	122	2.9×10^6		1.16×10^6	146	0.	---	857/0
Start Melt	121.5	21.4	228	111	2.9×10^6		1.23×10^6	146	0.	---	546/0
Start Slump	143.5	20.3	215	105	2.9×10^6		1.24×10^6	147	0.	---	315/0
Core Collapse	145.0										
Vessel Head Dry	149.2	22.4	224	116	2.9×10^6		1.43×10^6	145	0.	---	0/0
Bottom Head Fail	157.8	26.1	238	146	2.9×10^6		1.79×10^6	144	3.13×10^5	236	570/0
Concrete Attack	161.5				2.9×10^6						
Containment Fail	552.5	60.0	264	370	2.9×10^6		2.10×10^6	203	9.32×10^5	287	368/0
Ice Melt Complete	556.0				2.9×10^6						
End Calculation	761.6	15.1	211	210	2.9×10^6		2.18×10^6	213	9.74×10^5	213	80/32
					Sequoyah TML-Y						
Steam Gen. Dry	62.0	17.9	170	122	2.9×10^6		3.78×10^4	151	0.	---	1180/0*
Core Uncover	97.2	19.4	205	103	1.41×10^6		2.25×10^6	121	5.23×10^5	121	542/2
Start Melt	121.0	17.2	155	103	6.21×10^5		2.70×10^5	116	1.01×10^6	120	0/2
Spray Recirc.	126.0	17.1	147	103	3.95×10^5						
Start Slump	143.0	17.0	144	102	3.95×10^5		2.95×10^6	113	1.01×10^6	120	0/1
Core Collapse	144.5	19.9	200	103	3.95×10^5						

* Volume 1/Volume 2

TABLE 6.4 CONTAINMENT RESPONSE

Accident Event	Time, minutes	Compartment Pressure, psia	Compartment Temperature, F		RWST or CST Water Mass, lbm	Ice Weight, lbm	Sump Water Mass, lbm	Sump Water Temp., F	Reactor Cavity Water Mass, lbm	Reactor Cavity Water Temp., F	Steam Cond. on Walls lbm/min
			1	2							
Sequoyah TML-Y (Continued)											
Vessel Head Dry	148.8	20.4	204	102	3.95×10^5		3.11×10^6	113	1.01×10^6	120	333/0*
Hydrogen Burn	157.1	62.7	276	1364							
Bottom Head Fail	157.3	18.4	157	102	3.95×10^5						
Containment Fail	157.3	66.4	284	1389	3.95×10^5		3.81×10^6	114	9.64×10^5	237	0/0
Hydrogen Burn	159.7	37.9	455	1894							
End Calculation	262.1	14.7	212	219	3.95×10^5		4.65×10^6	127	9.75×10^5	212	330/0
Sequoyah TML-δ											
Steam Gen. Dry	62.0	17.9	170	122	2.9×10^6		3.78×10^4	151	0.	---	1180/0*
Core Uncover	97.2	19.4	205	103	1.33×10^6		2.25×10^6	120	6.00×10^5	121	542/2
Start Melt	121.0	17.3	155	103	5.43×10^5		2.77×10^6	116	1.01×10^6	120	0/2
Spray Recirc.	124.0	17.0	147	102	3.95×10^5						
Start Slump	143.0	17.0	146	105	3.95×10^5		2.95×10^6	112	1.01×10^6	120	0/0
Core Collapse	144.5	19.0	190	104	3.95×10^5						
Vessel Head Dry	148.3	20.4	203	102	3.95×10^5		3.12×10^6	112	1.01×10^6	120	693/0
Hydrogen Burn	150.5	44.5	1400	753							
Hydrogen Burn	155.2	51.5	435	851							
Bottom Head Fail	155.3	20.1	251	135	3.95×10^5						

* Volume 1/Volume 2

TABLE 6.4 CONTAINMENT RESPONSE

Accident Event	Time, minutes	Compartment Pressure, psia	Compartment Temperature, F		RWST or CST Water Mass, lbm	Ice Weight, lbm	Sump Water Mass, lbm	Sump Water Temp., F	Reactor Cavity Water Mass, lbm	Reactor Cavity Water Temp., F	Steam Cond. on Walls lbm/min
			1	2							
					Sequoyah TML-6						
Concrete Attack	155.3	46.2	407	674	3.95×10^5						
Hydrogen Burn	198.7	31.9	936	510							
Hydrogen Burn	264.7	33.6	294	618							
Hydrogen Burn	301.5	32.5	271	518							
Hydrogen Burn	335.5	32.0	262	510							
Hydrogen Burn	364.3	33.8	275	544							
Ice Melt Complete	531.1	25.8	187	101	3.95×10^5		4.88×10^6	116	9.63×10^5	240	364/1139*
End Calculation	760.4	34.4	171	123	3.95×10^5		4.89×10^6	130	9.55×10^5	257	75/0
					Sequoyah S_2HF						
Core Uncover	162.9	19.2	192	105	3.81×10^5		9.46×10^5	157	0.	---	229/0
Start Melt	195.9	19.3	308	105	3.81×10^5		1.29×10^6	150	0.	---	0/0
Ice Melt End	197.9	19.6	321	111	3.81×10^5						
Hydrogen Burn	201.7	26.8	1663	227	3.81×10^5						
Hydrogen Burn	203.7	27.1	1737	232	3.81×10^5						
Hydrogen Burn	205.1	27.9	1937	238	3.81×10^5						
Hydrogen Burn	206.2	27.9	1774	233	3.81×10^5						
Hydrogen Burn	207.2	30.0	2217	265	3.81×10^5						
Start Slump	207.9	24.6	923	164	3.81×10^5						

* Volume 1/Volume 2

TABLE 6.4 CONTAINMENT RESPONSE

Accident Event	Time, minutes	Compartment Pressure, psia	Compartment Temperature, F		RWST or CST Water Mass, lbm	Ice Weight, lbm	Sump Water Mass, lbm	Sump Water Temp., F	Reactor Cavity Water Mass, lbm	Reactor Cavity Water Temp., F	Steam Cond. on Walls lbm/min
			1	2							
Sequoyah S_2HF (Continued)											
Hydrogen Burn	208.1	29.8	2035	253	3.81×10^5						
Core Collapse	208.7	26.1	1002	187	3.81×10^5						
Hydrogen Burn	208.9	33.0	2596	309	3.81×10^5						
Hydrogen Burn	210.3	31.5	1964	268	3.81×10^5						
Vessel Head Dry	216.0	27.4	412	178	3.81×10^5		1.32×10^6	149	0.	---	0/1012*
Bottom Head Fail	259.6	35.7	230	261	3.81×10^5		1.32×10^6	149	0.	---	0/0
Hydrogen Burn	352.2	117.9	1768	1582	3.81×10^5						
Containment Fail	352.2	120.8	1802	1654	3.81×10^5		1.32×10^6	149	0.	---	0/0
End Calculation	860.3	15.0	345	349	3.81×10^5		1.31×10^6	140	0.	---	0/0

* Volume 1/Volume 2

TABLE 6.5 SUMMARY OF CONTAINMENT FLOWS AND LEAKAGES

Subsequence	CSIS Start, min	CSIS End, min	CSRS Start, min	CSRS End, min	Leakage in Compartment 1: Time Interval, min	Leak Rate,(a) v/hr	Pressure MPa	Pressure psia	Temp °F	Temp °C	Leakage in Compartment 2: Leak Rate,(b) v/hr	Pressure MPa	Pressure psia	Temp °F	Temp °C	Remarks
TMLB-Y	--	--	--	--	99.8	9.6	0.15	22	234	112	4.2E-4	0.15	22	124	51	Core uncovers
					99.8-121.5	2.0	0.15	22	232	111	4.2E-4	0.15	22	117	47	Core heats
					121.5-143.5	0.1	0.14	21	220	104	4.2E-4	0.14	21	104	40	Core melts
					143.5-144.5	25.4	0.14	21	217	103	4.2E-4	0.14	21	105	41	Core slumps and collapses
					144.5-155.6	15.2	0.16	23	227	109	4.2E-4	0.16	23	124	51	Reactor vessel heatup
					155.6-155.75	752.4	0.17	26	351	177	4.2E-4	0.17	26	145	63	
					155.75	733.3	0.17	26	359	181	4.2E-4	0.17	26	149	65	Reactor vessel fails
					157.8	4.2E-4	0.52	77	811	433	23.6	0.52	77	2125	1163	Hydrogen burn, cont. fails
					157.8-158.0	19.0	0.32	47	596	313	22.1	0.32	47	1612	878	Boiloff of H_2O
					158.0-158.2	253.9	0.19	28	1110	599	19.2	0.19	28	1107	597	Hydrogen burns
					158.2-158.9	30.2	0.20	29	1299	704	21.3	0.20	29	1442	783	Boiloff of H_2O
					158.9-159.6	36.3	0.14	21	483	250	18.9	0.14	21	1016	547	Initial concrete attack
					159.6-159.7	13.3	0.14	21	460	238	18.1	0.14	21	1302	706	Hydrogen burns
					159.7-242.4	3.6	0.10	15	218	103	0.3	0.10	15	308	154	Concrete decomposition
					242.4-407.8	3.3	0.11	16	212	100	0.9	0.11	16	357	180	Concrete decomposition
					407.8	2.1	0.11	16	228	109	2.3	0.11	16	452	234	Hydrogen burns
					407.8-412.8	7.6	0.11	16	251	122	4.3	0.11	16	728	386	Concrete decomposition
					412.8-428.5	2.5	0.10	15	202	94	4.2E-4	0.10	15	418	214	Concrete decomposition
					428.5	2.6	0.10	15	203	95	2.9E-2	0.10	15	368	187	Ice melt complete
					428.5-760.0	4.0	0.10	15	207	97	1.7	0.10	15	192	89	Concrete decomposition

(a) Normalized to a containment free volume of 3.877×10^5 ft^3. Units are volume fraction/hr. Leakage is from Compartment 1 to Compartment 2.
(b) Normalized to a compartment free volume of 8.979×10^5 ft^3. Units are volume fraction/hr. Leakage is from Compartment 2 to the environment.

TABLE 6.5 SUMMARY OF CONTAINMENT FLOWS AND LEAKAGES

Subsequence	CSIS Start, min	CSIS End, min	CSRS Start, min	CSRS End, min	Leakage in Compartment 1: Time Interval, min	Leak Rate,(a) v/hr	Pressure MPa	Pressure psia	Temp °F	Temp °C	Leakage in Compartment 2: Leak Rate,(b) v/hr	Pressure MPa	Pressure psia	Temp °F	Temp °C	Remarks
TMLB-6	--	--	--	--	97.75	9.6	0.15	22	234	112	4.2E-4	0.15	22	124	51	Core uncovers
					97.75-121.5	2.0	0.15	22	232	111	4.2E-4	0.15	22	117	47	Core heats
					121.5-143.5	0.05	0.14	21	220	104	4.2E-4	0.14	21	104	40	Core melts
					143.5-144.5	1.2	0.14	21	220	104	4.2E-4	0.14	21	104	40	Core slumps and collapses
					144.5-157.8	18.9	0.15	22	222	106	4.2E-4	0.15	22	114	46	Reactor vessel heatup
					157.8	645.5	0.18	26	237	114	4.2E-4	0.18	26	145	63	Reactor vessel fails
					157.8-161.5	4.9	0.18	26	232	111	4.2E-4	0.18	26	147	64	Boiloff of H_2O
					161.5-552.5	0.9	0.30	44	257	125	4.2E-4	0.30	44	305	152	Concrete decomposition
					552.5	0.5	0.41	60	275	135	4.2E-4	0.41	60	376	191	Compartment 2 fails
					552.5-556.02	32.8	0.25	37	252	122	13.7	0.25	37	263	129	Ice melt complete
					556.02-762.4	3.7	0.10	15	227	109	1.4	0.10	15	199	93	Concrete decomposition
TML-6	62.0	126.0	126.0	--	97.2	59.3	0.13	20	210	99	4.2E-4	0.13	20	103	40	Core uncovers
					97.2-121.0	10.4	0.12	18	180	82	4.2E-4	0.12	18	102	39	Core heats
					121.0-124.0	7.3	0.12	18	151	66	4.2E-4	0.12	18	102	39	Core melts
					124.0-143.0	7.2	0.11	17	140	60	4.2E-4	0.11	17	102	39	Spray recirculation begins
					143.0-144.0	34.2	0.12	18	162	72	4.2E-4	0.12	18	102	39	Core slumps and collapses
					144.0-150.5	21.9	0.14	21	202	94	4.2E-4	0.14	21	102	39	Reactor vessel heatup
					150.5-150.6	138.2	0.20	29	885	474	4.2E-4	0.20	29	322	161	Hydrogen burns
					150.6	23.7	0.29	42	1427	775	4.2E-4	0.29	42	667	353	Hydrogen burns

(a) Normalized to a containment free volume of 3.877×10^5 ft^3. Units are volume fraction/hr. Leakage is from Compartment 1 to Compartment 2.

(b) Normalized to a compartment free volume of 8.979×10^5 ft^3. Units are volume fraction/hr. Leakage is from Compartment 2 to the environment.

TABLE 6.5 SUMMARY OF CONTAINMENT FLOWS AND LEAKAGES

Subsequence	CSIS Start, min	CSIS End, min	CSRS Start, min	CSRS End, min	Leakage in Compartment 1: Time Interval, min	Leak Rate,(a) v/hr	Pressure MPa	Pressure psia	Temp. °F	Temp. °C	Leakage in Compartment 2: Leak Rate,(b) v/hr	Pressure MPa	Pressure psia	Temp. °F	Temp. °C	Remarks
TML-δ (Continued)					150.6-151.1	26.1	0.21	31	993	534	4.2E-4	0.21	31	295	146	Reactor vessel heatup
					151.1-153.0	4.3	0.16	24	450	232	4.2E-4	0.16	24	160	71	Reactor vessel heatup
					153.0-155.2	82.4	0.14	21	256	125	4.2E-4	0.14	21	136	58	Reactor vessel heatup
					155.2	56.1	0.29	43	388	198	4.2E-4	0.29	43	592	311	Reactor vessel fails
					155.2-155.3	36.6	0.29	43	342	172	4.2E-4	0.29	43	538	281	Hydrogen burns
					155.3-198.7	6.9	0.12	18	162	72	4.2E-4	0.12	18	109	43	Concrete decomposition
					198.7-198.8	46.3	0.19	28	860	460	4.2E-4	0.19	28	378	192	Hydrogen burns
					198.8-264.8	7.7	0.12	18	165	74	4.2E-4	0.12	18	104	40	Concrete decomposition
					264.8-265.0	17.7	0.19	28	249	121	4.2E-4	0.19	28	382	194	Hydrogen burns
					265.0-301.5	9.6	0.13	20	173	78	4.2E-4	0.13	20	107	42	Concrete decomposition
					301.5-301.6	59.4	0.20	29	282	139	4.2E-4	0.20	29	316	158	Hydrogen burns
					301.6-335.6	8.7	0.14	21	169	76	4.2E-4	0.14	21	107	42	Concrete decomposition
					335.6	4.2E-4	0.21	31	253	123	4.2E-4	0.21	31	482	250	Hydrogen bruns
					335.6-364.4	8.8	0.14	21	165	74	4.2E-4	0.14	21	109	43	Concrete decomposition
					364.4	4.2E-4	0.23	33	267	131	4.2E-4	0.23	33	523	273	Hydrogen burns
					364.4-760.4	7.9	0.18	27	170	77	4.2E-4	0.18	27	115	46	Concrete decomposition

(a) Normalized to a containment free volume of 3.877×10^5 ft^3. Units are volume fraction/hr. Leakage is from Compartment 1 to Compartment 2.

(b) Normalized to a compartment free volume of 8.979×10^5 ft^3. Units are volume fraction/hr. Leakage is from Compartment 2 to the environment.

TABLE 6.5 SUMMARY OF CONTAINMENT FLOWS AND LEAKAGES

Subsequence	CSIS Start, min	CSIS End, min	CSRS Start, min	CSRS End, min	Leakage in Compartment 1: Time Interval, min	Leak Rate,(a) v/hr	Pressure MPa	Pressure psia	Temp. °F	Temp. °C	Leakage in Compartment 2: Leak Rate,(b) v/hr	Pressure MPa	Pressure psia	Temp. °F	Temp. °C	Remarks
TML-Y	62.0	126.0	126.0	157.2	97.2	60.1	0.13	20	210	99	4.2E-4	0.13	20	103	40	Core uncovers
					97.2-121.0	10.4	0.12	18	180	82	4.2E-4	0.12	18	102	39	Core heats
					121.0-126.0	7.3	0.12	18	149	65	4.2E-4	0.12	18	102	39	Core melts
					126.0-143.0	7.2	0.11	17	139	60	4.2E-4	0.11	17	102	39	Spray recirculation begins
					143.0-144.0	34.9	0.12	18	161	72	4.2E-4	0.12	18	102	39	Core slumps and collapses
					144.0-151.16	18.0	0.13	20	184	84	4.2E-4	0.13	20	102	39	Reactor vessel heatup
					151.16	4.2E-4	0.29	43	251	122	4.2E-4	0.29	43	703	373	Hydrogen burns
					157.17-157.25	216.2	0.45	66	282	139	21.1	0.45	66	1451	788	Hydrogen burn, cont. fails
					157.25	263.1	0.45	66	284	140	21.0	0.45	66	1397	758	Reactor vessel fails
					157.25-158.5	15.0	0.34	49	263	128	19.7	0.34	49	1154	624	Boiloff of H_2O
					158.5-159.8	24.8	0.19	28	229	110	17.5	0.19	28	783	417	Boiloff of H_2O
					159.8	4.2E-4	0.24	35	403	206	21.3	0.24	35	1643	895	Hydrogen burns
					159.8-159.9	14.6	0.27	40	502	261	24.6	0.26	40	241	116	Hydrogen burns
					159.9-161.1	64.5	0.18	27	329	165	21.7	0.18	27	1487	808	Hydrogen bruns
					161.1-162.8	79.6	0.11	16	213	101	6.2	0.11	16	796	424	Hydrogen burns
					162.8-263.1	4.7	0.10	15	212	100	4.2E-4	0.10	15	243	117	Concrete decomposition

(a) Normalized to a containment free volume of 3.877×10^5 ft^3. Units are volume fraction/hr. Leakage is from Compartment 1 to Compartment 2.

(b) Normalized to a compartment free volume of 8.979×10^5 ft^3. Units are volume fraction/hr. Leakage is from Compartment 2 to the environment.

TABLE 6.5 SUMMARY OF CONTAINMENT FLOWS AND LEAKAGES

Subsequence	CSIS Start, min	CSIS End, min	CSRS Start, min	CSRS End, min	Leakage in Compartment 1: Time Interval, min	Leak Rate,(a) v/hr	Pressure MPa	Pressure psia	Temp. °F	Temp. °C	Leakage in Compartment 2: Leak Rate,(b) v/hr	Pressure MPa	Pressure psia	Temp. °F	Temp. °C	Remarks
S2HF-Y	40.9	52.7	52.7	107.7	162.9	12.6	0.13	20	192	89	4.2E-4	0.13	20	103	40	Core uncovers
					162.9-195.9	12.9	0.13	20	296	102	4.2E-4	0.13	20	105	41	Core heats
					195.9-197.7	12.7	0.13	20	313	156	4.2E-4	0.13	20	105	41	Ice melt complete
					197.7-201.68	13.8	0.13	20	458	167	4.2E-4	0.13	20	102	39	Core heats
					201.68-201.73	569.5	0.16	23	916	491	4.2E-4	0.16	23	154	68	Hydrogen burns
					201.73-201.75	224.0	0.18	27	1689	921	4.2E-4	0.18	27	231	110	Hydrogen burns
					201.75-201.9	4.2E-4	0.18	27	1474	801	4.2E-4	0.18	27	212	100	Core melts
					201.9-203.68	6.5	0.15	22	702	372	4.2E-4	0.15	22	123	51	Core melts
					203.68-203.73	509.0	0.16	24	1042	561	4.2E-4	0.16	24	164	74	Hydrogen burns
					203.73-203.88	42.2	0.18	27	1609	876	4.2E-4	0.18	27	236	113	Hydrogen burns
					203.88-204.43	1.6	0.16	24	1019	548	4.2E-4	0.16	24	170	76	Core melts
					204.43-205.06	22.3	0.15	22	690	366	4.2E-4	0.15	22	126	52	Core melts
					205.06-205.11	426.6	0.17	26	1406	763	4.2E-4	0.17	26	192	89	Hydrogen burns
					205.11-205.18	66.1	0.19	28	1889	1031	4.2E-4	0.19	28	245	118	Core melts
					205.18-206.0	2.3	0.17	26	1100	594	4.2E-4	0.17	26	188	86	Core melts
					206.0-206.21	33.0	0.15	22	765	407	4.2E-4	0.15	22	138	59	Core melts
					206.21-206.40	63.6	0.19	28	1673	912	4.2E-4	0.19	28	242	117	Hydrogen burns
					206.40-207.18	2.9	0.17	26	976	525	4.2E-4	0.17	26	169	76	Core melts
					207.18-207.23	448.9	0.18	27	1408	765	4.2E-4	0.18	27	196	91	Hydrogen burns
					207.23-207.26	175.1	0.21	31	2228	1220	4.2E-4	0.21	31	268	131	Hydrogen burns
					207.26-207.93	1.7	0.18	27	1252	678	4.2E-4	0.18	27	205	96	Core melts

(a) Normalized to a containment free volume of 3.877×10^5 ft^3. Units are volume fraction/hr. Leakage is from Compartment 1 to Compartment 2.

(b) Normalized to a compartment free volume of 8.979×10^5 ft^3. Units are volume fraction/hr. Leakage is from Compartment 2 to the environment.

TABLE 6.5 SUMMARY OF CONTAINMENT FLOWS AND LEAKAGES

Subsequence	CSIS Start, min	CSIS End, min	CSRS Start, min	CSRS End, min	Leakage in Compartment 1: Time Interval, min	Leak Rate,(a) v/hr	Pressure MPa	Pressure psia	Temp. °F	Temp. °C	Leakage in Compartment 2: Leak Rate,(b) v/hr	Pressure MPa	Pressure psia	Temp. °F	Temp. °C	Remarks
S2HF-Y (Continued)					207.93-208.1	89.8	0.17	26	935	502	4.2E-4	0.17	26	158	70	Core slump begins
					208.1-208.2	173.7	0.20	30	2091	1144	4.2E-4	0.21	31	261	127	Hydrogen burns
					208.2-208.5	5.2	0.19	28	1379	748	4.2E-4	0.19	28	232	111	Core slumps
					208.5-208.9	66.6	0.18	27	1100	594	4.2E-4	0.18	27	193	90	Core collapses
					208.9-208.97	52.1	0.22	33	2444	1340	4.2E-4	0.22	33	312	156	Hydrogen burns
					208.97-210.25	5.0	0.19	28	1097	592	4.2E-4	0.19	28	208	98	Reactor vessel heatup
					210.25-210.32	414.0	0.20	30	1432	778	4.2E-4	0.20	30	219	104	Hydrogen burns
					210.32-210.33	90.8	0.22	33	2111	1155	4.2E-4	0.22	33	286	141	Boiloff of H_2O
					210.33-211.31	4.2	0.19	28	1117	603	4.2E-4	0.19	28	218	103	Boiloff of H_2O
					211.31-213.68	10.7	0.18	27	583	306	4.2E-4	0.18	27	168	75	Boiloff of H_2O
					213.68-228.88	10.4	0.21	31	369	187	4.2E-4	0.21	31	191	88	Boiloff of H_2O
					228.88-259.6	6.2	0.24	35	264	129	4.2E-4	0.24	35	242	116	Boiloff of H_2O
					259.6	8.2	0.24	35	227	108	4.2E-4	0.24	35	261	127	Reactor vessel fails
					259.6-290.4	5.5	0.26	38	259	126	4.2E-4	0.26	38	280	138	Concrete decomposition
					290.4-352.2	6.1	0.32	47	401	205	4.2E-4	0.32	47	358	181	Concrete decomposition
					352.2-352.5	12.8	0.73	107	1681	916	64.3	0.73	107	1477	803	Hydrogen burn, cont. fails
					352.5-356.2	12.4	0.30	45	822	439	17.4	0.30	45	744	395	Concrete decomposition
					356.2-860.2	1.2	0.15	15	363	184	0.6	0.15	15	378	192	Concrete decomposition

(a) Normalized to a containment free volume of 3.877×10^5 ft^3. Units are volume fraction/hr. Leakage is from Compartment 1 to Compartment 2.

(b) Normalized to a compartment free volume of 3.979×10^5 ft^3. Units are volume fraction/hr. Leakage is from Compartment 2 to the environment.

TABLE 6.6. INVENTORIES OF RADIONUCLIDES AND STRUCTURAL MATERIALS FOR SEQUOYAH

Fission Products		Actinides/Structural	
Element	Mass (kg)	Element	Mass (kg)
Kr	17.0	U	101,156
Rb	18.7	Pu	596
Sr	60.9	Zr	20,897
Y	29.1	Sn	332
Zr	227	Ag	2,287
Mo	197	In	421
Tc	47.2	Cd	144
Ru	132	Fe	8,237
Rh	26.6		
Pd	66.8		
Te	31.7		
I	15.2		
Xe	330		
Cs	106		
Ba	77.7		
La	79.2		
Ce	167		
Pr	64.5		
Nd	217		
Sm	43.2		

TABLE 6.6b. INITIAL INVENTORIES OF ADDITIONAL SPECIES INCLUDED IN GROUPED RELEASE CALCULATIONS

Element	Mass (kg)
Eu	11.3
Nb	3.5
Np	33.0
Pm	9.2

TABLE 6.6c. CORSOR RESULTS WITH AND WITHOUT RSS GROUPING

	Without RSS Grouping		With RSS Grouping	
Group	Initial Inventory (kg)	Final CORSOR Releases (kg) S_2HF	Initial Inventory (kg)	Final CORSOR Releases (kg) S_2HF
Xe	347	347	347	347
I	15.2	15.2*	15.2	15.2*
Cs	166	166*	185	185*
Te	31.7	26.7	31.7	26.6
Sr	NA	NA	13.9	15.13
Ru	NA	NA	470	21.2
La	NA	NA	1480.0	0.30
Aerosol	134171	1533	133474	1499

	Not Grouped S_2HF	Grouped S_2HF
CsI	31.0	31.0
CsOH	169	190

*CORSOR releases these species in the form of CsI and CsOH.

TABLE 6.7. GEOMETRIC AND POWER PEAKING FACTORS FOR CORE CONFIGURATION OF THE SEQUOYAH PLANT

Radial Power Peaking Factor	Axial Power Peaking Factor	Fraction of Core in Radial Zone
1.03	0.09	0.047
1.05	0.26	0.062
1.04	0.43	0.083
1.04	0.59	0.062
1.06	0.74	0.062
1.05	0.89	0.062
1.03	1.02	0.083
1.04	1.14	0.124
0.95	1.24	0.166
0.71	1.32	0.249
	1.39	
	1.43	
	1.44	
	1.45	
	1.43	
	1.41	
	1.35	
	1.27	
	1.18	
	1.07	
	0.94	
	0.80	
	0.63	
	0.49	

TABLE 6.8. MATERIAL PRESENT IN MELT AT TIME OF RPV FAILURE FOR THE SEQUOYAH PLANT

Species	S_2HF Melt Content (kg)	TMLB Melt Content (kg)
Cs	0.1	1.5
I	--	0.1
Xe	0.1	3.1
Kr	--	0.2
Te	5.0	23.2
Ba	65.9	64.5
Sn	195	206
Ru	131	131
UO_2	100995	100992
Zr	7858	11800
ZrO_2	20580	15260
Fe	65220	49840
Mo	177	180
Sr	57.6	56.7
Ag	1217	1247
Cd	92	96
In	123	117
Sb	0.5	0.5

TABLE 6.9. MELT CONTENT AT RPV FAILURE FOR SPECIES NOT SPECIFICALLY INCLUDED IN CORSOR CALCULATIONS FOR SEQUOYAH PLANT

Species	S_2HF Melt Content (kg)	TMLB Melt Content (kg)	Reference Species (kg)
Rb	--	0.2	Cs
Y	29.1	29.1	UO_2
Tc	46.8	46.8	Ru
Rh	26.4	26.4	Ru
Pd	66.3	66.3	Ru
La	79.2	79.2	UO_2
Ce	167	167	UO_2
Pr	64.5	64.5	UO_2
Nd	217	217	UO_2
Sm	43.2	43.2	UO_2
Pu	596	596	UO_2
Cr	10220	7810	(a)
Mn	200	200	Fe
Ni	5679	4339	(a)

(a) These values are taken from the MARCH code predictions.

TABLE 6.10. AEROSOL COMPOSITION AND TOTAL RELEASE RATE FOR SEQUOYAH TMLB, CORE CONCRETE-INTERACTION

Species, %	Time, sec											
	0	1200	2400	3600	4800	6000	7200	8400	9600	10800	12000	13200
FeO	--	10.9	11.4	16.3	17.6	20.2	0.62	1.07	1.07	0.96	0.87	0.80
Cr_2O_3	--	--	--	--	--	--	0.64	0.74	0.01	0.016	0.019	0.022
Ni	0.3	0.28	0.30	0.45	0.38	0.24	1.20	1.16	0.73	0.59	0.53	0.50
Mo	--	1×10^{-7}	1×10^{-7}	2×10^{-7}	2×10^{-7}	6×10^{-8}	3×10^{-4}	3×10^{-4}	2×10^{-4}	2×10^{-4}	3×10^{-4}	6×10^{-4}
Ru	--	1×10^{-6}	1×10^{-6}	2×10^{-6}	1×10^{-6}	5×10^{-7}	2×10^{-6}	2×10^{-6}	7×10^{-7}	4×10^{-7}	3×10^{-7}	3×10^{-7}
Sn	0.3	0.22	0.23	0.34	0.31	0.24	3.20	3.48	3.29	3.40	3.68	4.09
Sb	7×10^{-5}	5×10^{-5}	5×10^{-5}	7×10^{-5}	7×10^{-5}	6×10^{-5}	3×10^{-4}	3×10^{-4}	3×10^{-4}	4×10^{-4}	4×10^{-4}	4×10^{-4}
Te	0.81	0.52	0.53	0.73	0.69	0.61	3.10	3.02	3.85	4.18	4.34	4.44
Ag + In	12.6	9.86	10.5	15.3	13.7	10.4	53.2	52.4	47.2	44.4	43.1	42.5
Mn	3.65	2.73	2.86	4.11	3.69	2.86	14.5	14.2	13.7	13.3	13.1	13.1
CaO	--	11.07	11.7	16.8	18.1	20.6	1.54	1.67	1.67	1.65	1.65	1.68
Al_2O_3	--	4×10^{-5}	8×10^{-5}	2×10^{-4}	2×10^{-4}	3×10^{-4}	2×10^{-3}	2×10^{-3}	3×10^{-3}	4×10^{-3}	5×10^{-3}	5×10^{-3}
Na_2O	--	2.48	2.50	3.55	3.01	1.93	0.54	0.70	1.00	1.13	1.17	1.16
K_2O	--	9.66	10.3	14.9	16.4	18.5	15.4	15.7	23.4	26.8	27.9	27.9
SiO_2	--	13.21	14.8	21.8	22.1	22.5	1.29	1.08	0.52	0.34	0.26	0.20
UO_2	0.37	0.29	0.28	0.38	0.29	0.18	4.59	4.64	3.23	2.98	3.06	3.30
ZrO_2	0.014	8×10^{-3}	9×10^{-3}	0.013	0.015	0.018	0.09	0.09	0.15	0.18	0.19	0.20
Cs_2O	1.04	0.49	0.44	--	--	--	--	--	--	--	--	--
BaO	4.40	2.13	1.76	1.94	1.42	0.72	0.06	0.06	0.07	0.076	0.081	0.087
SrO	5.94	3.09	2.49	2.69	1.82	0.80	7×10^{-3}	6×10^{-3}	6×10^{-3}	6×10^{-3}	6×10^{-3}	7×10^{-3}
La_2O_3	4×10^{-4}	2×10^{-4}	2×10^{-4}	3×10^{-4}	3×10^{-4}	3×10^{-4}	1×10^{-3}	1×10^{-3}	2×10^{-3}	3×10^{-3}	3×10^{-3}	3×10^{-3}
CeO_2	0.77	0.62	0.55	0.66	0.40	0.12	2×10^{-3}	2×10^{-3}	3×10^{-3}	4×10^{-3}	4×10^{-3}	4×10^{-3}
Nb_2O_5	4×10^{-6}	1×10^{-5}	1×10^{-5}	2×10^{-5}	1×10^{-5}	3×10^{-6}	1×10^{-5}	1×10^{-5}	2×10^{-5}	3×10^{-5}	3×10^{-5}	3×10^{-5}
CsI	0.88	0.010	6×10^{-5}	--	--	--	--	--	--	--	--	--
Cd	68.9	32.4	29.2	--	--	--	--	--	--	--	--	--
Source Rate (above pool) g/sec	13.4	24.7	29.1	32.6	42.9	37.6	6.21	4.44	1.82	0.98	0.66	0.51

TABLE 6.10. (Continued)

Species, %	Time, sec											
	T4400	T5600	T6800	T8000	T9200	20400	21600	22800	24000	25200	26400	27600
FeO	0.74	0.72	0.75	0.83	0.91	1.00	1.07	1.14	1.21	1.27	1.30	1.38
Cr_2O_3	0.023	0.024	0.025	0.025	0.024	0.024	0.024	0.024	0.023	0.023	0.023	0.022
Ni	0.49	0.48	0.47	0.46	0.46	0.45	0.45	0.44	0.44	0.44	0.44	0.46
Mo	1×10^{-3}	2×10^{-3}	2×10^{-3}	3×10^{-3}	3×10^{-3}	3×10^{-3}	3×10^{-3}	3×10^{-3}	3×10^{-3}	3×10^{-3}	3×10^{-3}	3×10^{-3}
Ru	--	--	--	--	--	--	--	--	--	--	--	--
Sn	4.66	5.26	5.66	5.82	5.89	5.92	5.94	5.95	5.96	5.97	6.06	6.16
Sb	4×10^{-4}	4×10^{-4}	4×10^{-4}	4×10^{-4}	4×10^{-4}	4×10^{-4}	5×10^{-4}	5×10^{-4}	5×10^{-4}	5×10^{-4}	5×10^{-4}	5×10^{-4}
Te	4.49	4.52	4.53	4.53	4.52	4.50	4.49	4.49	4.48	4.46	4.49	4.45
Ag + In	42.4	42.1	41.9	41.7	41.6	41.5	41.4	41.3	41.2	41.2	41.7	42.5
Mn	13.1	13.1	13.1	13.0	13.0	13.0	13.0	13.0	13.0	12.9	13.0	13.2
CaO	1.73	1.77	1.79	1.80	1.79	1.78	1.78	1.77	1.76	1.75	1.48	1.28
Al_2O_3	5×10^{-3}	5×10^{-3}	6×10^{-3}	6×10^{-3}	6×10^{-3}	6×10^{-3}	6×10^{-3}	6×10^{-3}	6×10^{-3}	6×10^{-3}	6×10^{-3}	6×10^{-3}
Na_2O	1.11	1.07	1.05	1.05	1.06	1.07	1.08	1.08	1.09	1.10	1.11	1.11
K_2O	27.1	26.4	26.0	26.1	26.2	26.3	26.5	26.6	26.8	26.9	26.5	25.7
SiO_2	0.16	0.14	0.12	0.11	0.11	0.11	0.10	0.10	0.10	0.10	0.10	0.10
UO_2	3.68	4.06	4.25	4.24	4.14	4.03	3.91	3.79	3.67	3.58	3.46	3.38
ZrO_2	0.20	0.20	0.20	0.20	0.20	0.19	0.19	0.19	0.19	0.18	0.18	0.18
CsO_2	--	--	--	--	--	--	--	--	--	--	--	--
BaO	0.095	0.102	0.105	0.105	0.103	0.100	0.098	0.096	0.094	0.092	0.071	0.056
SrO	7×10^{-3}	7×10^{-3}	7×10^{-3}	7×10^{-3}	7×10^{-3}	7×10^{-3}	7×10^{-3}	6×10^{-3}	6×10^{-3}	6×10^{-3}	5×10^{-3}	4×10^{-3}
La_2O_3	3×10^{-3}	3×10^{-3}	3×10^{-3}	3×10^{-3}	3×10^{-3}	3×10^{-3}	3×10^{-3}	3×10^{-3}	3×10^{-3}	3×10^{-3}	3×10^{-3}	2×10^{-3}
CeO_2	4×10^{-3}	4×10^{-3}	4×10^{-3}	4×10^{-3}	4×10^{-3}	4×10^{-3}	4×10^{-3}	4×10^{-3}	4×10^{-3}	4×10^{-3}	4×10^{-3}	4×10^{-3}
Nb_2O_5	3×10^{-5}	3×10^{-5}	3×10^{-5}	3×10^{-5}	3×10^{-5}	3×10^{-5}	3×10^{-5}	3×10^{-5}	3×10^{-5}	3×10^{-5}	3×10^{-5}	3×10^{-5}
CsI	--	--	--	--	--	--	--	--	--	--	--	--
Cd	--	-- --	--	--	--	--	--	--	--	--	--	--
Source Rate (above pool) g/sec	0.45	0.31	0.22	0.18	0.14	0.11	0.09	0.08	0.06	0.05	0.06	0.07

TABLE 6.11. (Continued)

Species, %	Time, sec											
	14400	15600	16800	18000	19200	20400	21600	22800	24000	25200	26400	27600
FeO	0.74	0.72	0.75	0.83	0.91	1.00	1.07	1.14	1.21	1.27	1.30	1.38
Cr_2O_3	0.023	0.024	0.025	0.025	0.024	0.024	0.024	0.024	0.023	0.023	0.023	0.022
Ni	0.49	0.48	0.47	0.46	0.46	0.45	0.45	0.44	0.44	0.44	0.44	0.46
Mo	1×10^{-3}	2×10^{-3}	2×10^{-3}	3×10^{-3}	3×10^{-3}	3×10^{-3}	3×10^{-3}	3×10^{-3}	3×10^{-3}	3×10^{-3}	3×10^{-3}	3×10^{-3}
Ru	--	--	--	--	--	--	--	--	--	--	--	--
Sn	4.66	5.26	5.66	5.82	5.89	5.92	5.94	5.95	5.96	5.97	6.06	6.16
Sb	4×10^{-4}	4×10^{-4}	4×10^{-4}	4×10^{-4}	4×10^{-4}	4×10^{-4}	5×10^{-4}	5×10^{-4}	5×10^{-4}	5×10^{-4}	5×10^{-4}	5×10^{-4}
Te	4.49	4.52	4.53	4.53	4.52	4.50	4.49	4.49	4.48	4.46	4.49	4.45
Ag + In	42.4	42.1	41.9	41.7	41.6	41.5	41.4	41.3	41.2	41.2	41.7	42.5
Mn	13.1	13.1	13.1	13.0	13.0	13.0	13.0	13.0	13.0	12.9	13.0	13.2
CaO	1.73	1.77	1.79	1.80	1.79	1.78	1.78	1.77	1.76	1.75	1.48	1.28
Al_2O_3	5×10^{-3}	5×10^{-3}	6×10^{-3}	6×10^{-3}	6×10^{-3}	6×10^{-3}	6×10^{-3}	6×10^{-3}	6×10^{-3}	6×10^{-3}	6×10^{-3}	6×10^{-3}
Na_2O	1.11	1.07	1.05	1.05	1.06	1.07	1.08	1.08	1.09	1.10	1.11	1.11
K_2O	27.1	26.4	26.0	26.1	26.2	26.3	26.5	26.6	26.8	26.9	26.5	25.7
SiO_2	0.16	0.14	0.12	0.11	0.11	0.11	0.10	0.10	0.10	0.10	0.10	0.10
UO_2	3.68	4.06	4.25	4.24	4.14	4.03	3.91	3.79	3.67	3.58	3.46	3.38
ZrO_2	0.20	0.20	0.20	0.20	0.20	0.19	0.19	0.19	0.19	0.18	0.18	0.18
Cs_2O	--	--	--	--	--	--	--	--	--	--	--	--
BaO	0.095	0.102	0.105	0.105	0.103	0.100	0.098	0.096	0.094	0.092	0.071	0.056
SrO	7×10^{-3}	7×10^{-3}	7×10^{-3}	7×10^{-3}	7×10^{-3}	7×10^{-3}	7×10^{-3}	6×10^{-3}	6×10^{-3}	6×10^{-3}	5×10^{-3}	4×10^{-3}
La_2O_3	3×10^{-3}	3×10^{-3}	3×10^{-3}	3×10^{-3}	3×10^{-3}	3×10^{-3}	3×10^{-3}	3×10^{-3}	3×10^{-3}	3×10^{-3}	3×10^{-3}	2×10^{-3}
CeO_2	4×10^{-3}	4×10^{-3}	4×10^{-3}	4×10^{-3}	4×10^{-3}	4×10^{-3}	4×10^{-3}	4×10^{-3}	4×10^{-3}	4×10^{-3}	4×10^{-3}	4×10^{-3}
Nb_2O_5	3×10^{-5}	3×10^{-5}	3×10^{-5}	3×10^{-5}	3×10^{-5}	3×10^{-5}	3×10^{-5}	3×10^{-5}	3×10^{-5}	3×10^{-5}	3×10^{-5}	3×10^{-5}
CsI	--	--	--	--	--	--	--	--	--	--	--	--
Cd	--	--	--	--	--	--	--	--	--	--	--	--
Source Rate (above pool) g/sec	0.09	0.08	0.07	0.07	0.07	0.07	0.07	0.06	0.06	0.06	0.07	0.09

TABLE 6.11. AEROSOL COMPOSITION AND TOTAL RELEASE RATE FOR SEQUOYAH TML, CORE-CONCRETE INTERACTION

Species, %	Time, sec											
	0	1200	2400	3600	4800	6000	7200	8400	9600	10800	12000	13200
FeO	--	10.9	11.4	16.3	17.6	20.2	0.62	1.07	1.07	0.96	0.87	0.80
Cr_2O_3	--	--	--	--	--	--	0.64	0.74	0.01	0.016	0.019	0.022
Ni	0.3	0.28	0.30	0.45	0.38	0.24	1.20	1.16	0.73	0.59	0.53	0.50
Mo	--	1×10^{-7}	1×10^{-7}	2×10^{-7}	2×10^{-7}	6×10^{-8}	3×10^{-4}	3×10^{-4}	2×10^{-4}	2×10^{-4}	3×10^{-4}	6×10^{-4}
Ru	--	1×10^{-6}	1×10^{-6}	2×10^{-6}	1×10^{-6}	5×10^{-7}	2×10^{-6}	2×10^{-6}	7×10^{-7}	4×10^{-7}	3×10^{-7}	3×10^{-7}
Sn	0.3	0.22	0.23	0.34	0.31	0.24	3.20	3.48	3.29	3.40	3.68	4.09
Sb	7×10^{-5}	5×10^{-5}	5×10^{-5}	7×10^{-5}	7×10^{-5}	6×10^{-5}	3×10^{-4}	3×10^{-4}	3×10^{-4}	4×10^{-4}	4×10^{-4}	4×10^{-4}
Te	0.81	0.52	0.53	0.73	0.69	0.61	3.10	3.02	3.85	4.18	4.34	4.44
Ag + In	12.6	9.86	10.5	15.3	13.7	10.4	53.2	52.4	47.2	44.4	43.1	42.5
Mn	3.65	2.73	2.86	4.11	3.69	2.86	14.5	14.2	13.7	13.3	13.1	13.1
CaO	--	11.07	11.7	16.8	18.1	20.6	1.54	1.67	1.67	1.65	1.65	1.68
Al_2O_3	--	4×10^{-5}	8×10^{-5}	2×10^{-4}	2×10^{-4}	3×10^{-4}	2×10^{-3}	2×10^{-3}	2×10^{-3}	4×10^{-3}	5×10^{-3}	5×10^{-3}
Na_2O	--	2.48	2.50	3.55	3.01	1.93	0.54	0.70	1.00	1.13	1.17	1.16
K_2O	--	9.66	10.3	14.9	16.4	18.5	15.4	15.7	23.4	26.8	27.9	27.9
SiO_2	--	13.21	14.8	21.8	22.1	22.5	1.29	1.08	0.52	0.34	0.26	0.20
UO_2	0.37	0.29	0.28	0.38	0.29	0.18	4.59	4.64	3.23	2.98	3.06	3.30
ZrO_2	0.014	8×10^{-3}	9×10^{-3}	0.013	0.015	0.018	0.09	0.09	0.15	0.18	0.19	0.20
Cs_2O	1.04	0.49	0.44	--	--	--	--	--	--	--	--	--
BaO	4.40	2.13	1.76	1.94	1.42	0.72	0.06	0.06	0.07	0.076	0.081	0.087
SrO	5.94	3.09	2.49	2.69	1.82	0.80	7×10^{-3}	6×10^{-3}	6×10^{-3}	6×10^{-3}	6×10^{-3}	7×10^{-3}
La_2O_3	4×10^{-4}	2×10^{-4}	2×10^{-4}	3×10^{-4}	3×10^{-4}	3×10^{-4}	1×10^{-3}	1×10^{-3}	2×10^{-3}	3×10^{-3}	3×10^{-3}	3×10^{-3}
CeO_2	0.77	0.62	0.55	0.66	0.40	0.12	2×10^{-3}	2×10^{-3}	3×10^{-3}	4×10^{-3}	4×10^{-3}	4×10^{-3}
Nb_2O_5	4×10^{-6}	1×10^{-5}	1×10^{-5}	2×10^{-5}	1×10^{-5}	3×10^{-6}	1×10^{-5}	1×10^{-5}	2×10^{-5}	3×10^{-5}	3×10^{-5}	3×10^{-5}
CsI	0.88	0.010	6×10^{-5}	--	--	--	--	--	--	--	--	--
Cd	68.9	32.4	29.2	--	--	--	--	--	--	--	--	--
Source Rate (above pool) g/sec	1.41	2.71	2.95	3.17	4.50	4.40	0.61	0.49	0.24	0.15	0.11	0.09

TABLE 6.12. AEROSOL COMPOSITION AND TOTAL RELEASE RATE FOR SEQUOYAH S_2HF, CORE-CONCRETE INTERACTION

Species, %	Time, sec											
	0	1200	2400	3600	4800	6000	7200	8400	9600	10800	12000	13200
FeO	--	11.7	12.4	19.1	0.23	1.18	1.60	1.82	1.65	1.44	1.30	1.21
Cr_2O_3	--	--	--	--	2×10^{-4}	1.04	1.08	1.05	0.02	0.02	0.03	0.03
Ni	0.34	0.32	0.32	0.40	1.68	1.49	1.44	1.44	0.92	0.71	0.62	0.59
Mo	8×10^{-8}	1×10^{-7}	1×10^{-7}	1×10^{-7}	2×10^{-4}	3×10^{-4}	3×10^{-4}	4×10^{-4}	2×10^{-4}	2×10^{-4}	2×10^{-4}	3×10^{-4}
Ru	6×10^{-7}	9×10^{-7}	8×10^{-7}	9×10^{-7}	3×10^{-6}	2×10^{-6}	2×10^{-6}	2×10^{-6}	7×10^{-7}	4×10^{-7}	3×10^{-7}	3×10^{-7}
Sn	0.15	0.12	0.12	0.16	2.49	2.51	2.63	2.78	2.37	2.27	2.34	2.50
Sb	2×10^{-5}	1×10^{-5}	1×10^{-5}	2×10^{-5}	1×10^{-4}	1×10^{-4}	1×10^{-4}	1×10^{-4}	1×10^{-4}	1×10^{-4}	1×10^{-4}	1×10^{-4}
Te	0.16	0.10	0.10	0.13	0.70	0.69	0.67	0.65	0.83	0.91	0.95	0.97
Ag	11.1	8.49	8.64	11.5	53.7	50.9	49.8	49.3	44.4	41.0	39.3	38.7
Mn	3.28	2.39	2.42	3.23	15.3	14.6	14.2	13.95	13.5	12.9	12.6	12.5
CaO	--	11.8	12.7	19.5	1.47	1.62	1.96	2.06	1.83	1.73	1.71	1.74
Al_2O_3	--	4×10^{-5}	8×10^{-5}	2×10^{-4}	1×10^{-3}	2×10^{-3}	2×10^{-3}	2×10^{-3}	3×10^{-3}	4×10^{-3}	5×10^{-3}	5×10^{-3}
Na_2O	--	2.51	2.54	3.34	0.44	0.84	0.98	1.06	1.45	1.62	1.68	1.68
K_2O	--	10.2	11.0	17.3	15.4	17.6	18.3	18.6	28.2	33.4	35.5	36.1
SiO_2	--	13.3	14.4	21.7	1.55	1.30	1.21	1.18	0.64	0.42	0.32	0.27
UO_2	0.38	0.30	0.27	0.31	6.82	5.94	5.83	5.87	3.91	3.33	3.22	3.31
ZrO_2	0.02	0.01	0.01	0.02	0.11	0.12	0.11	0.10	0.16	0.20	0.22	0.23
Cs_2O	0.07	0.03	0.03	--	--	--	--	--	--	--	--	--
BaO	3.41	1.57	1.25	1.26	0.10	0.10	0.11	0.10	0.10	0.10	0.10	0.11
SrO	4.56	2.28	1.76	1.67	0.01	0.01	0.01	0.01	0.01	0.01	9×10^{-3}	9×10^{-3}
La_2O_3	4×10^{-4}	2×10^{-4}	2×10^{-4}	3×10^{-4}	2×10^{-3}	2×10^{-3}	2×10^{-3}	1×10^{-3}	2×10^{-3}	3×10^{-3}	3×10^{-3}	3×10^{-3}
CeO_2	0.57	0.44	0.34	0.29	3×10^{-3}	3×10^{-3}	2×10^{-3}	2×10^{-3}	3×10^{-3}	4×10^{-3}	4×10^{-3}	5×10^{-3}
Nb_2O_5	5×10^{-6}	1×10^{-5}	1×10^{-5}	2×10^{-5}	2×10^{-5}	2×10^{-5}	2×10^{-5}	2×10^{-5}	3×10^{-5}	3×10^{-5}	3×10^{-5}	4×10^{-5}
CsI	--	--	--	--	--	--	--	--	--	--	--	--
Cd	75.97	34.40	31.69	--	--	--	--	--	--	--	--	--
Source Rate g/sec	66.8	142.0	163.0	158.0	30.3	18.5	12.8	14.9	8.50	4.84	3.16	2.57

TABLE 6.12. (Continued)

Species, %	Time, sec											
	14400	15600	16800	18000	19200	20400	21600	22800	24000	25200	26400	27600
FeO	1.13	1.07	1.02	0.99	1.00	1.04	1.11	1.18	1.26	1.34	1.41	1.48
Cr_2O_3	0.03	0.03	0.04	0.04	0.04	0.04	0.04	0.04	0.04	0.04	0.04	0.04
Ni	0.57	0.56	0.56	0.55	0.55	0.54	0.54	0.53	0.53	0.53	0.53	0.52
Mo	4×10^{-4}	6×10^{-4}	9×10^{-4}	1×10^{-3}	2×10^{-3}	2×10^{-3}	2×10^{-3}	2×10^{-3}	3×10^{-3}	3×10^{-3}	3×10^{-3}	3×10^{-3}
Ru	--	--	--	--	--	--	--	--	--	--	--	--
Sn	2.73	3.02	3.37	3.75	4.07	4.28	4.39	4.45	4.47	4.50	4.51	4.51
Sb	1×10^{-4}	1×10^{-4}	1×10^{-4}	1×10^{-4}	2×10^{-4}	2×10^{-4}	2×10^{-4}	2×10^{-4}	2×10^{-4}	2×10^{-4}	2×10^{-4}	2×10^{-4}
Te	0.99	1.00	1.01	1.01	1.02	1.02	1.02	1.02	1.02	1.01	1.01	1.01
Ag	38.5	38.5	38.6	38.6	38.6	38.5	38.4	38.3	38.2	38.3	38.2	38.2
Mn	12.5	12.6	12.6	12.7	12.7	12.8	12.7	12.7	12.7	12.7	12.7	12.7
CaO	1.77	1.82	1.87	1.92	1.96	1.98	1.99	1.99	1.99	1.99	1.99	1.98
Al_2O_3	6×10^{-3}	6×10^{-3}	6×10^{-3}	6×10^{-3}	6×10^{-3}	7×10^{-3}	7×10^{-3}	7×10^{-3}	7×10^{-3}	7×10^{-3}	7×10^{-3}	7×10^{-3}
Na_2O	1.65	1.61	1.55	1.50	1.46	1.44	1.43	1.43	1.44	1.44	1.44	1.44
K_2O	36.0	35.5	34.8	34.0	33.4	33.2	33.2	33.1	33.3	33.2	33.3	33.4
SiO_2	0.23	0.20	0.18	0.16	0.14	0.13	0.13	0.13	0.12	0.12	0.12	0.12
UO_2	3.48	3.72	4.04	4.35	4.60	4.70	4.68	4.62	4.52	4.44	4.34	4.24
ZrO_2	0.23	0.24	0.24	0.24	0.23	0.23	0.23	0.23	0.22	0.22	0.22	0.22
Cs_2O	--	--	--	--	--	--	--	--	--	--	--	--
BaO	0.11	0.12	0.12	0.13	0.14	0.14	0.14	0.14	0.13	0.13	0.13	0.13
SrO	9×10^{-3}	0.01	0.01	0.01	0.01	0.01	0.01	0.01	0.01	9×10^{-3}	9×10^{-3}	9×10^{-3}
La_2O_3	3×10^{-3}	3×10^{-3}	3×10^{-3}	3×10^{-3}	3×10^{-3}	3×10^{-3}	3×10^{-3}	3×10^{-3}	3×10^{-3}	3×10^{-3}	3×10^{-3}	3×10^{-3}
CeO_2	5×10^{-3}	5×10^{-3}	5×10^{-3}	5×10^{-3}	5×10^{-3}	5×10^{-3}	5×10^{-3}	5×10^{-3}	5×10^{-3}	4×10^{-3}	4×10^{-3}	4×10^{-3}
Nb_2O_5	4×10^{-5}	4×10^{-5}	4×10^{-5}	4×10^{-5}	4×10^{-5}	4×10^{-5}	4×10^{-5}	4×10^{-3}	4×10^{-3}	3×10^{-5}	3×10^{-5}	3×10^{-5}
CsI	--	--	--	--	--	--	--	--	--	--	--	--
Cd	--	--	--	--	--	--	--	--	--	--	--	--
Source Rate g/sec	2.27	2.10	1.98	1.89	1.83	1.78	1.74	1.71	1.66	1.64	1.61	1.60

7. RESULTS AND DISCUSSION

7.1 Introduction

Results of calculations for the transport and deposition of radionuclides are presented and discussed in this section. The plants and sequences selected for consideration were discussed in Chapter 4, the analytical and calculational methods were described in Chapter 5, and the assumptions and bases for the calculations were described in Chapter 6. Results presented in this chapter include the deposition and release from the reactor coolant system of radionuclides leaving the core region. These results are based on TRAP-MELT code calculations. Also included as results are the masses of radionuclides airborne and deposited in the containment as well as the airborne materials leaked to the environment. These results are based on ICEDF calculations for retention in the ice condenser and NAUA-4 calculations for transport in the containment.

Three system sequences are considered in the analyses: TMLB', TML, and S_2HF. Depending upon the accident sequence, an overpressure failure mode and/or hydrogen burning were examined.

7.2 Transport and Deposition in Reactor Coolant System (RCS)

The analyses of the transport and deposition within the RCS of materials released from the melting core have been performed using the TRAP-MELT code which was described in Volume I of this report. The time frame of interest in the RCS for core meltdown accidents such as those considered here spans the period of time starting with the onset of core melting and ending with failure of the bottom head of the RPV. For accidents involving only minor fuel damage, the gap release term, which occurs prior to melting of fuel, may be the major release and require careful consideration. For the accidents examined here, however, this release term is insignificant in comparison with the melt release and the period immediately prior to the onset of core melting is not considered. Rather, the gap releases calculated by CORSOR are added to the initial material emitted by the melting core.

Releases from the melting core and their behavior in the RCS are simulated beyond the time of core collapse in these analyses. It should be recognized that the uncertainties in the behavior of the molten core in the lower plenum region are quite large. The analyses performed by the MARCH 2 code for this phase of the accident are greatly simplified. The rates of steam production as molten core material enters the lower plenum and the duration of time to failure of the reactor vessel have large associated uncertainties.

The heatup of the RCS structures downstream of the core is not modeled following dryout of the vessel. This is not expected to be a significant source of error since the surface temperatures in the core region are too high to permit condensation of the volatile species considered in these analyses prior to this period and there is little subsequent emission of these species from the core.

At the time of bottom head failure, the materials suspended in the RCS are assumed to exit the primary system through the bottom head without further attenuation. This results in a short duration "puff" release of aged material into the drywell at the time of vessel failure. Reentrainment of previously deposited particles or vapors is not considered to occur during this process.

One further aspect of the time frame of the primary system analyses which should be noted is that the primary system is not considered in the analyses after the molten core has left the RPV. Air ingress into the RPV and deposition of materials evolved during the core-concrete interaction is not considered, nor is the primary system considered as a potential source of fission products due to reevolution of previously deposited materials.

The analyses presented in the following section are subject to a number of uncertainties. Principal among these are the source rates of materials emitted by the core, and the details of the flow patterns in the RCS.

The results of the analyses of the transient sequences and the small pipe break sequence for the Sequoyah plant are discussed separately in the following sections. The transient sequences, TMLB' and TML, are identical with respect to their RCS behavior and so are not analyzed separately. The flow paths, associated geometry, and the timing of the core-melt period in the RCS can be found in Chapter 6.

7.2.1 RCS Transport and Deposition for Sequences TMLB' and TML

These sequences are characterized, from the perspective of the RCS, as high pressure, low gas flow rate scenarios for most of the in-vessel phase of the core melt. The principal contributors to fission product retention in the primary system for these sequences are the core region, the upper plenum, and the pressurizer. The behavior of the pressurizer quench tank and the potential for scrubbing in a water-filled quench tank are not addressed here.

Tables 7.1 and 7.2 illustrate the extent and location of fission product retention predicted by the TRAP-MELT code. Table 7.1 contains the cumulative mass of each species released as a function of time since the start of core melting and the current total mass retained throughout the RCS. Clearly, the materials released from the molten core experience significant depletion before reaching the containment atmosphere. Tellurium retention is due to its chemical reaction with the interior surfaces of the RCS to which it is exposed. The rapid rate of this interaction, coupled with the long residence time the emitted vapor experiences, results in its being nearly perfectly scavenged by the surfaces in the RCS, principally in the upper plenum. This is indicated in Figure 7.1.

CsOH has a lower surface reaction rate than does Te, while CsI has a rate so low as to be insignificant in comparison with the other retention processes. The mechanism which is almost totally responsible for the RCS retention of these species in this sequence is condensation on particles which are deposited in the RCS. It is seen in Table 7.2 that from the start of core melting to about 1200 s, the CsI and CsOH retention is under 20 percent of the material released from the core. This fraction retained then increases dramatically until at the time of bottom head failure approximately 80 percent of the emitted CsOH and CsI have been retained. The cause of this is that approximately 1200 s after the start of core melting the gas flow rate increases by two orders of magnitude, sweeping the vapors from the core--in which the temperature is too hot for condensation to occur--and into cooler regions such as the core plate and pressurizer where condensation on particles and subsequent deposition occurs. This behavior can be seen in Figures 7.2 and 7.3 also.

TABLE 7.1. CORSOR PREDICTIONS OF MASSES OF SPECIES RELEASED FROM THE CORE (TOTAL) AND TRAP-MELT PREDICTIONS OF MASSES RETAINED IN THE RCS (RET) DURING THE TMLB SEQUENCE FOR THE SEQUOYAH PLANT

(Times Measured from Start of Core Melting)

Time (s)	CsI		CsOH		Te		Aerosol	
	Ret (kg)	Total (kg)	Ret (kg)	Total (kg)	Ret (kg)	Total (kg)	Ret (kg)	Total (kg)
110	0.3	9.8	1.5	52.9	--	0.3	349	376
220	1.4	12.5	7.9	71.9	--	0.5	449	469
320	1.9	15.4	11.1	92.1	--	0.7	536	553
430	2.5	17.9	14.6	101	--	1.0	617	631
540	3.1	20	17.5	111	--	1.4	690	702
650	3.7	21.7	20.4	119	0.1	1.9	759	771
760	4.1	23.1	23.5	127	0.1	2.5	829	840
860	4.5	24.5	25.9	135	0.2	3.0	897	908
970	5.0	25.8	28.2	142	0.2	3.4	963	973
1080	5.3	26.9	30.4	147	0.3	3.9	1025	1035
1190	4.7	27.9	27.3	152	0.6	4.3	1090	1100
1300	12.4	27.6	69.4	156	3.3	4.7	1150	1180
1400	23.0	29.2	125	159	4.9	5.5	1205	1300
1510	24.4	29.8	134	161	5.9	6.2	1280	1400
1620	24.7	30.1	135	164	6.1	6.7	1320	1430
2160	25.2	30.8	137	168	7.8	8.5	1370	1490

TABLE 7.2. TRAP-MELT PREDICTIONS OF PRIMARY SYSTEM RETENTION FACTORS (RF) AND VOLUME SPECIFIC RETENTION FACTORS AS FUNCTIONS OF TIME FOR THE TMLB SEQUENCE FOR THE SEQUOYAH PLANT

Time (s)	CsI				CsOH				Te			Aerosol	
	RF	Core	Core Plate	Pres-surizer	RF	Core	Core Plate	Pres-surizer	RF	Core	Core Plate	RF	Core
110	.03	.02	.01	--	.03	.02	.01	--	.01	0	.01	.93	.93
220	.11	.10	.01	--	.11	.10	.01	--	.02	0	.02	.96	.95
320	.13	.10	.02	--	.12	.10	.02	--	.02	0	.02	.97	.97
430	.14	.11	.03	--	.15	.11	.03	--	.03	0	.03	.98	.98
540	.15	.12	.04	--	.16	.12	.04	--	.03	0	.03	.98	.98
650	.17	.12	.05	--	.17	.12	.05	--	.04	0	.04	.98	.99
760	.18	.12	.06	--	.19	.12	.06	--	.05	0	.05	.99	.99
860	.18	.11	.07	--	.19	.12	.07	--	.05	0	.05	.99	.99
970	.19	.11	.08	--	.20	.12	.08	--	.06	0	.06	.99	.99
1080	.20	.11	.09	--	.21	.12	.09	--	.07	0	.07	.99	.99
1190	.17	.04	.13	--	.18	.05	.13	--	.14	0	.14	.99	.99
1300	.43	--	.42	--	.45	--	.43	--	.69	0	.68	.97	.96
1400	.79	.07	.46	.23	.80	.06	.47	.23	.99	.11	.86	.93	.89
1510	.82	.07	.45	.27	.83	.06	.47	.27	.94	.14	.77	.91	.84
1620	.82	.07	.45	.27	.83	.07	.46	.27	.92	.14	.73	.92	.82
2160	.82	.07	.45	.27	.83	.07	.46	.27	.91	.14	.73	.92	.82

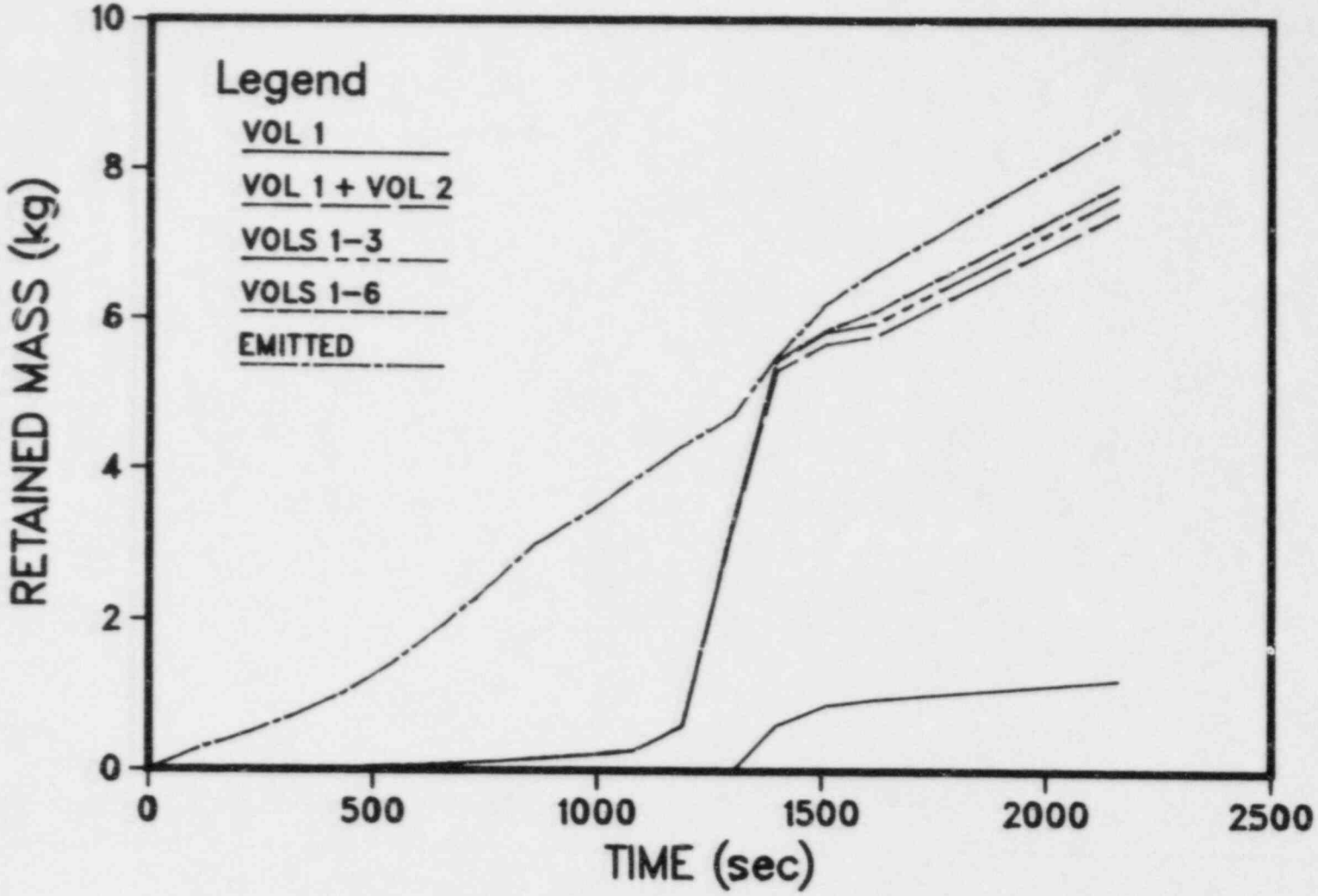

FIGURE 7.1. MASSES OF Te EMITTED FROM CORE AND RETAINED IN THE RCS CONTROL VOLUMES AS FUNCTIONS OF TIME FOR THE TMLB' SEQUENCE (Vol 1 = Core, Vol 2 = Upper Grid, Vol 3 = Guide Tubes, Vol 4 = Upper Plenum Annulus, Vol 5 = Hot Leg, Vol 6 = Pressurizer). Times measured from start of core melting.

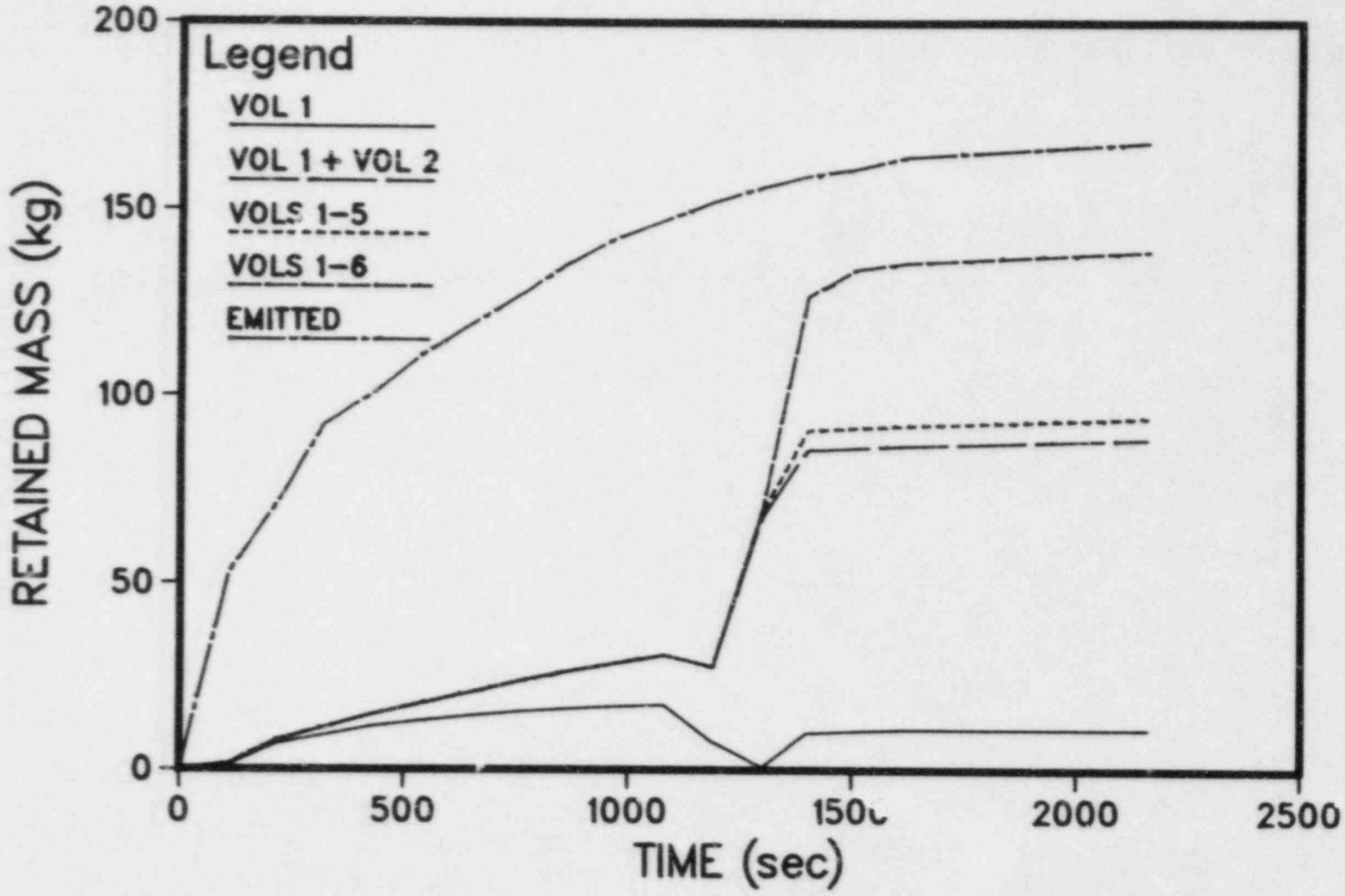

FIGURE 7.2. MASSES OF CsOH EMITTED FROM CORE AND RETAINED IN THE RCS CONTROL VOLUMES AS FUNCTIONS OF TIME FOR THE TMLB' SEQUENCE (Vol 1 = Core, Vol 2 = Upper Grid, Vol 3 = Guide Tubes, Vol 4 = Upper Plenum Annulus, Vol 5 = Hot Leg, Vol 6 = Pressurizer). Times measured from start of core melting.

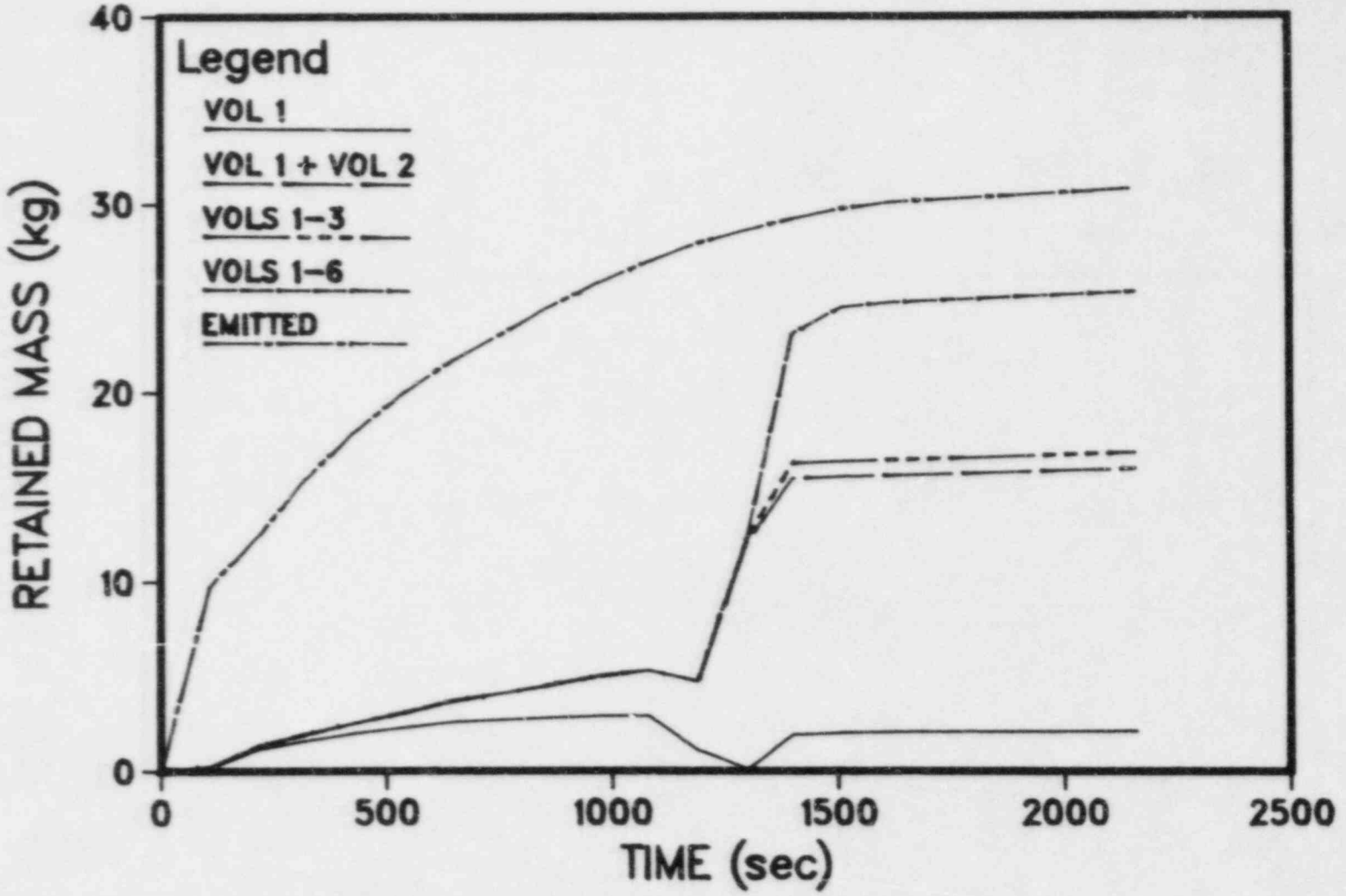

FIGURE 7.3. MASSES OF CsI EMITTED FROM CORE AND RETAINED IN THE RCS CONTROL VOLUMES AS FUNCTIONS OF TIME FOR THE TMLB' SEQUENCE (Vol 1 = Core, Vol 2 = Upper Grid, Vol 3 = Guide Tubes, Vol 4 = Upper Plenum Annulus, Vol 5 = Hot Leg, Vol 6 = Pressurizer). Times measured from start of core melting.

The increase in the gas flow rate is also reflected in the aerosol retention predictions contained in these tables. As the flow rate increases, the time available for deposition decreases, and the aerosol concentration decreases, leading to a reduction in the retention factor for the core and the entire RCS, even though the overall retention remains quite high as can be seen in Figure 7.4. The reduction in particle growth which occurs in the core region due to the higher flow rates is also indicated by the mass median diameter of the particles in this volume which is predicted to drop from 5.0 μm at 1200 s to 2.0 μm at 1400 s.

7.2.2 RCS Transport and Deposition for Sequence S_2HF

Unlike the transient sequences described above, this small pipe break sequence is characterized by steam and hydrogen flows on the order of 3-80 lb/s for the first 1200 seconds following the start of core melting. These correspond to flows of 0.2-0.4 lb/s for the transients, and thus result in much shorter RCS residence times than for the sequences discussed above. From about 1250 s to the time of bottom head failure there is very low flow through the RCS as predicted by MARCH, and only approximately an additional 10 percent release of Te and the Cs species from the core region. This is reflected in the retention predicted by TRAP-MELT and presented for the RSS species groups, described in Chapter 6, in Tables 7.3 and 7.4.

As before, the tellurium which is released during the in-vessel portion of the core melting is seen to be efficiently retained by the surfaces in the upper plenum region due to chemical reaction with the surfaces. In this sequence there is no lag apparent in Figure 7.5 between emission and retention due to the higher flow rates which occur here. The CsOH, which also reacts with the RCS surfaces, is retained partly due to this mechanism on the upper plenum surfaces, though this is not a major contributor to the overall retention. About one-half of the CsOH retention proceeds via condensation on aerosol particles which are subsequently deposited in the steam generators and hot leg piping. This route--vapor condensation followed by particle deposition--also dominates the retention of CsI, which is mainly deposited in the steam generators and hot leg at the time of bottom head failure. The high gas temperatures in

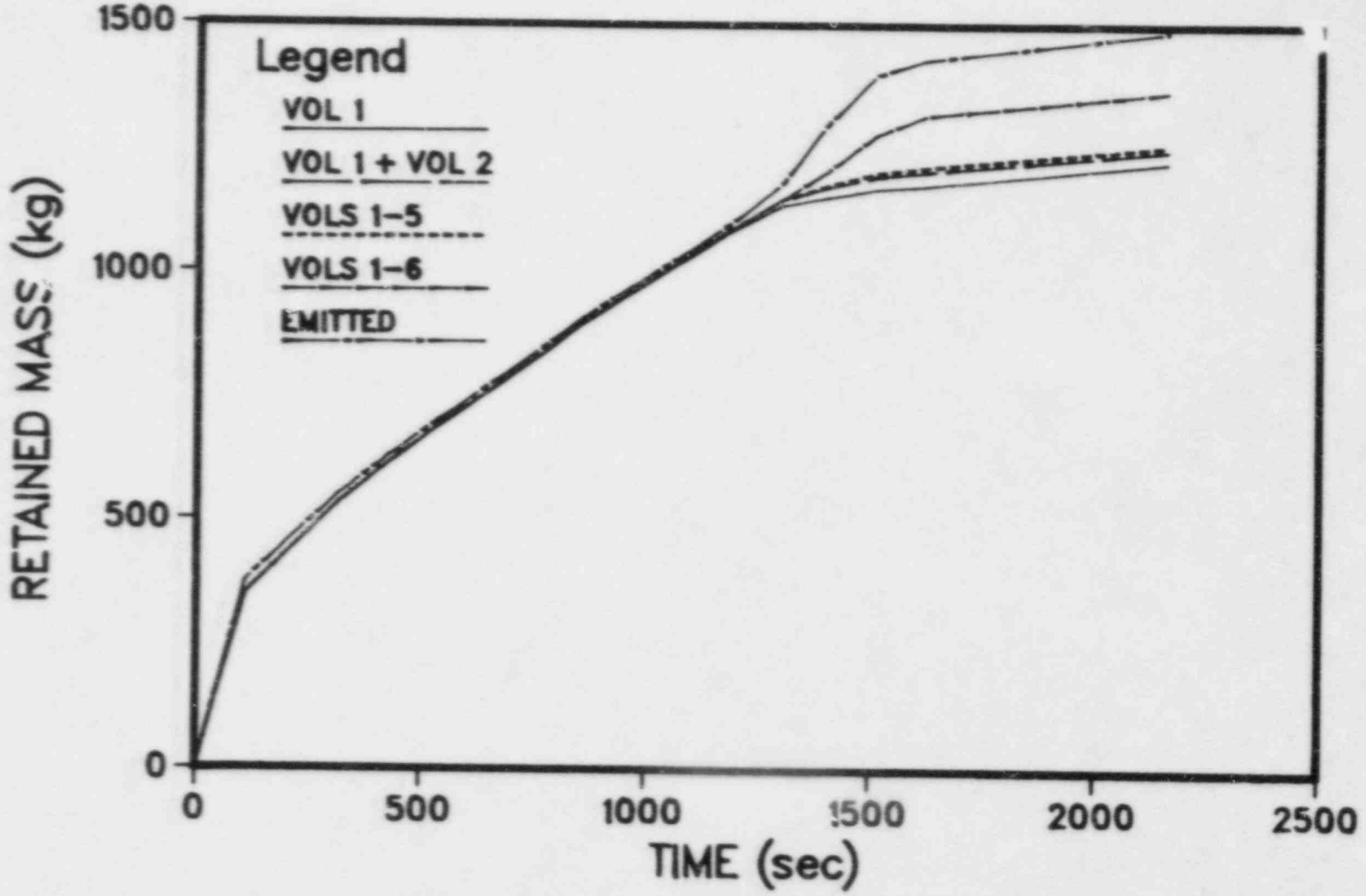

FIGURE 7.4. MASSES OF AEROSOL EMITTED FROM CORE AND RETAINED IN THE RCS CONTROL VOLUMES AS FUNCTIONS OF TIME FOR THE TMLB' SEQUENCE (Vol 1 = Core, Vol 2 = Upper Grid Plate, Vol 3 = Guide Tubes, Vol 4 = Upper Plenum Annulus, Vol 5 = Hot Leg, Vol 6 = Pressurizer). Times measured from start of core melting.

TABLE 7.3. CORSOR PREDICTIONS OF MASSES OF SPECIES RELEASED FROM THE CORE (TOTAL) AND TRAP-MELT PREDICTIONS OF MASSES RETAINED IN THE RCS (RET) DURING THE S_2HF SEQUENCE FOR THE SEQUOYAH PLANT BASED ON THE RSS GROUPINGS*

(Times Measured from Start of Core Melting)

Time (s)	CsI		CsOH		Te		Aerosol	
	Ret (kg)	Total (kg)	Ret (kg)	Total (kg)	Ret (kg)	Total (kg)	Ret (kg)	Total (kg)
200	3.1	7.3	24.4	50.4	2.1	2.7	250	390
397	10.2	16.2	67.5	102.9	6.8	8.6	495	662
594	17.6	23.4	113.2	145.3	15.5	16.4	771	952
792	23.3	27.0	145.6	166.1	20.5	20.6	1049	1267
990	22.6	27.7	142.7	170.4	21.2	21.3	1084	1309
1188	22.6	28.0	142.4	172.2	21.2	21.7	1084	1311
1386	22.6	28.2	142.4	173.6	21.3	22.0	1084	1313
1784	22.6	28.6	142.5	176	21.3	22.7	1090	1320
2378	22.7	29.7	143.0	182.1	21.5	24.3	1118	1350
2972	22.9	30.8	144.0	189.0	21.9	25.7	1183	1415
3762	22.9	31.3	144.2	191.7	22.0	26.6	1269	1499

*See Table 6.6c.

TABLE 7.4. TRAP-MELT PREDICTIONS OF PRIMARY SYSTEM RETENTION FACTORS (RF) AND VOLUME SPECIFIC RETENTION FACTORS AS FUNCTIONS OF TIME FOR THE S_2HF SEQUENCE FOR THE SEQUOYAH PLANT

Time	CsI			CsOH			Te		Aerosol			
(s)	RF	Hot Leg	Steam Gen	RF	Hot Leg	Steam Gen	RF	Core Plate	RF	Core	Hot Leg	Steam Gen
200	.42	.16	.13	.48	.17	.14	.77	.73	.64	.22	.15	.13
397	.63	.23	.20	.66	.23	.20	.80	.77	.75	.22	.20	.18
594	.75	.27	.31	.78	.25	.27	.94	.91	.81	.20	.23	.23
792	.86	.25	.43	.88	.24	.37	.99	.94	.83	.15	.21	.34
990	.82	.25	.44	.84	.23	.38	.99	.93	.83	.15	.21	.36
1188	.81	.25	.43	.83	.23	.38	.98	.91	.83	.15	.21	.36
1386	.80	.24	.43	.82	.23	.37	.97	.91	.83	.15	.21	.36
1784	.79	.24	.42	.81	.23	.37	.94	.87	.83	.15	.20	.36
2378	.77	.23	.41	.79	.22	.36	.89	.82	.83	.17	.20	.35
2972	.74	.22	.39	.76	.21	.34	.85	.79	.84	.21	.19	.33
3762	.73	.22	.39	.75	.21	.34	.82	.76	.85	.25	.18	.31

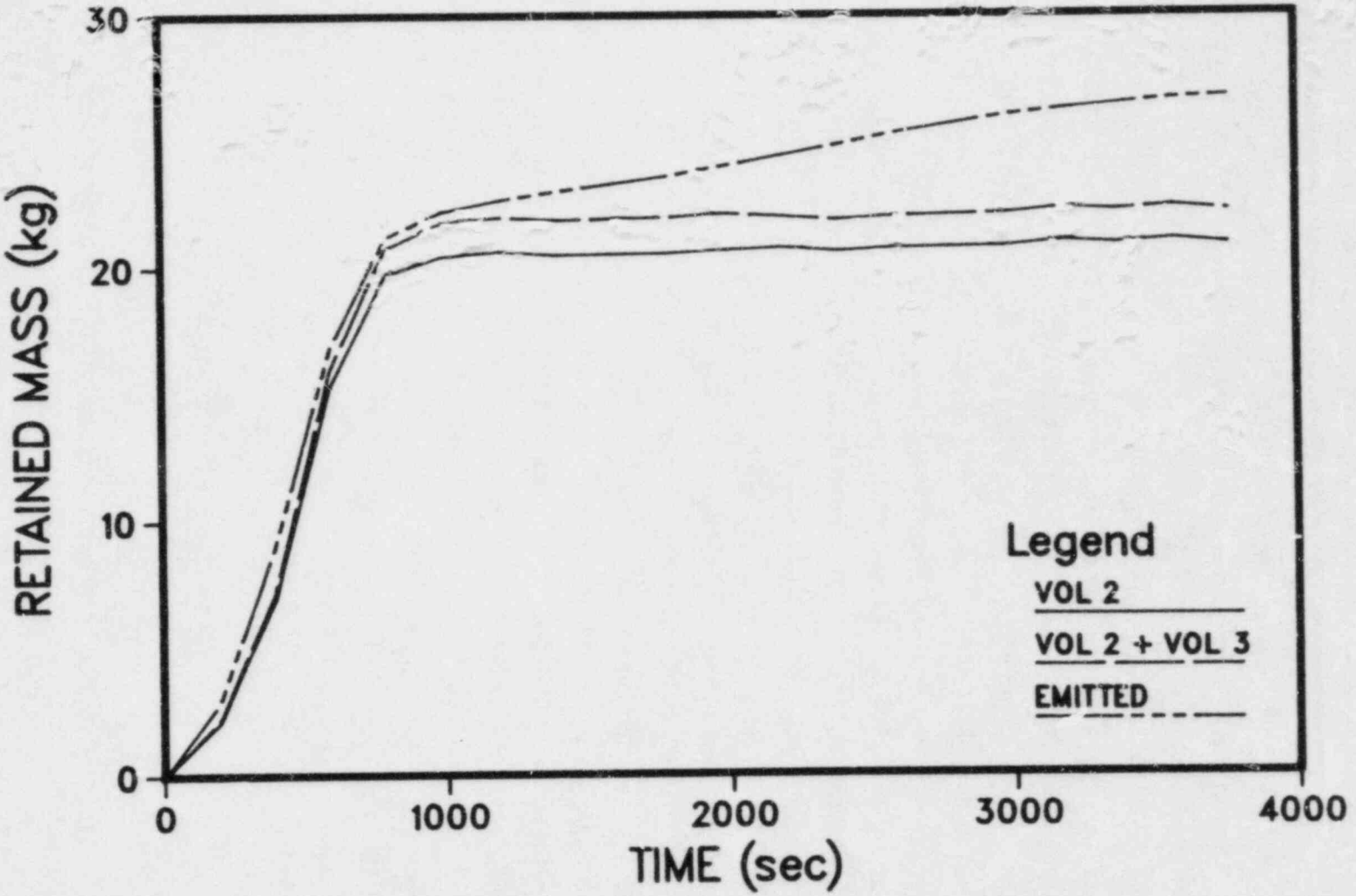

FIGURE 7.5. MASSES OF Te EMITTED FROM CORE AND RETAINED IN THE RCS CONTROL VOLUMES AS FUNCTIONS OF TIME FOR THE S_2HF SEQUENCE (Vol 1 = Core, Vol 2 = Upper Grid Plate, Vol 3 = Guide Tubes, Vol 4 = Upper Plenum Annulus, Vol 5 = Hot Leg, Vol 6 = Steam Generator). Time measured from start of core melting.

the core region prevent the vapor from condensing on the particles which settle out in this control volume. This is seen in Figures 7.6 and 7.7.

The aerosol behavior for this sequence is greatly influenced by the timing of the aerosol emissions from the core relative to the RCS gas flow rates. The fact that both are at their highest values during the same period results in a lower aerosol mass concentration than one would otherwise obtain, and therefore somewhat less coagulational growth and retention via settling. During the initial 650 s, the aerosol generation rate is high, resulting in mass median diameters in the core region of 3.5 μm, and, following additional growth in transit through the RCS, the distribution has a mass median diameter of 6.4 μm in the steam generators. These sizes are sufficient to lead to appreciable settling. From about 750 to 1200 s, the gas flow rates through the RCS are very high and prevent the concentration of aerosol to become very large, so that at t = 1200 s, the mass median diameter of the aerosol in the core region is approximately 0.5 μm. From 1200 s to the time of bottom head failure, the gas flow rate is minimal and the concentration of aerosol steadily increases, leading to a MMD value of 3.3, which again results in attenuation due to gravitational settling. This aspect of the aerosol dynamics is clearly reflected in the "core" column for the aerosol in Table 7.4, and is indicated in the Volume 1 curve in Figure 7.8 as well.

The S_2HF sequence was performed using TRAP-MELT to track the RCS retention of the WASH-1400 groups as defined in Chapter 6. In these analyses the Cs, I, and Te retention behaves as was the case for the previously discussed CsI, CsOH, and Te. While at various times in the sequence the extent of retention of the Sr, Ru, and La groups varies by as much as 15 percent from the retention of the inert aerosol, the extent of retention at the time of bottom head failure is very nearly the same for all forms of the aerosol. These results are summarized in Table 7.4a.

7.3 Transport of Fission Products Through Containment

Calculations of the transport and deposition of fission products within the containment were made for the various sequences and containment failure modes described previously and the results are presented in this section. For calculation purposes, the containment system was divided into

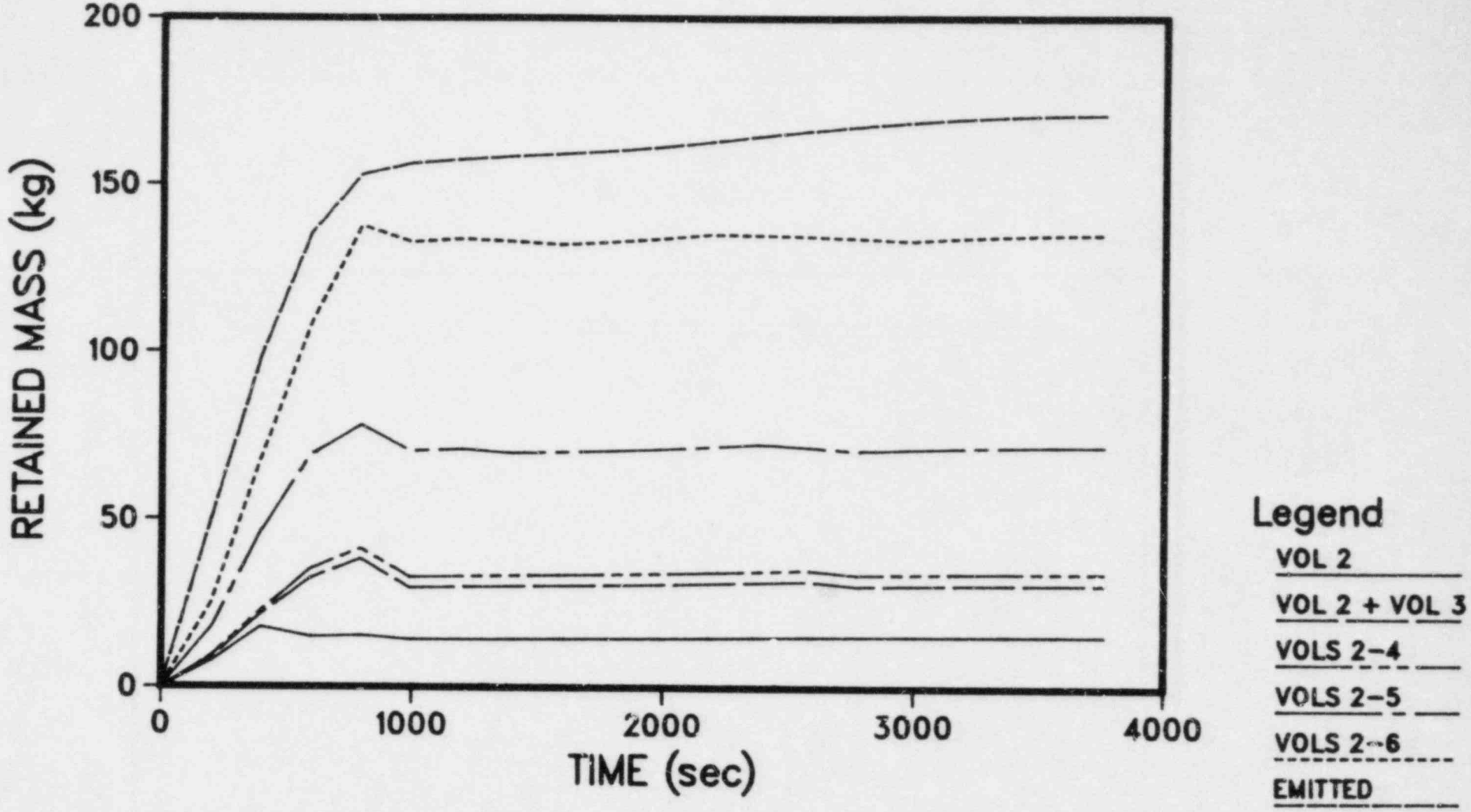

FIGURE 7.6. MASSES OF CsOH EMITTED FROM CORE AND RETAINED IN THE RCS CONTROL VOLUMES AS FUNCTIONS OF TIME FOR THE S_2HF SEQUENCE (Vol 1 = Core, Vol 2 = Upper Grid Plate, Vol 3 = Guide Tubes, Vol 4 = Upper Plenum Annulus, Vol 5 = Hot Leg, Vol 6 = Steam Generator). Time measured from start of core melting.

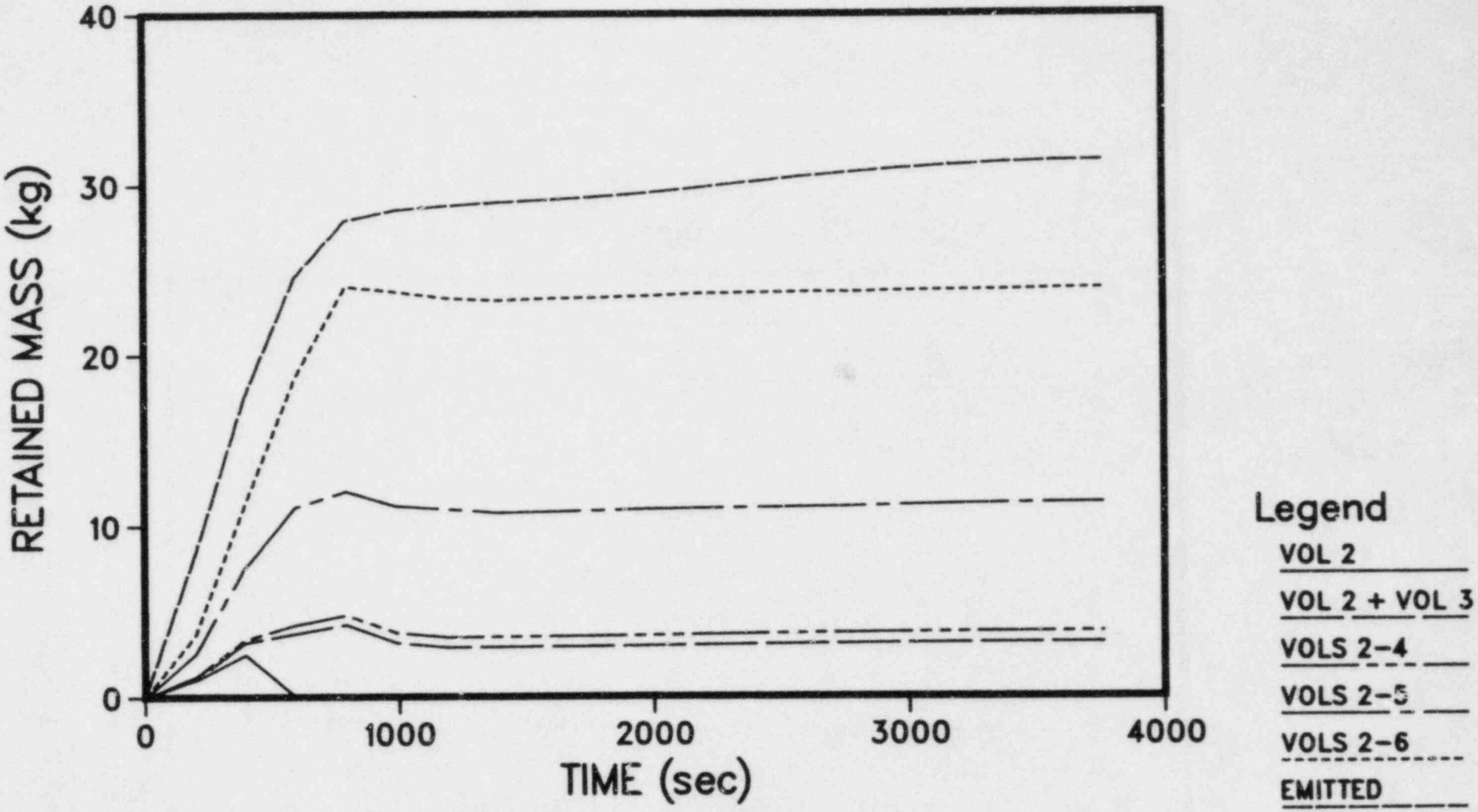

FIGURE 7.7. MASSES OF CsI EMITTED FROM CORE AND RETAINED IN THE RCS CONTROL VOLUMES AS FUNCTIONS OF TIME FOR THE S_2HF SEQUENCE (Vol 1 = Core, Vol 2 = Upper Grid Plate, Vol 3 = Guide Tubes, Vol 4 = Upper Plenum Annulus, Vol 5 = Hot Leg, Vol 6 = Steam Generator). Time measured from start of core melting.

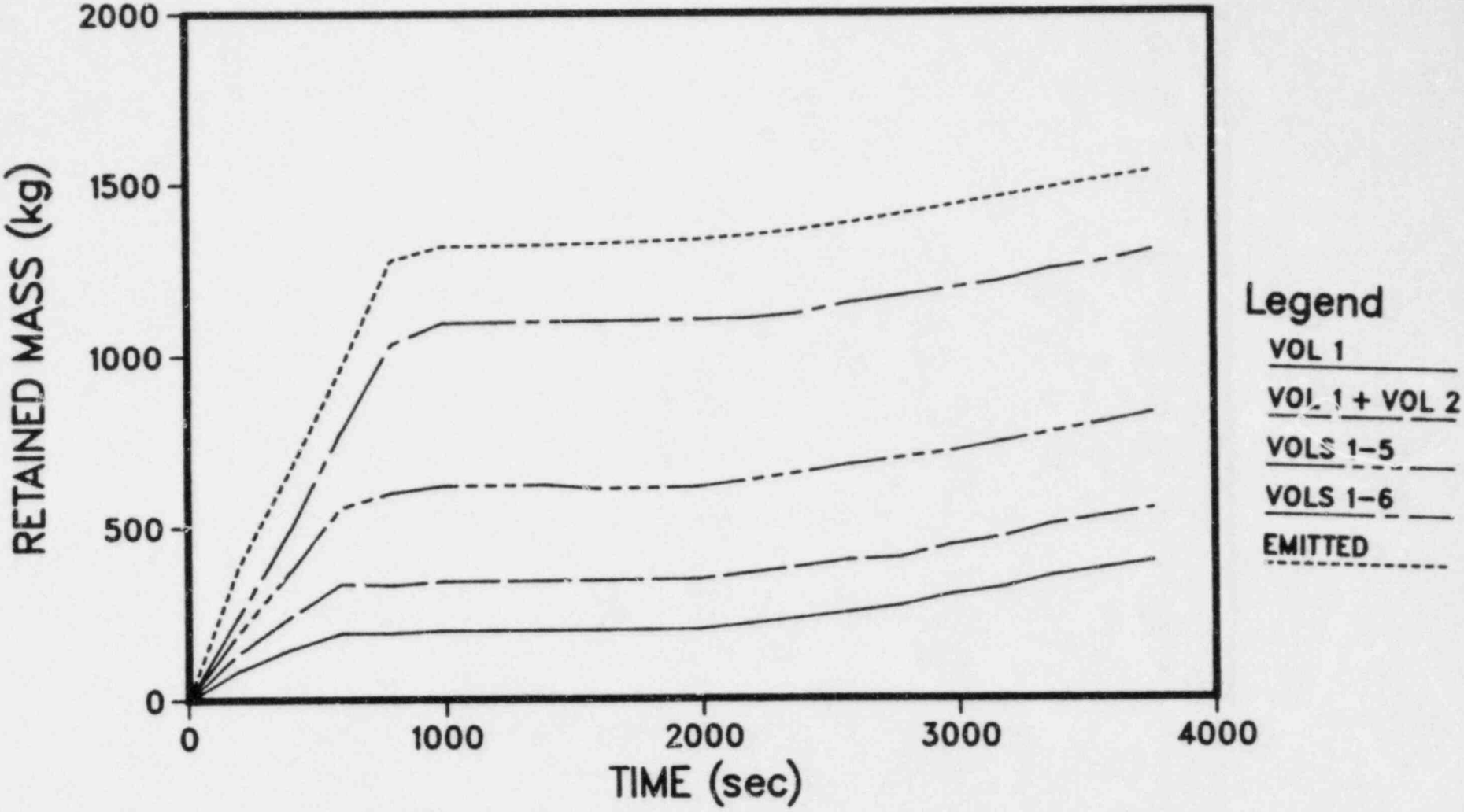

FIGURE 7.8. MASSES OF AEROSOL EMITTED FROM CORE AND RETAINED IN THE RCS CONTROL VOLUMES AS FUNCTIONS OF TIME FOR THE S_2HF SEQUENCE (Vol 1 = Core, Vol 2 = Upper Grid Plate, Vol 3 = Guide Tubes, Vol 4 = Upper Plenum Annulus, Vol 5 = Hot Leg, Vol 6 = Steam Generator). Time measured from start of core melting.

TABLE 7.4a. CORSOR PREDICTIONS OF RELEASE FROM CORE AND TRAP-MELT PREDICTIONS OF PRIMARY SYSTEM RETENTION OF WASH-1400 GROUPS FOR S_2HF SEQUENCE FOR THE SEQUOYAH PLANT

Group	Released (kg)	Retained (kg)
I	15.2	11.2
Cs	184.5	139.5
Te	26.6	22.0
Sr	15.1	13.4
Ru	21.2	18.9
La	0.26	0.23

three separate compartments in the present analyses, namely, the lower compartment, the ice condenser, and the upper compartment. The geometry of these compartments was given in Chapter 4.

The NAUA-4 code, which is basically a single-volume containment code, was utilized in these calculations and was run sequentially for each compartment. For certain accident sequences such as TML and S_2HF, both of which involve recirculation of fission products among the three compartments, the above sequential runs of the NAUA code were repeated until the prediction results converged. Details on this iterative calculation procedure will be discussed further later. For modeling the behavior of the ice condenser, the computer code designated ICEDF that was developed by Battelle's Pacific Northwest Laboratories was utilized.

In general, the NAUA code needs information on the thermal hydraulic conditions of an accident of interest. The conditions provided by the MARCH computer calculation were used. The typical required thermal hydraulic conditions are time-dependent containment temperature, pressure, wall temperature, and the rates at which steam enters the containment, condenses on the containment structure, and flows among various compartments.

Another important and critical input that containment codes need is the fission product source term for particulates. The source rates calculated as release from the primary system (TRAP-MELT code) and the VANESA code calculations for release during the core-concrete interaction were taken as the melt and vaporization releases, respectively. For the containment calculations, CsI, CsOH, and Te were distinguished and all the other species were treated as one group. All species were assumed to be in the particulate form in the containment atmosphere because the temperature and pressure under the containment conditions indicated that these species will remain as particulates for all practical circumstances. Although it was assumed in the calculation that individual species are distributed evenly over all sizes of particulates, differential amounts of these species at a given time due to different source timings were taken into consideration in the calculations.

Three different accident sequences, TMLB', TML, and S_2HF, were considered in the present calculations.

7.3.1 TMLB' Sequence

In this transient accident sequence heat and steam generated in the core are transmitted to the lower containment volume causing the temperature and the pressure to rise. The increase in the pressure opens the ice condenser doors allowing the steam to pass through the ice condenser. A substantial amount of steam subsequently condenses onto ice present in the ice condenser, causing the temperature and pressure to decrease. The fission products leaving the ice condenser are subsequently released into the upper containment volume. The ice in the ice condenser is expected to melt slowly as time elapses. Two different containment failure modes were considered in the present analysis. In the first mode, designated as TMLB'-γ, the containment failure occurs at the time the pressure vessel fails due to hydrogen burning. This takes place approximately 155 minutes after the accident is initiated. The second mode considered is the TMLB'-δ in which the containment fails at about 550 minutes (about 300 minutes after the bottom head of the reactor vessel fails) due to buildup of noncondensible gases. The containment failure is assumed to take place in the upper containment volume in both modes. No engineered safety features, such as air return fans and sprays, are assumed operating. The key accident events and containment conditions are given in Section 6.1.

TMLB'-γ

In this accident sequence, hydrogen ignitions are assumed to take place shortly after the bottom head fails causing the upper compartment to fail at a time of 155 minutes. The core debris is assumed to fall into and down through the water present in the reactor cavity to reach the concrete and the gases and particulate formed in the core-concrete interaction to rise up through the water pool. A water mass of 1.42×10^5 kg at 311 K was predicted in the reactor cavity at the time of bottom head failure from the discharge of the accumulators. The water depth is initially about 10 ft and then slowly increases due to ice melting to about 30 ft over a period of 550 minutes. Although no water-debris interactions were considered in the VANESA calculation, physical scrubbing of particulates passing up through the water pool has been considered. Decontamination factors ranging 4 to 40 were obtained by the VANESA code depending upon the particle size and the water temperature.

The NAUA calculation results show that the fission products released from the RCS enter the lower containment and quickly pass through the ice condenser. In the ice condenser, a considerable amount of fission products is removed by the ice. The most important mechanism is found to be that due to steam condensation. Table 7.5 shows the decontamination factor calculated for the ice condensers. Figures 7.9 and 7.10 show the airborne particle mass, the amount leaked into the environment, and the particle size distribution as calculated for the upper compartment. Table 7.6 summarizes the calculated distribution of radionuclide mass (as a fraction of core inventory) at the end of this sequence.

TMLB'-δ

For this sequence, input identical to that used for the TMLB'-γ was used for the fission product source. However, the thermal hydraulic conditions as calculated by the MARCH code show that the containment fails at a time of 552 minutes which is much delayed compared to the containment failure time for the TMLB'-γ case. The decontamination factor of the ice condenser for the TMLB'-δ sequence is shown in Table 7.5. Note that the mass retained in the ice compartment is also strongly influenced by the continued operation of the recirculating fan which in effect gives multiple passes through this compartment. The airborne mass, the leaked mass, and the particle size distribution for the upper containment are shown in Figures 7.11 and 7.12. The distribution of fission products after the accident is completed is shown in Table 7.6. It is seen that, as expected, the TMLB'-δ sequence is calculated to have considerably less mass leaked to the environment than for the TMLB'-γ case.

7.3.2 TML Sequence

This accident sequence occurs due to the failure of the water make-up systems. For the purpose of performing calculations, this sequence is similar to that for the TMLB' sequence in that the flow paths of fission products are similar. However, the major features that differ from the TMLB' sequence are that the air return fans and the containment spray system are operating in this sequence. The role of the air return fan that moves the gas from the upper containment into the lower containment volume causes an overall

TABLE 7.5. DECONTAMINATION FACTOR OF THE ICE CONDENSER BASED ON THE TOTAL MASS, TMLB'

Time, min	DF[a]	
	γ	δ
145	5.3	29.7
160	3.0	43.8
161	3.6	8.9
170	5.4	6.6
180	7.0	5.1
200	6.9	5.5
232	5.7	6.3
314	4.4	5.5
360	1.6	4.5
527	--	12.1

(a) Decontamination factor, DF, is defined as mass entering the ice compartments divided by the mass leaving.

TABLE 7.6. DISTRIBUTION OF SPECIES AFTER ACCIDENT IS COMPLETED AS CALCULATED BY THE NAUA CODE, TMLB'

Containment Failure Mode	Species	Fraction of Core Inventory				
		RCS	Lower Cont	Ice Bed	Upper Cont	Environment
γ	CsI	0.82	6.1×10^{-2}	0.10	1.5×10^{-3}	1.7×10^{-2}
	CsOH	0.83	3.9×10^{-2}	0.12	2.9×10^{-3}	2.3×10^{-2}
	Te	0.25	2.4×10^{-2}	3.7×10^{-2}	6.2×10^{-4}	1.4×10^{-2}
δ	CsI	0.82	8.6×10^{-3}	0.17	5.5×10^{-3}	3.9×10^{-4}
	CsOH	0.83	5.4×10^{-2}	0.13	5.0×10^{-3}	4.5×10^{-4}
	Te	0.25	4.0×10^{-2}	3.1×10^{-2}	3.8×10^{-3}	2.0×10^{-3}

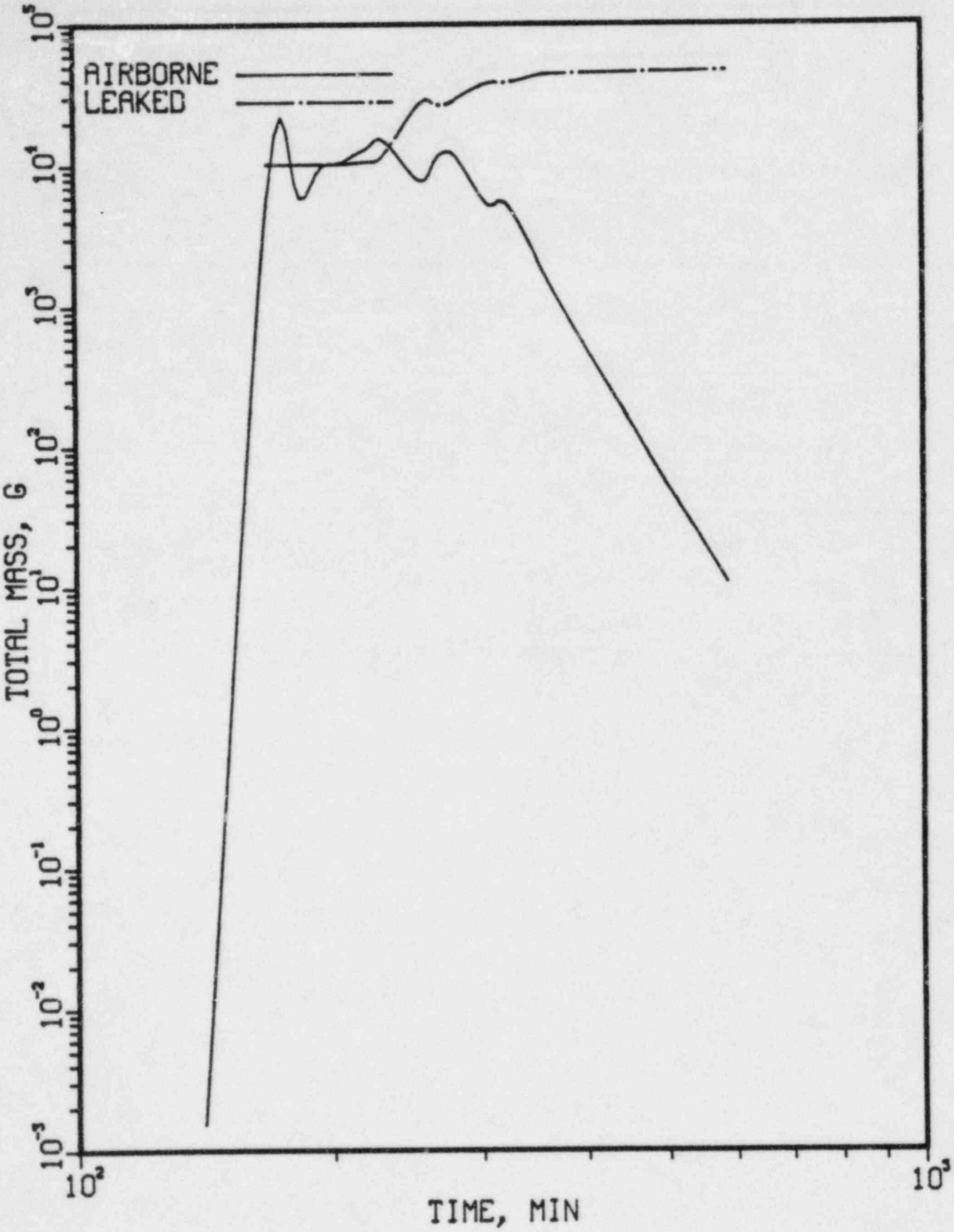

FIGURE 7.9. AIRBORNE AND LEAKED MASSES, TMLB'-γ

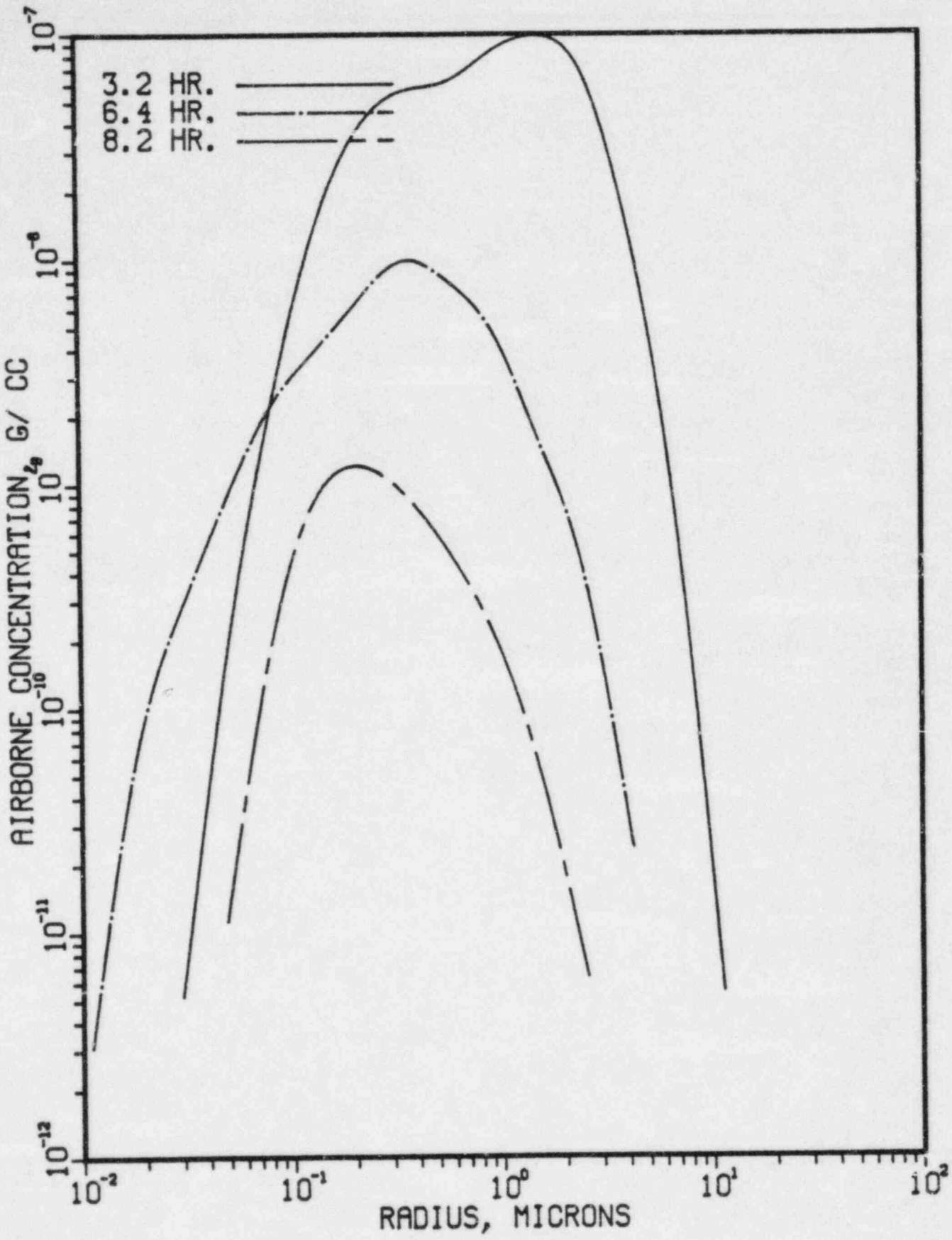

FIGURE 7.10. PARTICLE SIZE DISTRIBUTIONS, TMLB'-Y

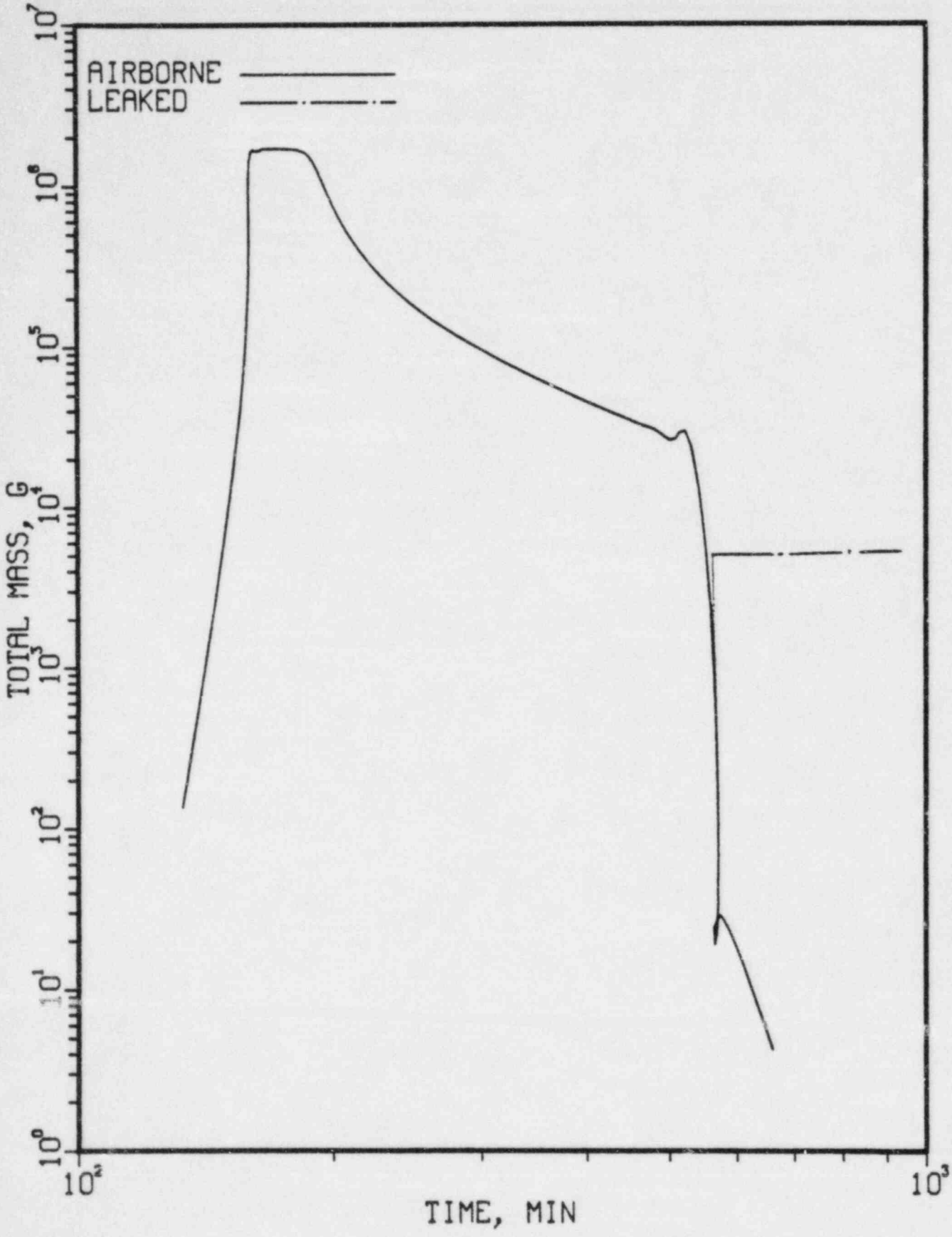

FIGURE 7.11. AIRBORNE AND LEAKED MASSES, TMLB'-6

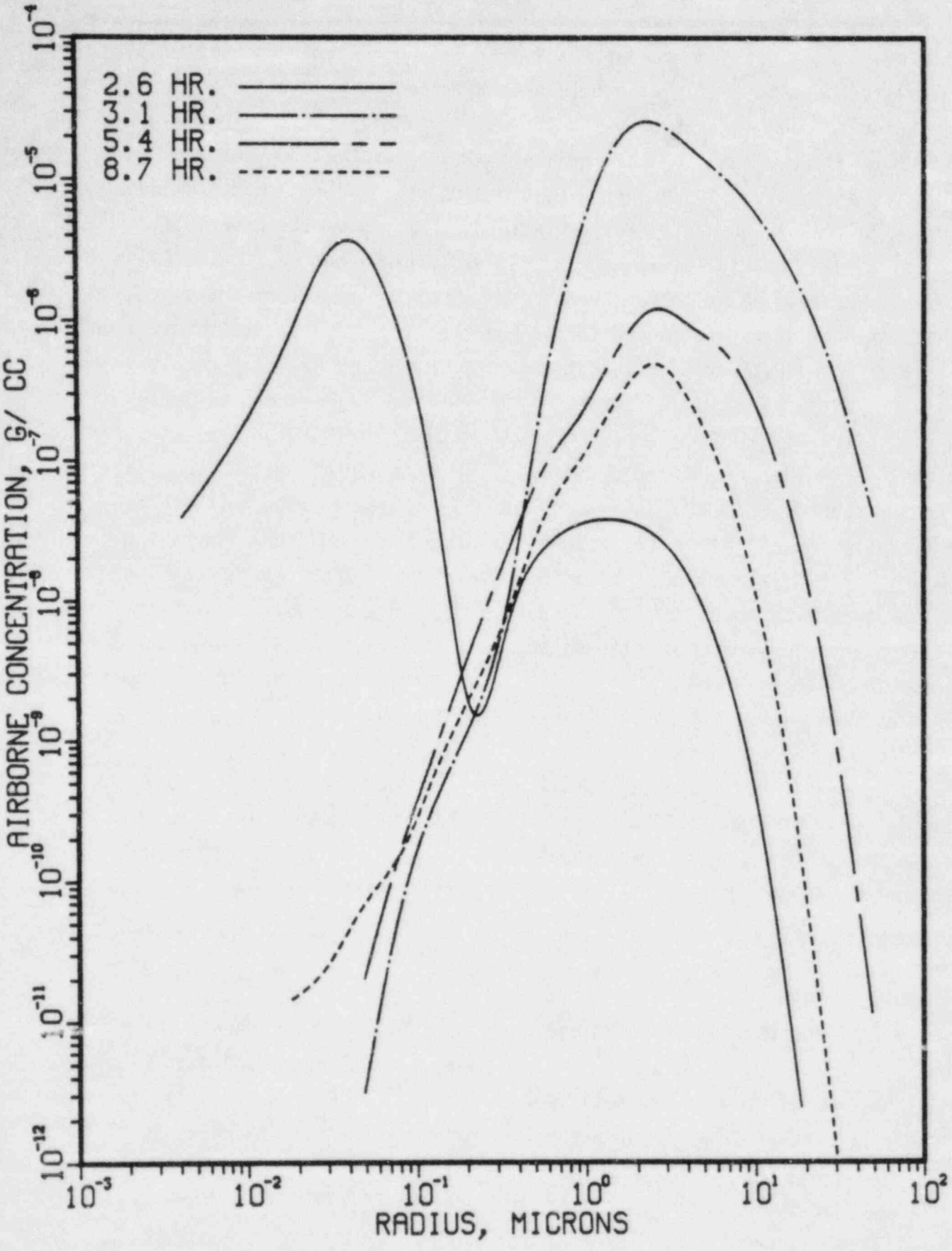

FIGURE 7.12. PARTICLE SIZE DISTRIBUTIONS, TMLB'-δ

containment flow with a circulatory pathway. In order to treat this recirculation pattern involving multiple compartments, the single-volume NAUA code has been used sequentially and iteratively as follows. Initially, the NAUA code has been run for modeling the lower compartment and the ice bed. Using the calculated fission products escaping the ice condenser, the upper compartment was subsequently modeled with another run of the NAUA code. A procedure identical to the above was then repeated except that the fission products transported by the air return fans from the upper compartment to the lower compartment are accounted for in the repeated run. These iterative calculation procedures were continued until the last two calculated results were close. Typically, three to four iterations were necessary in practice.

Two containment failure modes were considered in the present study. In the first mode, TML-γ, the containment fails at 157 minutes which coincides with the reactor vessel failure time, due to hydrogen burning. The second mode, designated as TML-δ, corresponds to failure due to the buildup of noncondensible gases. Since the calculation was not carried out to the point of failure, a nominal containment leak rate of 1 volume percent per day was utilized for the purpose of determining the fraction of fission products that escape into the environment. Details on the pertinent accident event times and the amount of fission products released into the containment can be referred to in Chapter 6.

As discussed in Section 7.2.1, the source rates identical to that calculated by the TRAP-MELT code for the TMLB' sequence were utilized as the source for the melt release and the VANESA calculation results described in Section 6 were utilized as the source for a period after the vessel failure.

TML-γ

The predicted decontamination factor for the ice condenser is shown in Table 7.7. Figures 7.13 and 7.14 show the total airborne solid particulate mass, the amount released into the environment, and the particle size distribution for the upper compartment where the containment integrity gives in at 157 minutes.

Table 7.8 is the predicted distribution of fission products after the accident is completed. The fractions of CsI, CsOH, and Te that are released into the environment are all less than 1 percent which are considerably lower

TABLE 7.7. DECONTAMINATION FACTOR FOR THE ICE CONDENSER BASED ON THE TOTAL MASS, TML

Time, min	Decontamination Factor	
	γ	δ
145	2.5	2.6
156	6.0	2.9
158	4.8	3.0
170	18.5	1.3
200	15.0	1.3
227	16.8	1.1
251	15.6	1.3
262	14.2	1.2
263	5.8	1.1
271	1.1	1.4

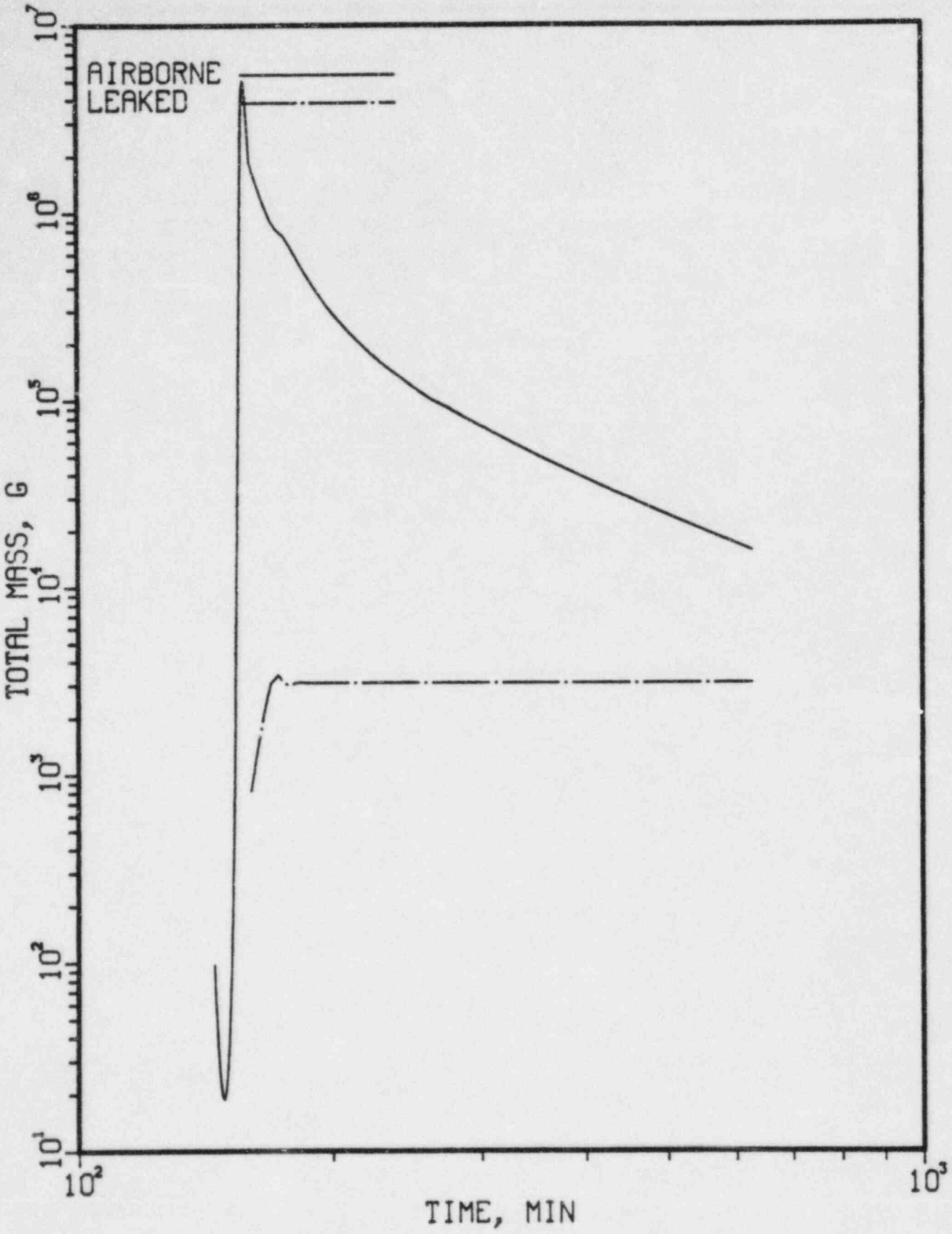

FIGURE 7.13. AIRBORNE AND LEAKED MASSES, TML-γ

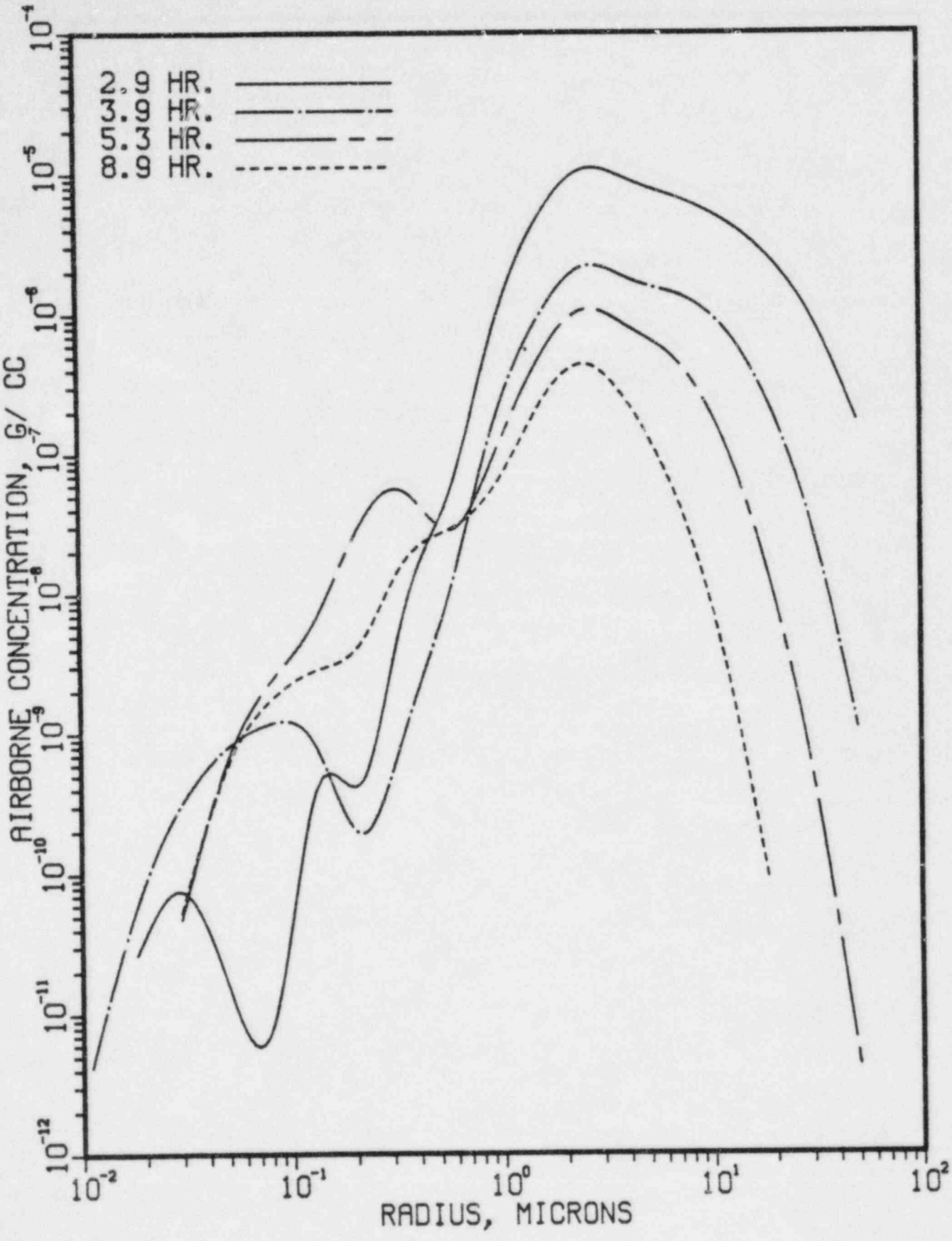

FIGURE 7.14. PARTICLE SIZE DISTRIBUTIONS, TML-Y

TABLE 7.8. DISTRIBUTION OF SPECIES AFTER ACCIDENT IS COMPLETED AS CALCULATED BY THE NAUA CODE, TML

Containment Failure Mode	Species	Fraction of Core Inventory				
		RCS	Lower Cont	Ice Bed	Upper Cont	Environment*
γ	CsI	0.82	4.2×10^{-2}	9.4×10^{-2}	4.6×10^{-2}	1.3×10^{-3}
	CsOH	0.83	3.1×10^{-2}	0.11	3.4×10^{-2}	7.0×10^{-3}
	Te	0.25	3.1×10^{-4}	1.2×10^{-2}	8.6×10^{-3}	5.5×10^{-4}
δ	CsI	0.82	5.7×10^{-2}	8.5×10^{-2}	3.4×10^{-2}	6.9×10^{-9}
	CsOH	0.83	5.8×10^{-2}	9.4×10^{-2}	3.5×10^{-2}	7.4×10^{-9}
	Te	0.25	8.1×10^{-3}	1.0×10^{-2}	9.5×10^{-3}	1.6×10^{-8}

*All iodine is assumed to be present as CsI and formation of volatile iodides in the containment was not considered. If production of volatile iodides is considered, the iodide release to the environment is estimated to be of the order of 10^{-3}.

than those for TMLB'-γ shown in Table 7.6, primarily due to availability of the air return fans and the containment sprays in this sequence. The role of the air return fans is, of course, to force the fission products suspended in the upper compartment to pass through the ice bed lowering the overall concentration in the containment.

TML-δ

In this failure mode, the containment integrity is maintained while a series of hydrogen burns take place. The containment pressure and temperature during the accident were already described in Chapter 6. Figures 7.15 through 7.17 show the airborne concentration, the leaked amount of radionuclides, and the particle size distribution. Decontamination factors of the ice condenser during this sequence are shown in Table 7.7. The fractions of the core inventory for CsI, CsOH, and Te that are released into the environment are summarized in Table 7.8. Due to the continued availability of the air return fans and containment sprays, very low releases are predicted for this sequence.

7.3.3 S_2HF Sequence

This sequence is initiated by a small pipe break. In this accident sequence, all engineered safeguards operate initially. As the core starts melting however, the containment sprays cease to operate and the ice bed does not contribute significantly to the removal of fission products due to complete melting of the ice. However, the air return fans operate during the entire period of accident time. As listed in Table 6.2, the core melting takes place at a time of 196 minutes and the reactor vessel fails at a time of 260 minutes followed by the containment failure at 352 minutes. Like in the TML accident sequence, the NAUA code has been run sequentially and iteratively to model the recirculatory paths involved in the S_2HF sequence.

The decontamination factors for this accident sequence are shown in Table 7.9. As expected, decontamination factors for the ice bed on removal of fission products are not as large as those for TMLB' and TML since the ice is essentially gone when fission product release takes place. However, the total mass removed in the ice compartment is still significant because of the continuing air recirculation. The airborne mass, leaked mass, and particle

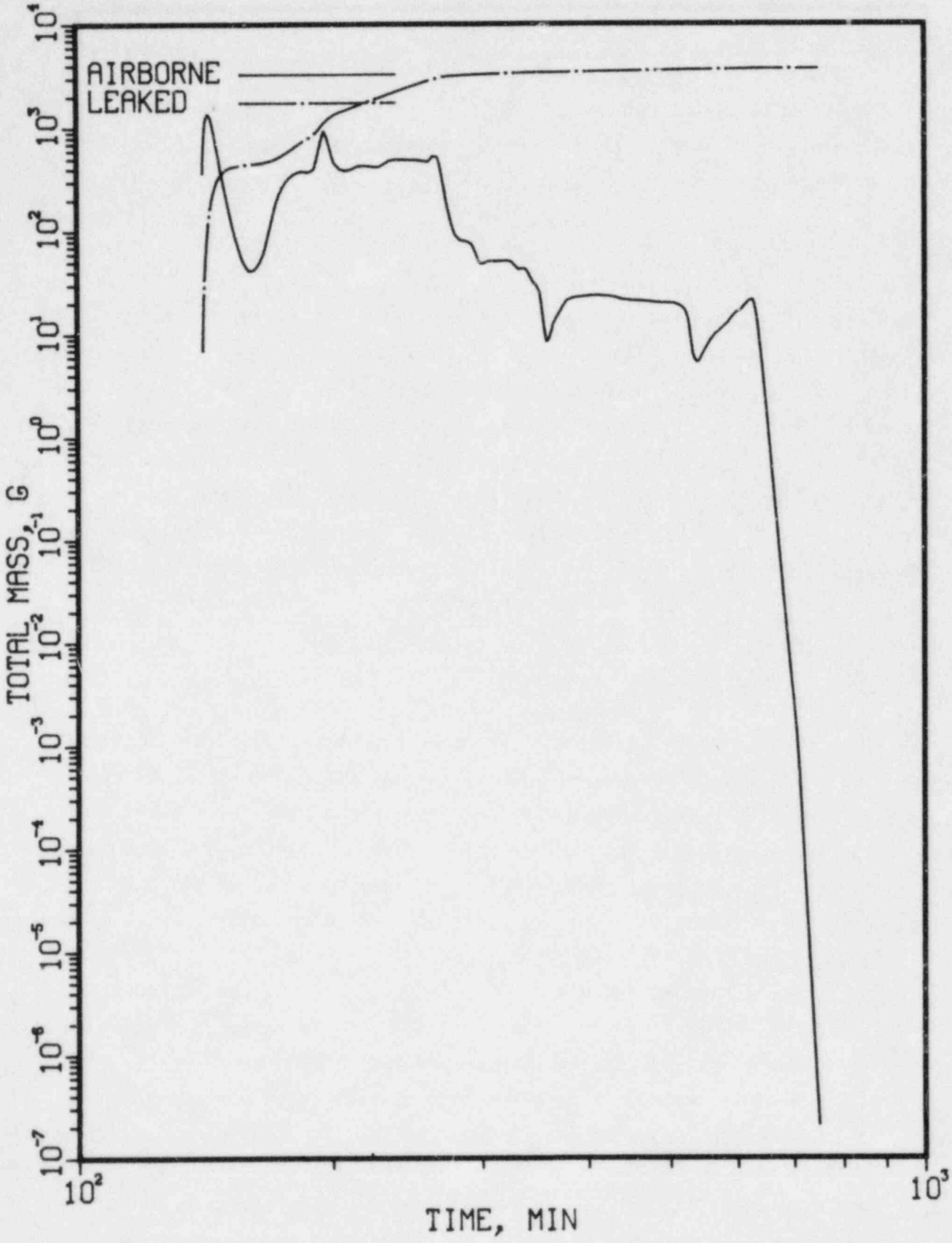

FIGURE 7.15. AIRBORNE AND LEAKED MASSES (TML-δ)

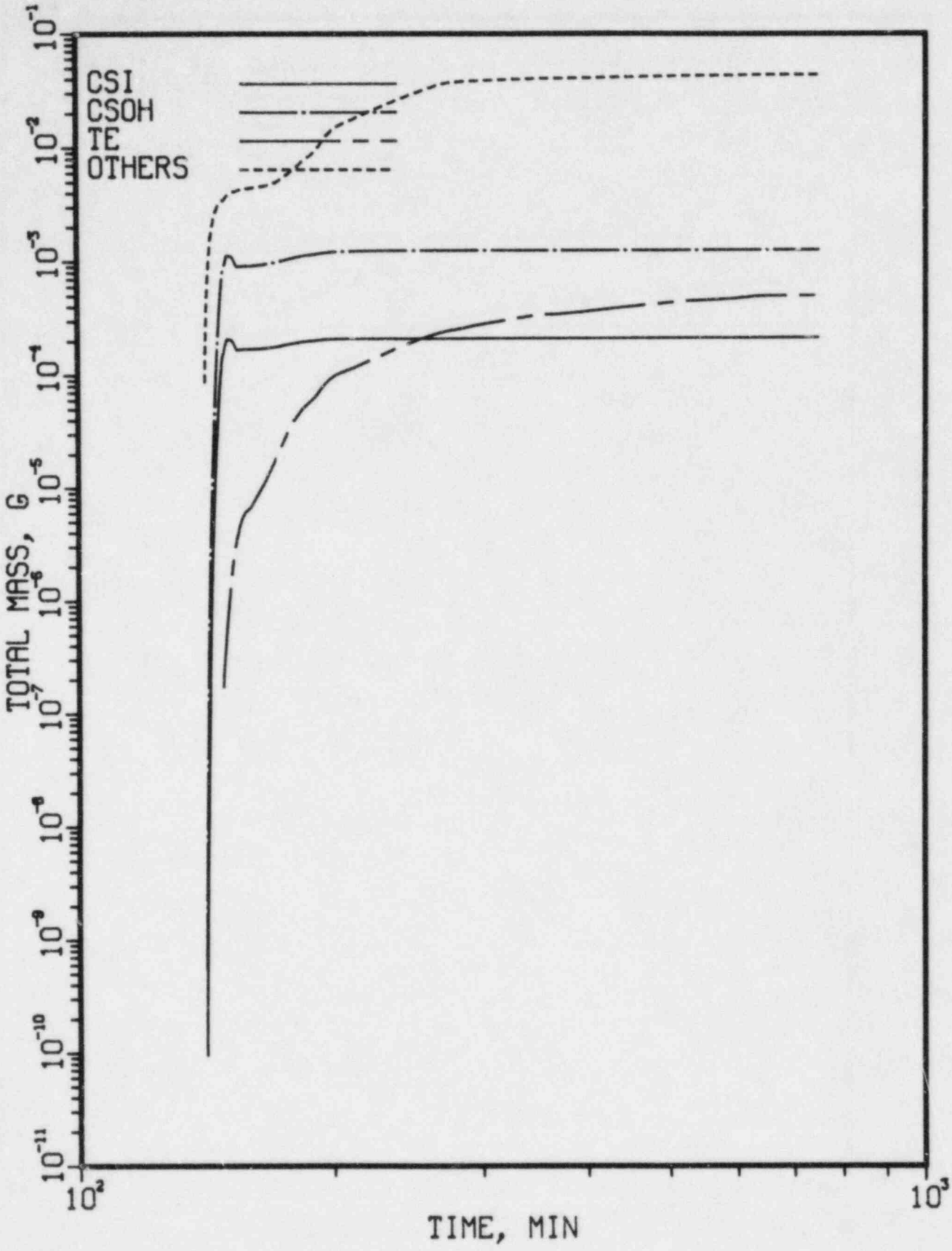

FIGURE 7.16. ACCUMULATED LEAKED NUCLIDES (TML-δ)

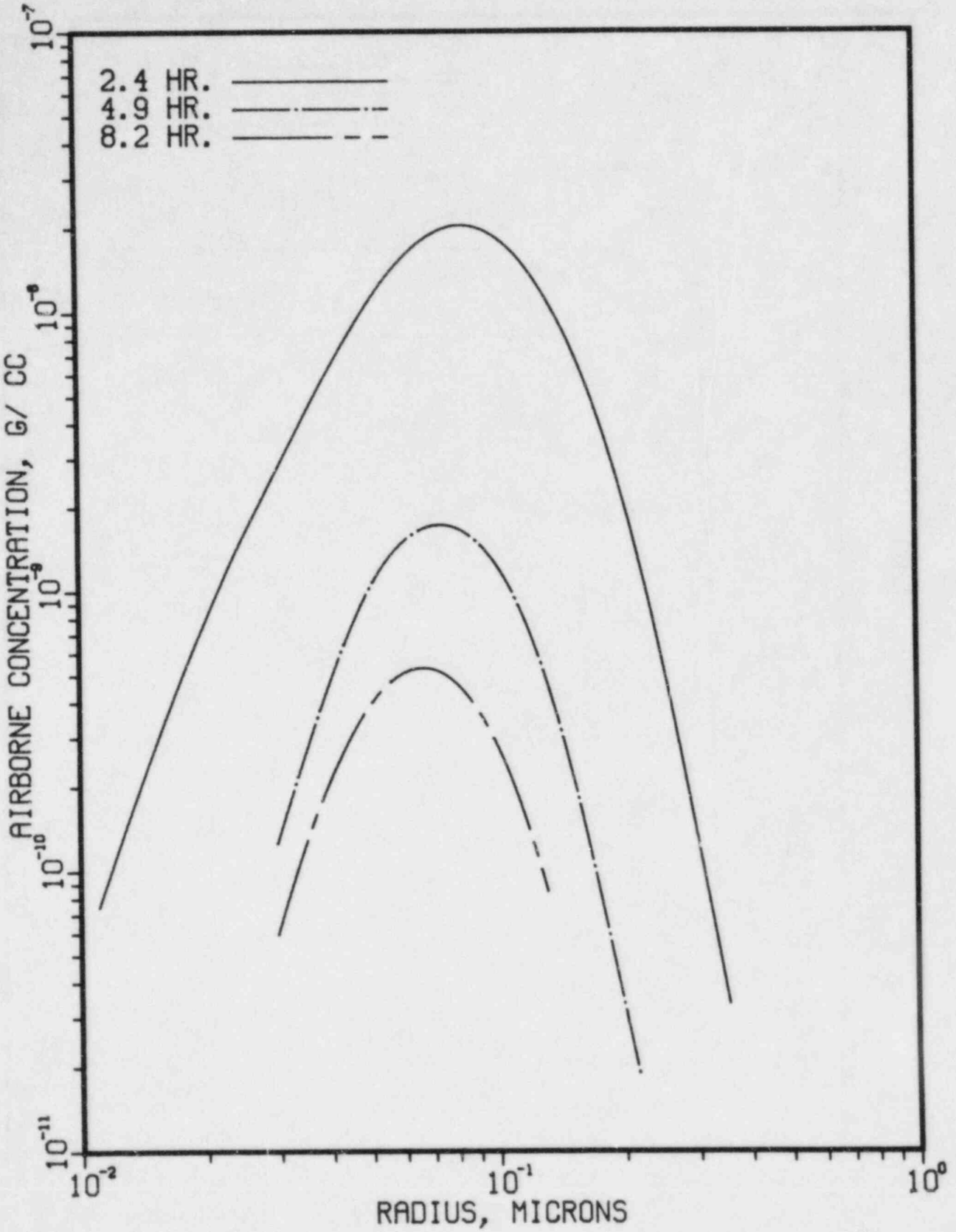

FIGURE 7.17. PARTICLE SIZE DISTRIBUTIONS (TML-6)

TABLE 7.9. DECONTAMINATION FACTOR FOR THE ICE CONDENSER BASED ON THE TOTAL MASS, S_2HF-Y

Time, min	Decontamination Factor
200	1.14
208	1.10
211	1.04
220	1.05
230	1.08
240	1.06
250	1.05
270	1.05
300	1.05
330	1.06
360	1.07
400	1.06
500	1.06
600	1.06
1000	1.06

size distribution for the upper compartment are shown in Figures 7.18 through 7.20. The final locational distribution of species after the accident is completed is shown in Table 7.10. It is interesting to note that the fractions of CsI and CsOH that are released to the environment are about 3 percent, comprising the second most severe accident among the Sequoyah accident sequences as examined in this study. On the other hand the release fraction of Te is 5.5 percent, being the highest number. This is primarily due to the increased amount of Te released into the containment in this sequence. In the TMLB' and TML sequences, about 35 percent of the Te inventory is released from the fuel (note that the fraction not released includes that retained by the overlying layer of water). Approximately 90 percent of Te is released in this sequence; the enhanced Te release is due to the absence of water in the reactor cavity.

7.3.4 Results for Fission Product Groups of Reactor Safety Study

As discussed, the results of calculations presented so far distinguished CsI, CsOH, and Te. In general, one can keep track of an increased number of species in the calculation. In order to demonstrate this capability, an additional NAUA calculation was performed for the S_2HF sequence. The groups and the corresponding species accounted for in this additional calculation were already discussed in Section 6.2.1. Since the VANESA calculations for the release during the core-concrete interaction did not include all the species to be tracked, it was assumed that the species in a group not included in the original VANESA calculation are released at a rate identical to that for the species in the same group. For example, the release rate for Tc, Rh, and Pd in Group 6 was assumed to be the same as that for Ru and Mo combined after accounting for their core inventories. It should also be noted that Group 1 was not included in the NAUA calculation since Kr and Xe are in the gaseous form. Table 7.11 lists the calculated fraction of core inventory released to the environment as a function of both time and group for the S_2HF-γ sequence.

Compared with the results of the calculations for CsI, CsOH, and Te given earlier in Table 7.10, the results listed in Table 7.11 for Groups 2, 3, and 4 are consistent with the regrouping of the species.

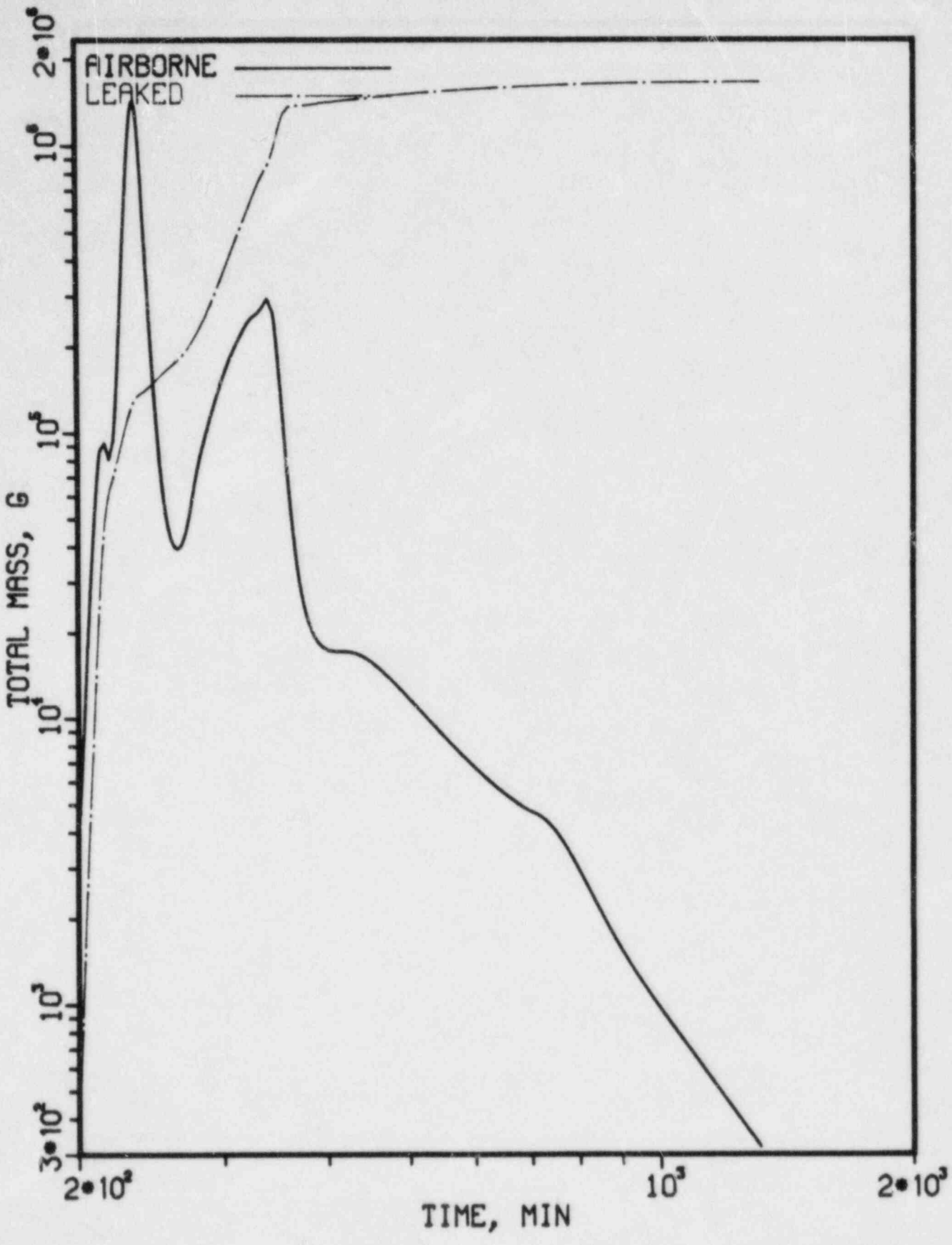

FIGURE 7.18. AIRBORNE AND LEAKED MASSES (S_2HF-Y)

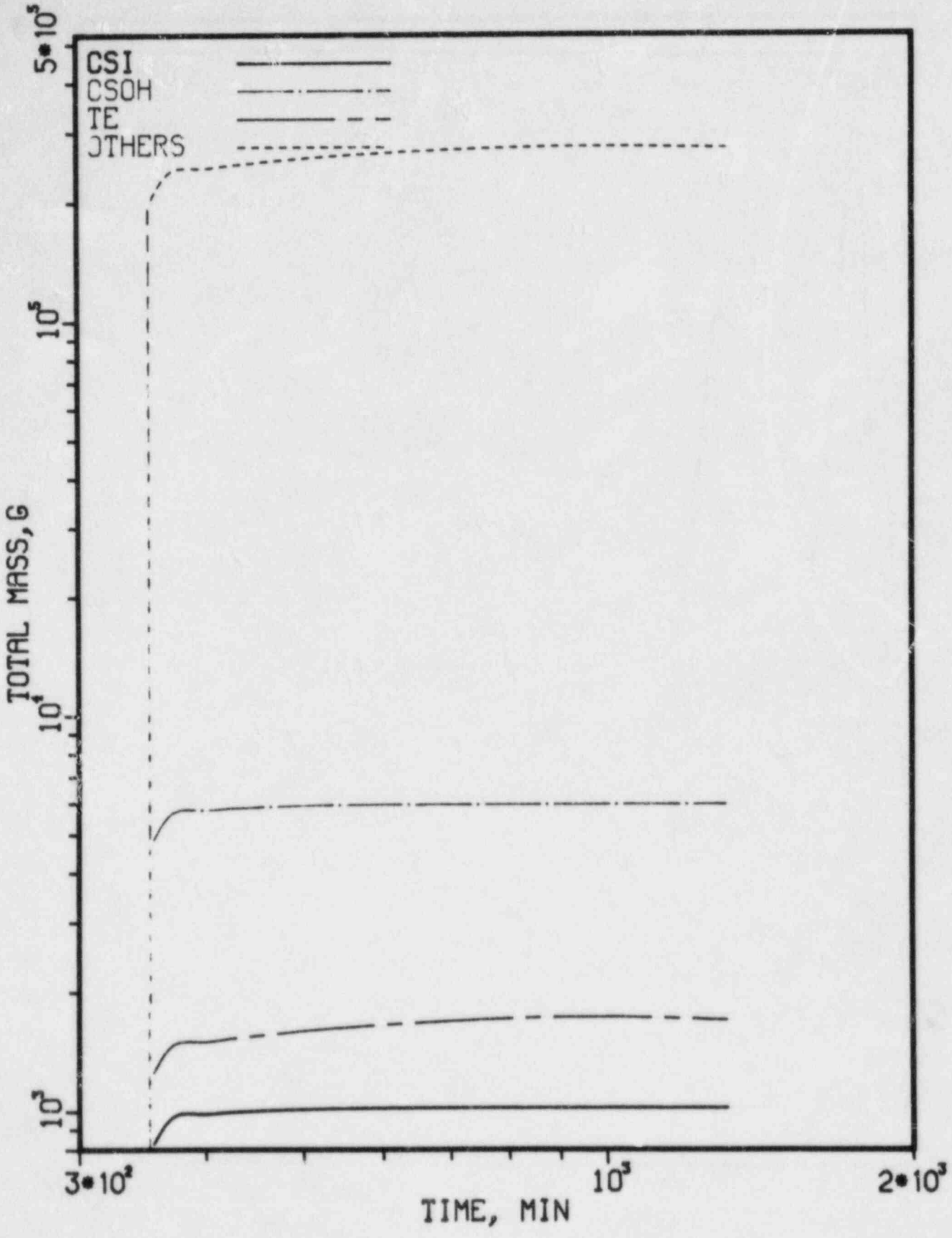

FIGURE 7.19. ACCUMULATED LEAKED NUCLIDES (S_2HF-Y)

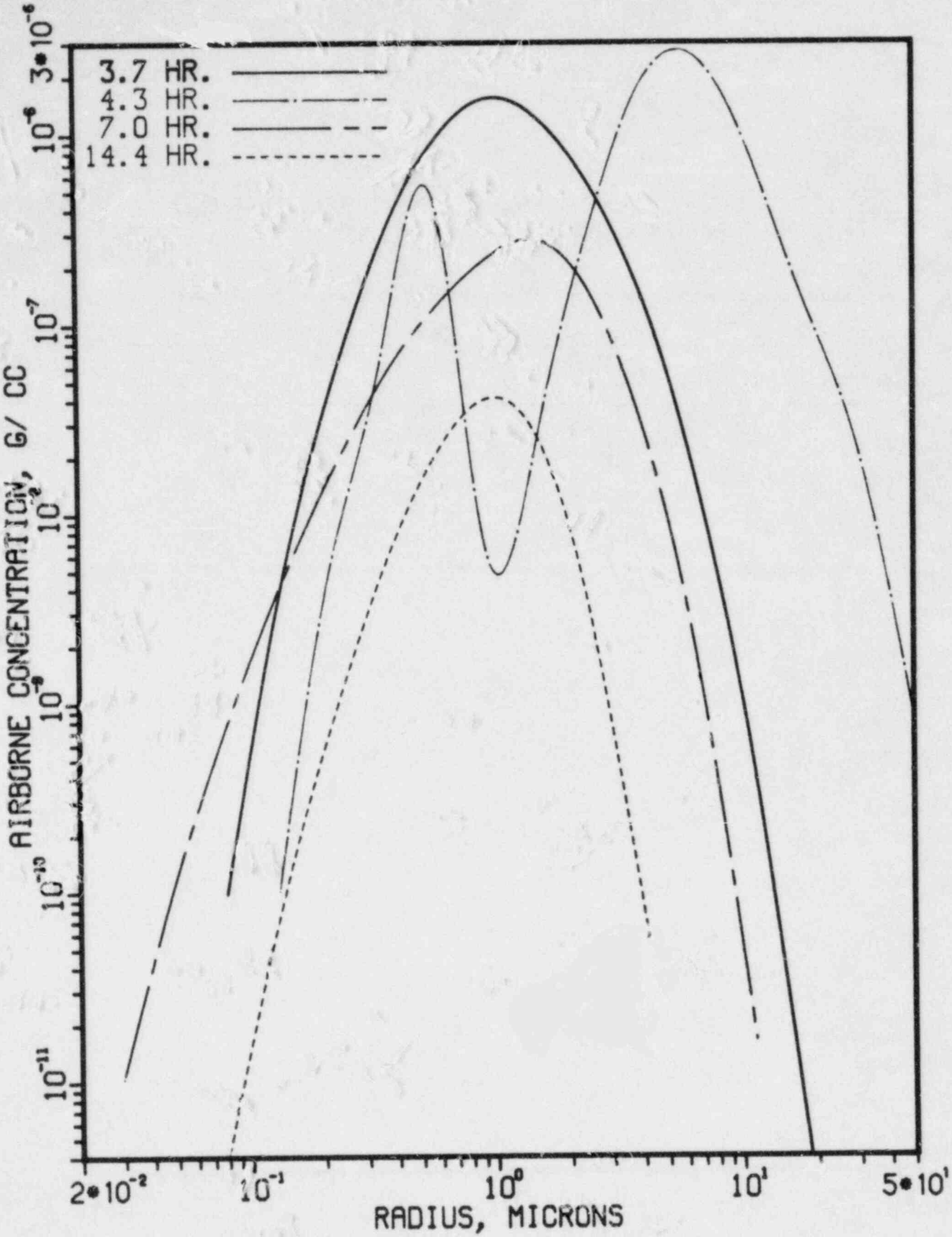

FIGURE 7.20 PARTICLE SIZE DISTRIBUTIONS (S_2HF-Y)

TABLE 7.10. DISTRIBUTION OF SPECIES AFTER ACCIDENT IS COMPLETED AS CALCULATED BY THE NAUA CODE, S_2HF-Y

Species	Fraction of Core Inventory				
	RCS	Lower Volume	Ice Bed	Upper Volume	Environment
CsI	0.73	4.5×10^{-2}	8.3×10^{-2}	0.109	3.3×10^{-2}
CsOH	0.75	4.2×10^{-2}	7.6×10^{-2}	0.100	3.2×10^{-2}
Te	0.69	6.4×10^{-2}	6.5×10^{-2}	0.045	5.5×10^{-2}

TABLE 7.11. FRACTION OF CORE INVENTORY RELEASED TO THE ATMOSPHERE FOR GROUPS OF REACTOR SAFETY STUDY

Time (hr)	I Group 2*	Cs Group 3	Te Group 4	Sr Group 5	Ru Group 6	La Group 7
4	0	0	0	0	0	0
7	3.2×10^{-2}	3.1×10^{-2}	4.8×10^{-2}	4.7×10^{-2}	4.0×10^{-4}	2.5×10^{-3}
10	3.3×10^{-2}	3.1×10^{-2}	5.2×10^{-2}	4.9×10^{-2}	4.1×10^{-4}	2.6×10^{-3}
15	3.3×10^{-2}	3.2×10^{-2}	5.5×10^{-2}	4.9×10^{-2}	4.2×10^{-4}	2.6×10^{-3}
20	3.3×10^{-2}	3.2×10^{-2}	5.5×10^{-2}	4.9×10^{-2}	4.2×10^{-4}	2.6×10^{-3}

*Contribution of volatile iodides to the iodine release is not included, but should be small compared with these values.

7.3.5 General Observations

The containment calculation results of three accident sequences involving five different containment failure modes have been presented. From these results, several interesting observations can be made for the Sequoyah plant. As concluded in previous analyses performed for other types of plants, the fraction of radionuclides released into the environment is largely dependent upon the magnitude and timing of the release from fuel and dependent upon the containment failure time. Among the accident sequences examined, the TMLB'-γ sequence results in the highest release fractions for CsI and CsOH. The assumed early containment failure combined with unavailability of the active engineered safety features are a direct reason for the high release. The TML-δ sequence was found to result in the lowest release fraction, largely due to the effect of the engineered safety features.

The role the ice condenser plays on removal of fission products is found to be relatively significant, yielding a decontamination factor as high as 43 in a certain instance during the TMLB'-δ sequence. Based on the comparison of the amount of fission products removed with those released into the containment from fuel and from the core-concrete interaction, roughly half of the fission products available in the containment were found to be removed by the ice condenser (see Tables 7.6, 7.8, and 7.10). It should be noted however that the present analyses represent one of the first attempts to model the performance of the ice condenser on removal of fission products and that the validity and range of the uncertainties involved in the used model have not been determined. For this reason it may be necessary in the future to conduct a series of controlled separate effect experiments and integral large-scale tests to identify all pertinent removal mechanisms, such as inertial impaction, diffusiophoresis, gravitational settling, Brownian diffusion, and reentrainment of captured fission products into the gas stream, and to determine quantitatively the importance of each mechanism.

7.4 Discussion of Results

The release from the fuel and in-vessel transport of fission products for the Sequoyah sequences considered here was found to be substantially the

same as for the other PWR's considered. In particular, significant retention within the primary system of the released radioactivity was predicted for the accident sequences evaluated. The analyses presented here did not, however, take into account the possible long term reevolution of these fission products due to the heating of the surfaces by the decay of the plated out radioactivity.

The low design pressure and relatively small free volume of the ice condenser containment result in greater vulnerability of this type of containment to the loads that may be encountered during severe reactor accidents. While the ice bed provides an effective heat sink for steam that is released to the containment, the long term buildup of noncondensible gases can pose a threat to containments of this type. Also, the ice has a finite lifetime in the event of an accident, and after it is melted other means of steam condensation may be required; the containment spray systems are provided for this purpose. Hydrogen burning is seen to be a potential threat to the integrity of ice condenser containment. For this reason hydrogen igniters are provided in these containments to burn off the hydrogen that may be generated before it can accumulate to excessive concentrations. For the types of accidents and under the modeling assumptions considered here, however, significant containment pressure rises were predicted even with the operation of the hydrogen igniters considered in the analyses. No representation is made here regarding the likelihood of containment failure due to these burns, but it is considered prudent to address the possibility that failures may take place.

The ice condenser was found to have significant potential for the removal of fission products passing through it. For cases where the air return fans were not available and the released radioactivity made only a single pass through the ice condenser, approximately one-half of the fission products released to the containment were removed by the ice bed. With the air return fans available to continually recirculate the containment atmosphere, even greater retention by the ice bed can be seen. It is interesting to that in the S_2HF sequence the ice is essentially melted by the time that core melting starts, but significant retention is still predicted in the ice condenser compartment; this is due to the plateout of aerosols on the ice baskets and other surfaces, with the air return fans ensuring continuing recirculation of the airborne materials.

In the TMLB and TML sequences as analyzed here, there was significant water in the reactor cavity following reactor vessel failure. This water was found to have significant potential for the removal of radioactivity, particularly tellurium, released from the corium-concrete interaction. In the TML sequence this pool of water offers the possibility of terminating the accident sequence if a coolable debris bed is formed, since the water is cooled and continuously resupplied to the reactor cavity by the spray recirculation system.

In the analyses considered here, essentially all the flow from the lower compartment to the upper compartment passed through the ice condenser. In the normal configuration of the ice condenser containment, there is some relatively limited potential for ice condenser bypass; there are two 6-inch diameter drain lines for the return of containment spray water to the containment sump. Since the flow area of these drain lines is very small compared to that of the ice condenser, such bypass would not be expected to have an appreciable effect on fission product release to the environment. In situations where the containment sprays and/or air return fans are operating, this bypass flow would have no effect; in the absence of sprays and air return fans and with early containment failure, such as TMLB'-γ, this bypass could possibly increase the predicted environmental releases somewhat.

The calculated releases of fission products to the environment show the expected sensitivity to the timing of containment failure, with earlier failure times leading to greater releases. The magnitudes of the environmental releases in the present study are lower than in some earlier studies. The removal of airborne radioactivity by passage through the ice condenser was found to contribute considerably to the reduction in environmental source terms. The predicted retention of fission products within the reactor primary system also serves to reduce the potential magnitudes of environmental releases. In this regard it should be noted that the potential later reevolution, which has not been considered here, could have an impact on the ultimate releases. This would be particularly significant if such reevolution were to take place after the containment as failed.

UNITED STATES
NUCLEAR REGULATORY COMMISSION
WASHINGTON, D.C. 20555